21211

NAME OF AUTHOR/*NOM DE L'AUTEUR*_____ Mr. Murray J. PRESS

TITLE OF THESIS/*TITRE DE LA THÈSE*_____ The Molecular Configurations in Nematic Liquid

Crystal Droplets as Calculated and Observed

UNIVERSITY/*UNIVERSITÉ*_____ Simon Fraser University

DEGREE FOR WHICH THESIS WAS PRESENTED/
*GRADE POUR LEQUEL CETTE THÈSE FUT PRÉSENTÉE*_____ Doctor of Philosophy

YEAR THIS DEGREE CONFERRED/*ANNÉE D'OBTENTION DE CE DEGRÉ*_____ 1974

NAME OF SUPERVISOR/*NOM DU DIRECTEUR DE THÈSE*_____ A. S. Arrott, Professor of Physics

DATED/*DATE*_____ July 25, 1974 _____ SIGNED/*SIGNÉ*_____

PERMANENT ADDRESS/*RÉSIDENCE FI*

NL-91 (11-73)

THE MOLECULAR CONFIGURATIONS

IN NEMATIC LIQUID CRYSTAL DROPLETS

AS CALCULATED AND OBSERVED

by

Murray J. Press

B.Sc., McGill University, 1967

M.Sc., McGill University, 1969

A DISSERTATION SUBMITTED IN PARTIAL FULFILLMENT

OF THE REQUIREMENTS FOR THE DEGREE OF

DOCTOR OF PHILOSOPHY

in the Department

of

Physics

© Murray J. Press 1974

SIMON FRASER UNIVERSITY

June 1974

APPROVAL

Name: Murray J. Press

Degree: Doctor of Philosophy

Title of Thesis: The Molecular Configurations in Nematic Liquid
Crystal Droplets as Calculated and Observed

Examining Committee:

Chairman: A. E. Curzon

_____
A. S. Arrott
Senior Supervisor

_____
K. S. Viswanathan

_____
L. H. Palmer

_____
B. P. Clayman

_____
Etienne Guyon
External Examiner
Laboratoire de Physique des Solides
University of Paris
Paris, Orsay, France

Date Approved: __June 7, 1974__

Title of Thesis/Dissertation:

The Molecular Configurations in Nematic Liquid

Crystal Droplets as Calculated and Observed

Author: _____
          (signature)

Murray J. PRESS
_____
          (name)

July 25, 1974
_____
          (date)

ABSTRACT

Minimum energy solutions have been found for the configurations of the molecules in lens-shaped nematic liquid crystal droplets. These solutions account for most of the phenomena observed in these droplets on liquid substrates when viewed between crossed polarizers. Such droplets are shown to have cylindrical symmetry and to produce three distinct patterns which are called the normal, right-handed, and left-handed configurations. The optical patterns have circular fringes crossed by extinction brushes. In the normal case these brushes form a cross which lies parallel to the cross of the crossed polarizers. In the other cases these brushes are similar at large radii, but near the center of the drops they form a cross rotated with respect to the cross of the crossed polarizers.

The problem is one of the elasticity theory of the nematic liquid crystal with particular boundary conditions. The calculus of variations is used to derive the torque equations, the solutions of which are found by relaxation methods on a digital computer. These solutions are used to draw pictures of the molecular arrangements and with the aid of Maxwell's equations to predict the observed optical patterns, including the case of magnetic fields applied along the symmetry axis.

ACKNOWLEDGMENTS

TABLE OF CONTENTS

CHAPTER I

I.1 INTRODUCTION

A nematic liquid crystal is a fluid composed of elongated molecules which tend to be parallel to one another. This tendency is sufficiently strong to produce considerable long range orientational order but is not strong enough to overcome the effects of local reorientation produced by an interface. The molecular configuration of the fluid is determined from a competition between the volume and surface energies.

The calculation to be discussed arose from the question of the orientation of the molecules in a free drop of a nematic liquid crystal. One quickly reaches the conclusion that the molecules in a spherical droplet should not align in a spherically symmetric fashion. Optimistically one might expect the molecules to display cylindrical symmetry, the axis of which would be infinitely degenerate. This degeneracy is removed if the drops are placed at the interface between two media (for example, air and water). This results in a lens-shaped droplet with a unique axis of symmetry. A typical preparation of droplets of Methoxybenzylidene-Butylaniline (MBBA) on a water substrate in air is shown in Fig. I.1 as it appears in approximately parallel white light between crossed polarizers. Attention is drawn to the dark brushes

- 1 -
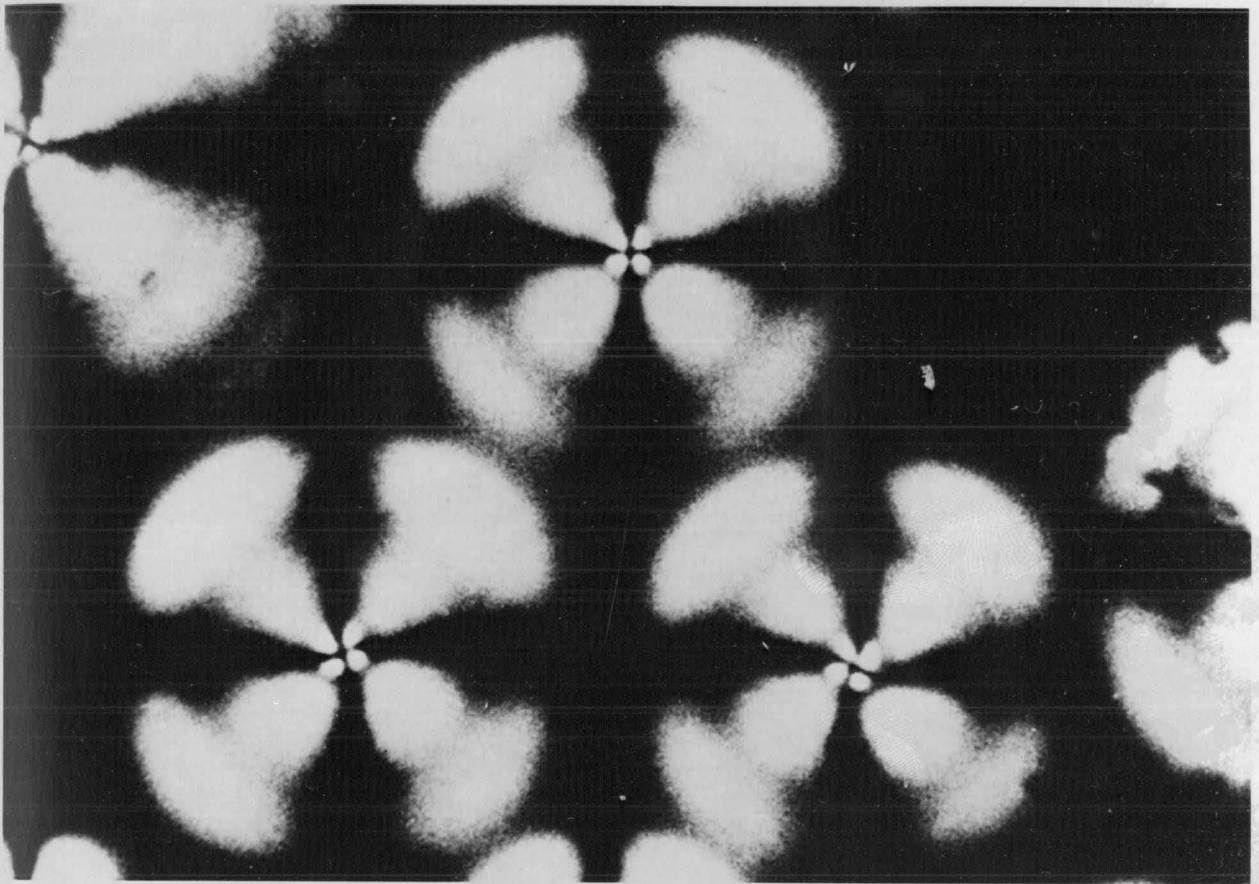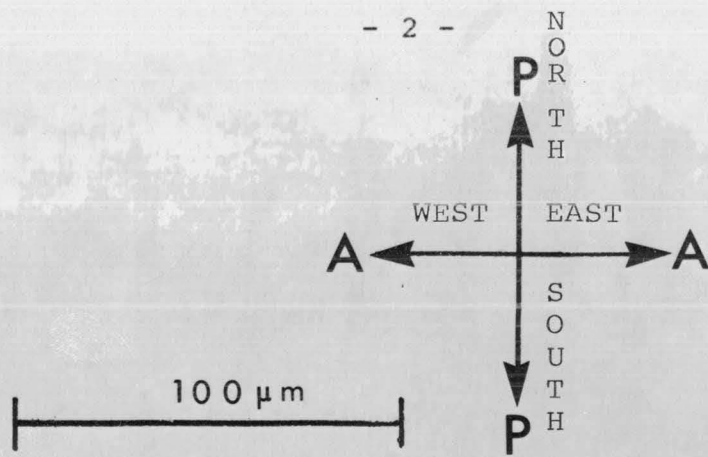
Figure I.1

MBBA droplets on a water substrate observed between crossed polarizers with white light.

rather than the fringe pattern. Three different configurations are observed on the same preparation. These are referred to as the left- and right-handed and the normal configurations. In the normal configuration the dark brushes are oriented as a cross coinciding with the cross of the crossed polarizer-analyzer pair. This type of optical pattern is what one would expect from a configuration in which the projections of the molecules perpendicular to the direction of the light are strictly radial or strictly circumferential about the axis of symmetry. The left- and right-handed species show a rotated cross in the center of the droplet which slowly rotates towards the normal cross as one proceeds outwards. These have surely been observed by others, but have received scant attention.

The calculations to be described show that the rotated optical cross can be accounted for in terms of a rather complex pattern of molecular orientation which minimizes the energy of the system. In this pattern the mean orientation at each point in space is described by two polar angles τ and ϕ. The energy is expressed in terms of these angles, their spatial derivatives, and three elastic constants (splay, twist, and bend). It will be shown that when the twist elastic constant is less than the splay elastic constant the left- and right-handed species are stable and

equal in energy while the normal configuration is apparently
metastable and only slightly higher in energy ($\sim 10^{-9}$ ergs).

An attempt will be made to keep the mathematics in the
main body of the text to a minimum. Thus most manipulations
will be relegated to the appendices as will the discussion of
the computer calculations used to treat the problem.

The introduction will conclude with a brief description
of nematic liquid crystals. This will be followed in Ch. II
by a description of the simple experiments performed and the
conclusions one can reach from the observed optical patterns.

The energetics of distortions in nematics as derived
by Frank (Fr-58) will be presented in Ch. III. Then the
technique of deriving the energy and torque equations in a
geometry slightly simpler than the actual drop will be pre-
sented. This will include a discussion of which terms in
the energy most influence the configuration, the role of
the relative values of the elastic constants, and the effects
of the magnetic field term in the energy. The manipulations
will appear in App. I. The calculation required for the full
droplet will be indicated in App. II along with details of
the justification for the approximations made in the simpli-
fied calculation.

The presentation and discussion of the results of this
calculation will take place in Ch. IV. In Ch. V the method
of handling the propagation of light through the liquid

crystal medium will be discussed. This involves the solution of Maxwell's equations in a birefringent medium in which the optic axis has non-zero spatial derivatives. Ch. V. concludes with a comparison of theory and experiment in which the optical patterns observed, their relation to the molecular orientation, and the effects of a magnetic field will be discussed. In Ch.VI the problem and solutions are reviewed, comparisons are made with other authors, and some interesting extensions of the ideas discovered are indicated.

I.2 NEMATIC LIQUID CRYSTALS

The liquid crystalline phase is intermediate in order between the crystalline solid and the isotropic liquid and is separated from these phases by first order transitions as demonstrated by such experiments as heat capacity measurements (Jo-69) and volume expansion (Pr-73).

The simplest type of liquid crystal ordering is the nematic phase, the main feature of which is the presence of long range orientational order of the molecules. The molecules tend to be parallel to a common axis, called the director, $\hat{n}$, about which there appears to be rotational symmetry. This property is demonstrated in all macroscopic tensor properties. The nematic phase behaves like a uniaxial medium with the principal axis along the director. It shows a large birefringence effect, the difference between the indices of refraction is typically 0.2 compared with 0.01 for quartz. The magnetic and electric susceptibilities as well as the

thermal conductivity and viscosity tensors also show large anisotropies.

The lack of Bragg peaks in the X-ray diffraction patterns indicates that there is no long range order to the spacing of the centers of gravity of the molecules.

In an infinite medium there is no preferred direction for the director. In a finite sample the molecules close to an interface generally have certain preferred orientations. For example, on a crystalline substrate the crystal axes may be preferred. At an isotropic interface, the preferred orientation is degenerate, that is, the molecules like to make an angle θ with respect to the normal to the surface but the azimuthal angle is undetermined. This produces an "easy cone" of surface pinning. Experimentally all values for the angle θ have been found, from $\theta = 0$, the homeotropic configuration, to $\theta = 90°$, where the molecules lie in the surface. The exact angle depends on the nature of the liquid crystal material and the substrate. It can also be somewhat temperature dependent.

Principal among several effects contributing to the molecular interaction in nematics are attractive van der Waals interactions and repulsive hard core interactions. The latter are principally quadrupolar in symmetry, even though the ends of the molecules are not completely identical. The van der Waals interaction is anisotropic because the electric susceptibility is highly

anisotropic. A dipolar fluctuation in one molecule induces a dipole moment in a neighbouring molecule, with the resulting interaction possessing quadrupolar symmetry. With quadrupolar symmetry the director $\hat{n}$ is indistinguishable from $-\hat{n}$. That is, the reversal of a group of molecules will not change its energy with respect to a neighbouring group. This is in contrast to ferromagnetism where the reversal of regions of magnetization is energetically unfavorable. However if one only compares cases where the director or the magnetization direction varies slowly with respect to molecular distances, the mathematical formulations of the two problems have considerable similarity.

The nematic phase can occur only in materials which cannot distinguish right from left, thus the molecules must be identical to their mirror images. Molecules with handedness tend to form cholesteric liquid crystals. It would be an extension of the present work to include the elastic properties of such materials.

CHAPTER II

II.1 OBSERVATIONAL TECHNIQUES

Lens-shaped droplets were obtained by spraying a small quantity of the desired nematic liquid crystal onto a suitable substrate. The material most frequently worked with was Methoxybenzylidene-Butylaniline (MBBA) which is nematic in the temperature range of 10°C-47°C. The MBBA was obtained from Varilight and was used without purification. Its elastic and optical constants have been measured by several workers, making it possible to compare some of the predicted results quantitatively with experiment.

The substrate that proves most convenient to use with the MBBA droplets is water. The advantage of water is that it is not too highly soluble in MBBA and even though it does cause hydrolysis, the reaction rate is sufficiently slow as to allow a sample to be observed for several hours. The isotropic surface presented by the water to MBBA proved far superior to any solid substrate because the local irregularities of the solid usually destroyed the desired cylindrical symmetry.

Two techniques of preparing MBBA droplets for observation were employed. The first consisted in placing a small drop of water (~1/2 cm diameter) on the underside of a cover

- 8 -

glass and then spraying the water drop using an atomizer bottle containing the MBBA. This produced a group of small nematic droplets which gather about the bottom of the water drop as shown in Fig. II.1a. In the second technique the water drop was contained in a capillary about 3 mm in diameter and the MBBA was sprayed on the top surface as shown in Fig. II.1b. Studies were also made of Licrystal Nematic Phase 4 from E. Merck Co. which is nematic between 16°C and 76°C. The Licrytal doesn't interact as strongly with the glass as the MBBA does and thus samples showing cylindrical symmetry could be obtained by spraying directly on glass slides. The samples were viewed optically using a Reichert metallurgical microscope, shown in Fig. II.2. The droplets could be viewed in light of any polarization with the insertion of the appropriate linear polarizers and quartz wedges. The light used was provided by a quartz lamp which could be viewed directly or after having passed through a monochromator when the dependence of the image on wavelength was of interest. To produce a clearer image of the fringe pattern a sodium lamp could be used in place of the quartz lamp. Also shown in Fig. II.2 is a small water-cooled magnet that could provide up to 10 kG along the direction of the light and the axis of symmetry of the droplets. To improve the optics the light was conducted from the monochromator to the hollow pole tip of the magnet with a light tube.
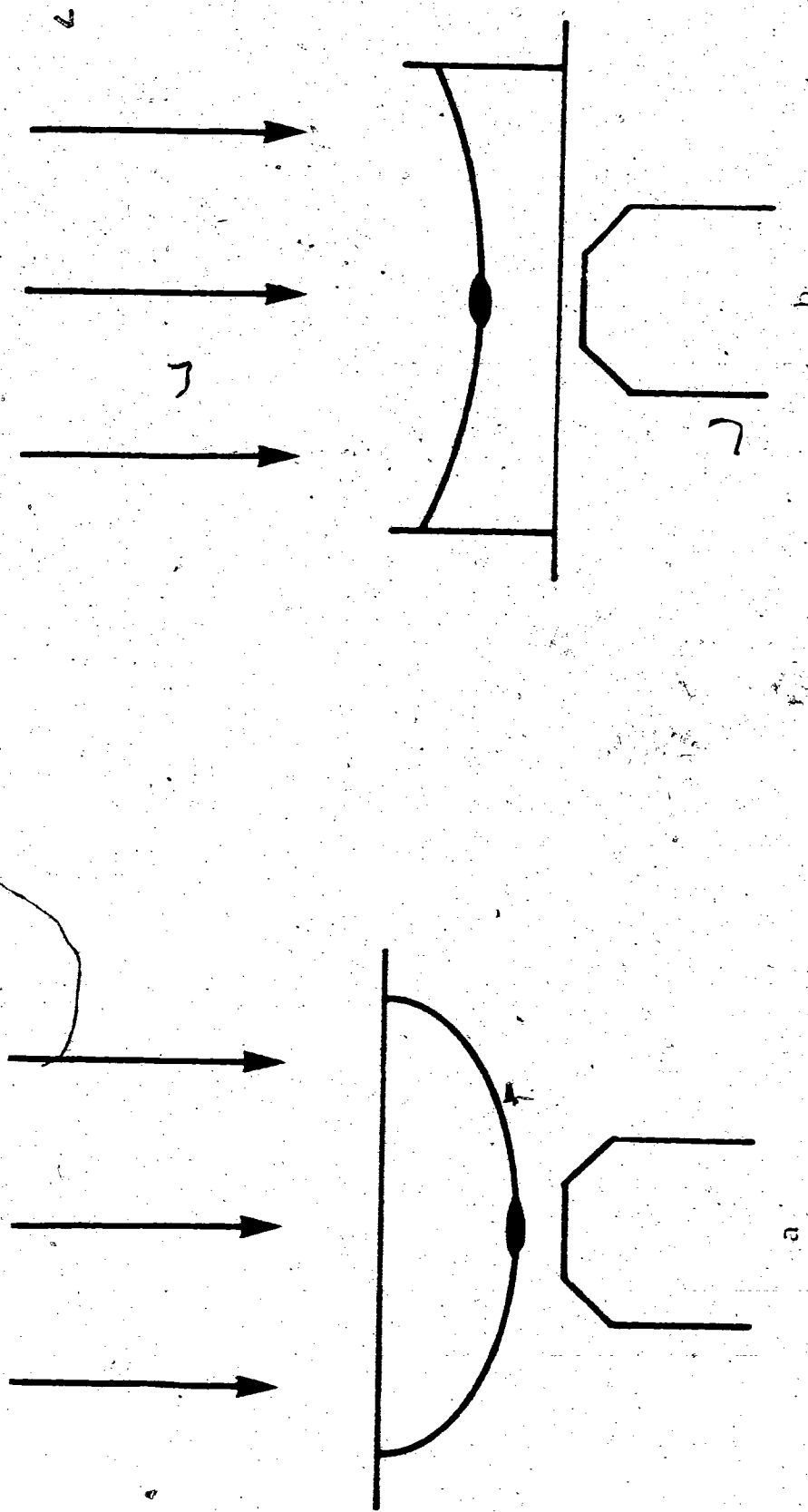
<u>Figure II.1</u>

Schematic of experimental apparatus showing the incident light, water substrate, liquid crystal droplet, and microscope objective. In (a) the liquid crystal droplet is suspended from a water drop approximately 5 mm in diameter while in (b) it is floating on a water column about 3 mm in diameter.
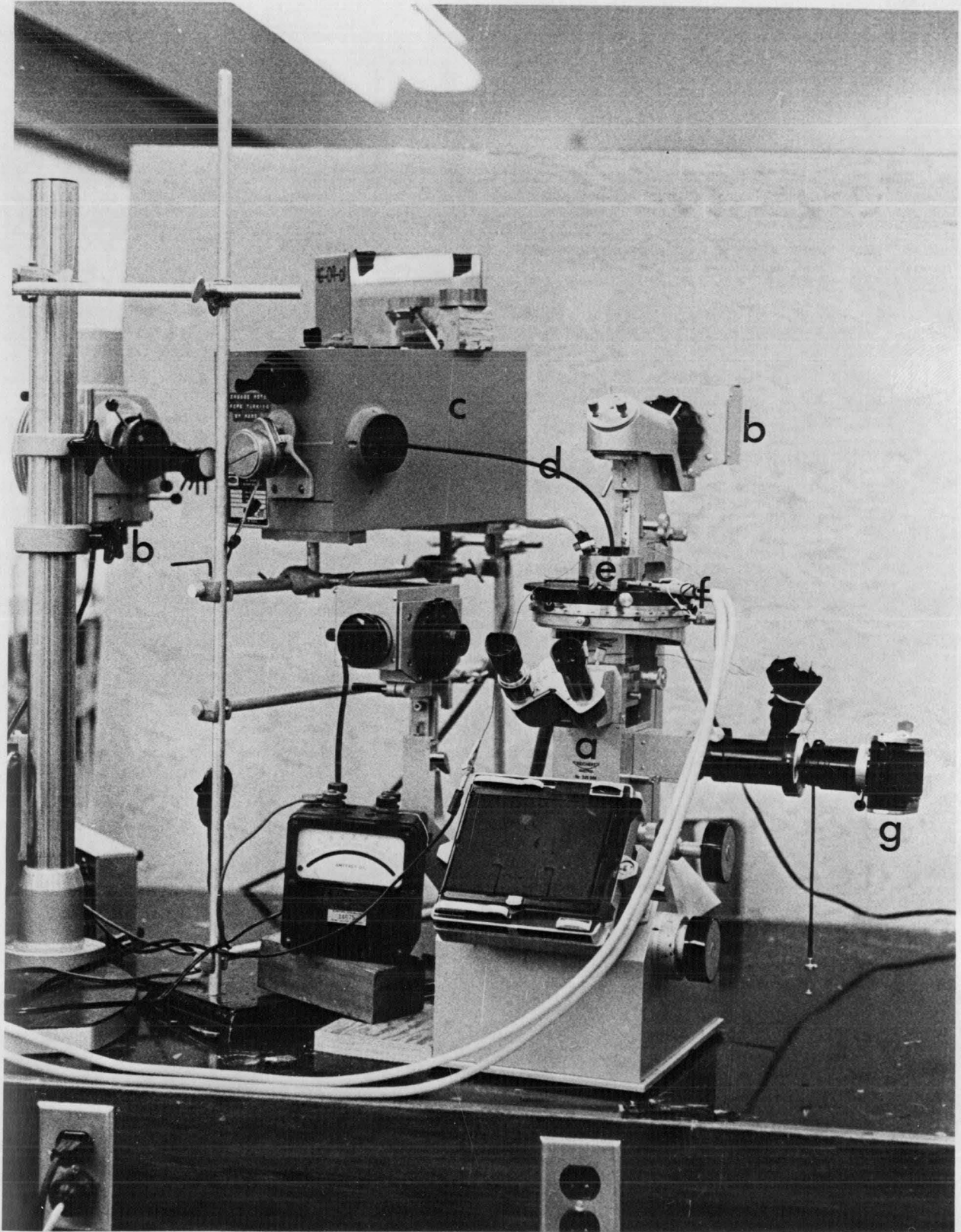
Figure II.2

Experimental apparatus showing the: (a) Reichert microscope,
(b) quartz lamps, (c) Jarrell Ash monochromator, (d) optical
light pipe, (e) water-cooled magnet, (f) temperature-controlled
sample-holder, and (g) Leica 35 mm. camera.

Pictures were taken using a Leica 35 mm camera and either Kodak Tri-X black and white film or Kodak High Speed Ektachrome EH-135 color film. For the color pictures between crossed polarizers it was sometimes found useful to use a Xenon flashgun to avoid excessive exposure times.

The sample holder consisted of a copper block inside which the sample was placed. The temperature could be controlled by passing water through channels milled in the copper block. The whole assembly could be inserted into a slot in the magnet placing the sample between the pole tips in the path of the light.

II.2   OBSERVATIONS

The droplets were observed with approximately parallel light propagating along their axes of symmetry. The light is usually linearly polarized in the NS direction with respect to the microscope before encountering the droplets (See Fig.I.1). After emerging from the droplets the light encounters an analyzer whose polarization axis is rotated 90° from the polarizer, i.e., along the EW direction of the microscope. The most common objective employed has a magnification of sixteen while the eyepieces have a magnification of eight or twelve. The droplets vary between 30 and 1000 microns in diameter. In Figs. I.1 and II.3 are some examples of MBBA droplets on water. The patterns have a strong resemblance

100 μm

a

b
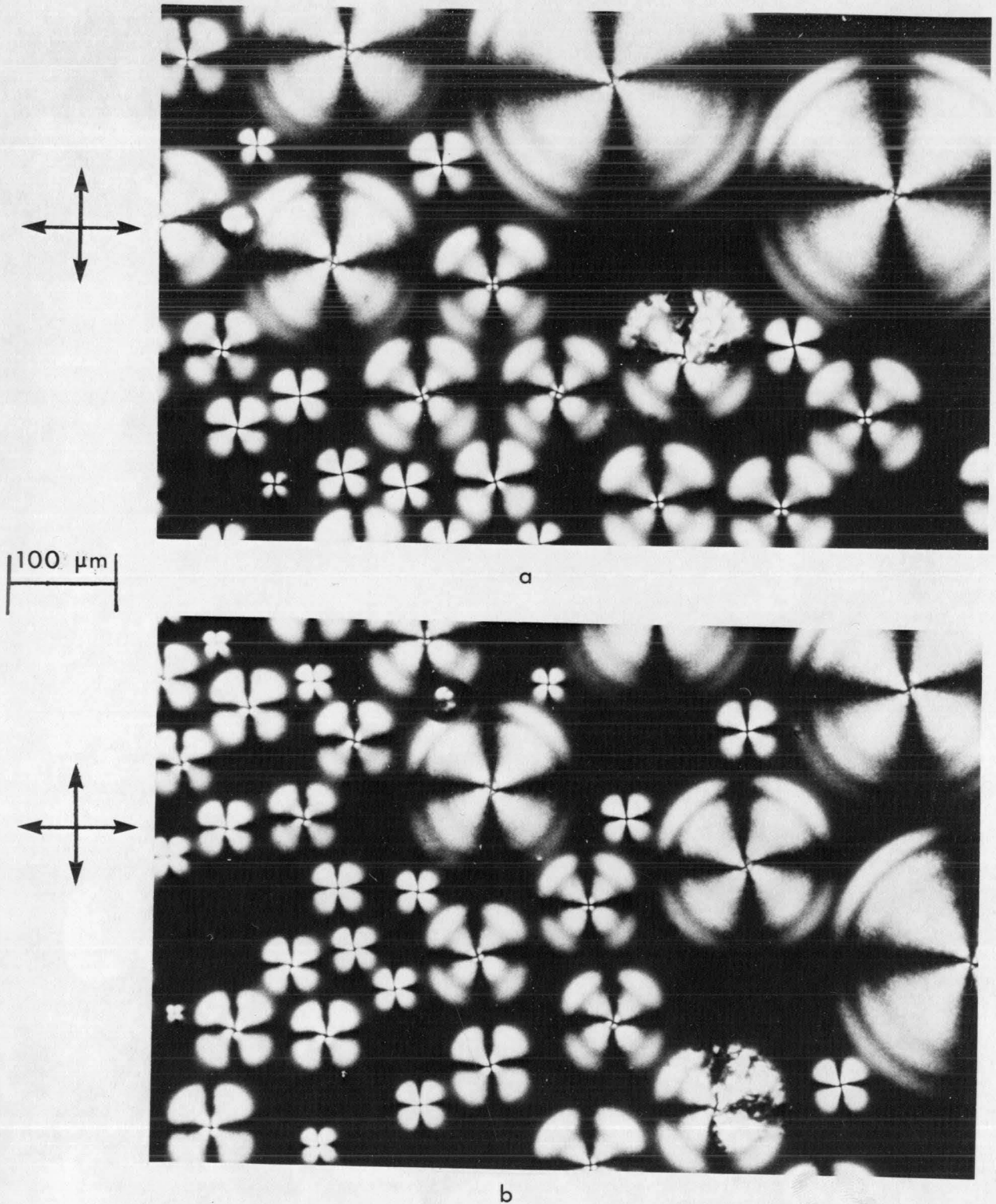
Figure II.3

MBBA droplets on a water substrate observed between crossed
polarizers with white light. In (b) the droplets have been
rotated by about 45° from their position in (a).

to conoscopic images of a uniaxial crystal cut perpendicular
to the optic axis.

The pattern is characterized by dark brushes that lie
roughly parallel to the NS and EW directions, that is,
parallel to the cross of the crossed polarizers. In some
drops the brushes are purely radial in character, this is
called the normal configuration. In most of the drops,
however, the brushes have some curvature to them. Some of
the drops show their brushes rotating clockwise as one
approaches the center of the drop while in others the brushes
rotate counter-clockwise. These are called the right- and
left-handed configurations respectively. At the center of
the droplets there appears to be a cross rotated about 45°
to the polarizer axis which occupies a region of about 10μ
in radius. All three types can be present in a single pre-
paration as shown in Fig. I.1. In addition to the brushes
there are concentric circular fringes.

The droplets are cylindrically symmetric as shown
by the invariance of the optical patterns in Figs. II.3a and
II.3b as the droplets are rotated. These patterns have a
strong resemblance to the Airy (Ai-31) spirals produced by
two pieces of quartz of opposite handedness placed on top
of each other and observed between crossed polarizers in
divergent light.

The Licrystal droplets on glass, shown in Fig. II.4, produce patterns very similar to the ones shown in Fig. I.1. Again one has the existence of the rotated cross and the outer brushes. The fringe patterns are generally more diffuse than those in MBBA, due to the Licrystal being optically thinner. This shows that the effect of the rotated brushes to be explained is not peculiar to MBBA.

When a magnetic field is applied perpendicular to the substrate there is a change in the fringe patterns. This is the result of the molecules being anisotropically diamagnetic. Their long axes align with the magnetic field. Aligning the molecules parallel to the light direction reduces the amount of birefringence present which reduces the optical retardation of the droplets. This causes a reduction in the number of fringes with a resultant increase in the width of the remaining fringes. The nature of the rotated cross does not appear to be affected by the presence of the field.

The magnetic field, applied parallel to the axis of symmetry of the drops usually maintains the symmetry as demonstrated by the invariance of the optical pattern as the sample is rotated between the polarizers. However for some larger droplets (radii in excess of 100μm) and magnetic fields of 6-10 kG, the symmetry sometimes gets broken. This is demonstrated by the slow nucleation of tiny bubbles in the droplets. As time goes on the bubbles
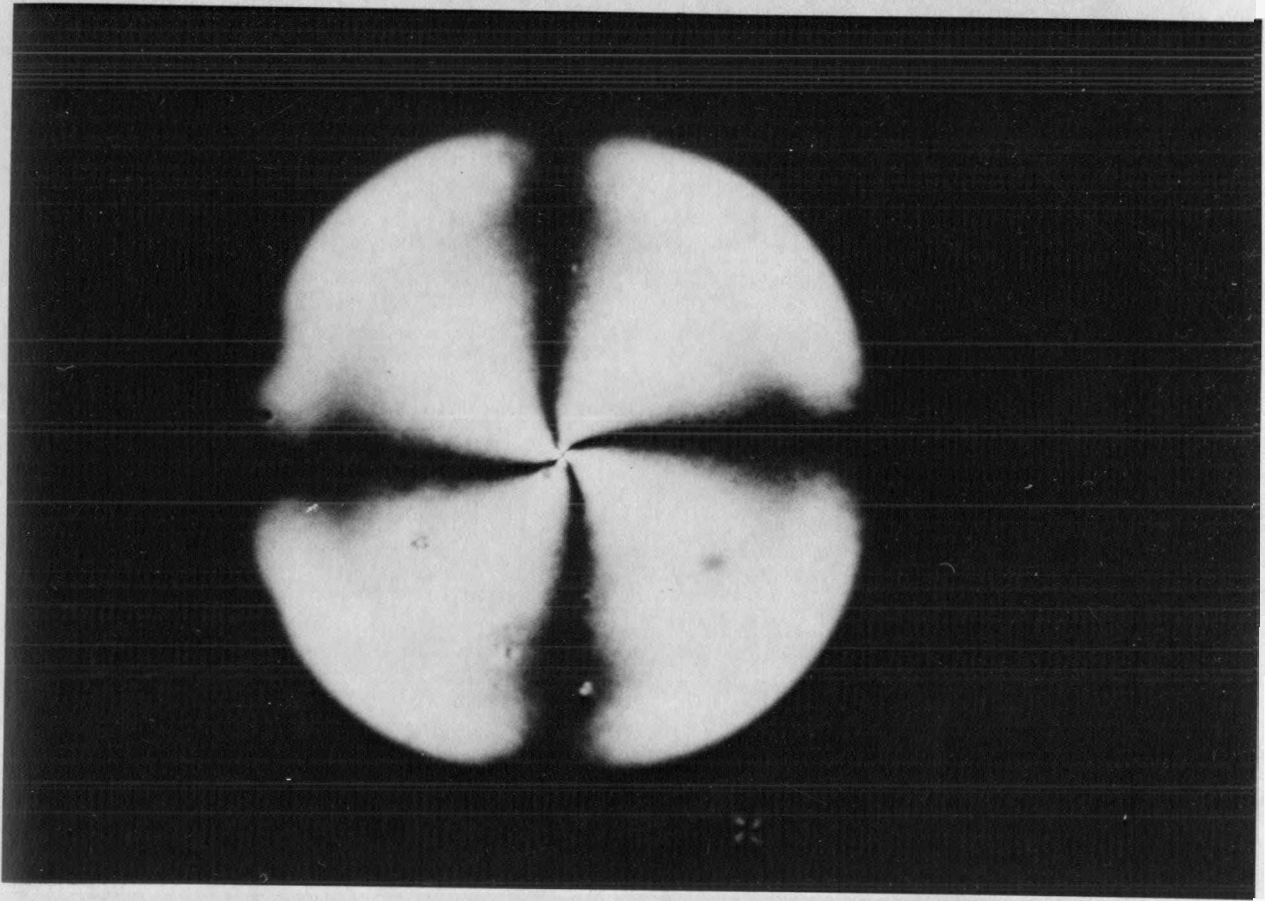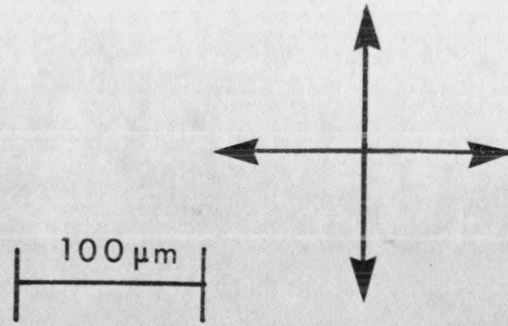
Figure II.4

Licrystal Nematic Phase 4 droplet on a glass slide observed between crossed polarizers with white light.

become more numerous, grow bigger, and start to merge. The process is reversible as demonstrated by their slow disappearance when the magnetic field is decreased. The droplet symmetry is then restored. The presence of the bubbles does not seem to greatly affect the brush pattern or the pattern of the fringes. The droplets can be recycled in such a fashion many times. Such "decorative" effects were first seen by Rault (Ra-71) who obtained them by placing a film of MBBA on ethylene glycol. There are two possible explanations. The bubbles could be regions of impurities that are expelled by the magnetic field. The second possibility is that the molecules are reorienting themselves discontinously to minimize the energy.

An observed pattern can be changed by inserting a quartz wedge or a quarter wave plate. When a quartz wedge is inserted between the droplets and the analyzer with its fast axis in the NE-SW direction the outer fringes in the NE and SW quadrants move inwards while those in the NW and SE quadrants move outwards. When the wedge is withdrawn the movement of the fringe pattern reverses.

When the droplets are observed with only the polarizer or the analyzer most of the birefringence effects disappear. What does remain is a flickering pattern in the two quadrants parallel to the direction of the polarization of the light.

II.3 QUALITATIVE INTERPRETATIONS OF THE OUTER BRUSH PATTERN

When viewing the droplets with light propagating parallel
to their symmetry axes the effect of the optical anisotropy
of the molecules can be qualitatively determined by examining
the effect on the light of the projections of the molecules
in a plane perpendicular to the direction of the light pro-
pagation. In the two simplest configurations possible for
large radii the projections of the molecules in the horizon-
tal plane can be radial or circumferential. When light that
is linearly polarized in the NS direction encounters the
radial configuration, at the points close to the NS axis of
the drop the electric field is vibrating parallel to the
direction of the molecules and hence the light polarization
lies in the local principal plane. The principal plane is
defined as that plane which contains the direction of pro-
pagation and the optic axis. Light whose polarization is in
the principal plane behaves as an extraordinary wave, that
is, its index of refraction depends on the angle between
the direction of propagation and the optic axis. Since the
assumption is that all the principal planes along the NS
axis are radial, the light propagating here is completely
e-ray and thus its direction of polarization is unchanged
as it propagates through the droplet. When it emerges, its
polarization is perpendicular to the polarization axis of

the analyzer and so it gets absorbed producing a dark region. This effect produces a dark brush in the NS direction. Light entering the droplet along the EW axis is polarized perpendicular to the principal plane and thus becomes the ordinary or o-ray. When it emerges its polarization is still perpendicular to the analyzer direction and it gets absorbed producing the dark brush in the EW direction. Light entering the droplet along the NE-SW and NW-SE axes gets broken into two components, travelling parallel and perpendicular to the principal plane, producing the e- and o-rays respectively. These travel at different velocities and then recombine after leaving the droplet. However, their phases can be different and thus they can produce any degree of elliptical polarization. Since the light is no longer polarized perpendicular to the analyser a bright region can occur along the NE-SW and NW-SE axes. The same argument can be applied to the circumferential configuration, only now along the NS axis the light propagates as an o-ray while along the EW axis it propagates as an e-ray. Thus both the radial and circumferential configuration droplets can explain the outer brush pattern observed.

Differentiating the two configurations is possible by analyzing the movement of the fringe pattern when a quartz wedge is inserted. It is necessary to recall that

nematics show positive birefringence, which means the o-ray
propagates more quickly than the e-ray.

The objects that are being looked at are droplets that
have zero thickness and thus zero optical retardation at the
outer edge and which become thicker as one moves towards the
center. Thus as the quartz wedge is inserted if the fringes
at some point move towards the outer edge, the optical retarda-
tion of the system at that point is increasing, i.e., the
effect of the quartz wedge is adding to that due to the droplet.
If at some point the fringes move away from the outer edge, the
optical retardation of the system at that point is decreasing,
i.e., the effect of the quartz wedge is subtracting from that
due to the droplet. Addition occurs in those regions in which
the fast axes of the droplet are aligned parallel to the fast
axis of the quartz wedge. Since for a nematic liquid crystal
the slow axis corresponds to the e-ray and thus to the direction
of the principal plane, the observed subtraction in the NE and
SW quadrants when the quartz wedge is inserted with its fast
axis along the NE-SW direction indicates that the projections
of the molecules perpendicular to the symmetry axis must be
radial.

This configuration is confirmed by the speckling pattern
observed when only a polarizer is used. The speckling results
from the vibrations of the molecules about their equilibrium
positions. The ordinary index of refraction is independent of
the orientation of the molecules, but the extraordinary index of
refraction depends on the direction of propagation of the light

with respect to the optic axis. Thus as the molecules fluctuate, the local index of refraction for the e-rays varies and they are refracted whereas the o-rays are unaffected. The speckling patterns are observed to be parallel to the polarizer axis, which again indicates that the projections of the molecules in a plane perpendicular to the axis of symmetry at large radii are radial.

II.4 CONJECTURES ON THE CENTRAL CROSS

The central rotated cross can have some simple explanations related to the configuration of the molecules. One can visualize the simple case where all the horizontal projections of the molecules in a vertical column through the droplet lie along the same direction. Since the crosses are extinction lines all the horizontal projections of the molecules on the rotated cross must be aligned parallel to either the polarizer or the analyzer. Joining these molecular projections with a continuous line would produce a spiral pattern in the horizontal plane (see Fig. IV.1b). The equation of the spiral can be shown to be

$$r = r_o\, e^{-(\cot\theta_o)\theta} \qquad\qquad (II.1)$$

where θ_0 is the angle between the analyzer and the arms of the cross in which the molecules are parallel to the analyzer. In particular, when $\theta_0 = 45°$, the equation for the direction of the projections of the molecules in the horizontal plane becomes

$$r = r_0 \, e^{-\theta} \qquad\qquad (II.2)$$

an equation of exceeding simplicity and beauty. The appearance in nature of a spiral described by the base of natural logarithms raised to a power in radian measure was a major motivation for the calculations carried out.

To appreciate a second situation one must go back to 1831 when Airy (Ai-31) published some observations on the optics of quartz crystals and the mathematics to explain them. One of the more interesting observations was that involving two quartz crystals of opposite optical activity, cut perpendicular to their optic axis, placed on top of each other, and observed between crossed polarizers with divergent light. The pattern he observed consists of a rotated cross with continually spiralling arms which bears a stong resemblance to the optical pattern of the liquid crystal droplets.

Since nematics do not show optical activity this raised the possibility that the handedness might arise from the physical rotation of the molecules. One could have the

molecules first rotating in one direction and then symmetri-
cally in the opposite direction to produce the two types of
handedness to complete the analogy with the quartz experi-
ment. Such a configuration does produce a rotated optical
cross. However, the same cross can be obtained by rotating
in one direction only. The position of the cross is thus
some weighted average of the directions of the molecules.
Again one finds that the rotated cross is associated with a
twisted configuration of the molecules. The reason for
producing this twist will be demonstrated in the analysis of
the energy performed in the next chapter.

CHAPTER III

III.1 ENERGY AND TORQUE EQUATIONS

Frank (Fr-58) has shown that the continuous distortions that can be produced in a liquid crystal are of three distinct types. There is a splay-like distortion if there is a divergence in the director, $\hat{n}$. A twist-like distortion occurs if there is a component of the curling pattern of the molecules parallel to the director. A bend-like distortion is present if there is a component of the curling pattern perpendicular to the director. These three distortions are shown in Fig. III.1 in a cylindrically symmetric medium. A general distortion can contain components of each type in various amounts. Frank has derived an expression for the energy associated with these distortions. For a nematic the bulk energy density can be written as the sum of three terms, one associated with each type of primary distortion. The expression he derived for the energy density is

$$F = \tfrac{1}{2} S |\nabla \cdot \hat{n}|^2 + \tfrac{1}{2} T |\hat{n} \cdot (\nabla \times \hat{n})|^2 + \tfrac{1}{2} B |\hat{n} \times (\nabla \times \hat{n})|^2$$

$$(III.1)$$

where S, T, and B are the elastic constants associated with splay, twist, and bend respectively. Experimentally the elastic constants have values of the order of 10^{-6} dynes.

Because the experimental observations on the droplets

- 24 -
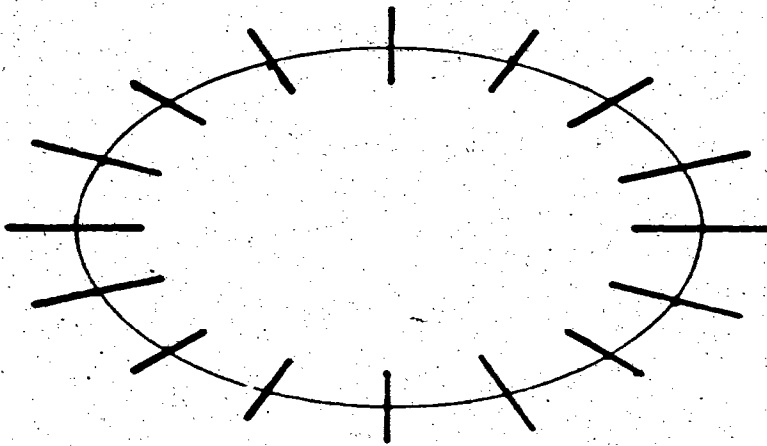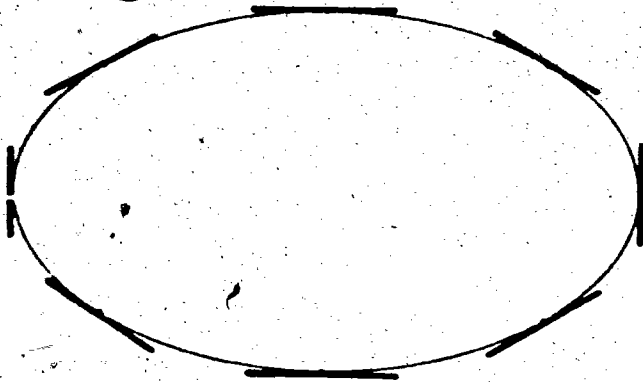
SPLAY
DIV $\hat{n} \neq 0$

BEND
CURL $\hat{n} \perp \hat{n}$
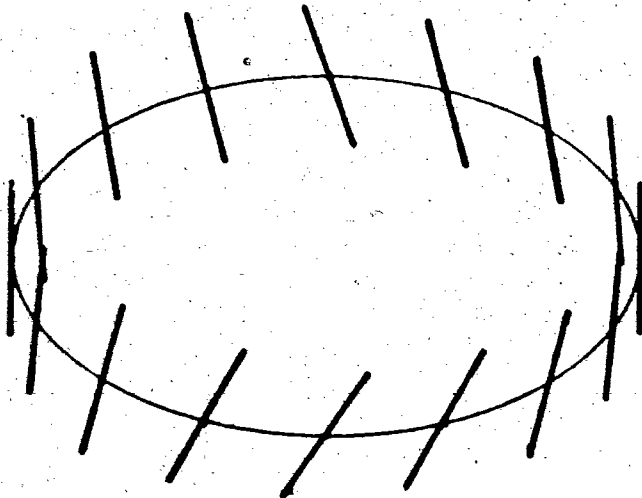
TWIST
CURL $\hat{n} \parallel \hat{n}$

Figure III.1

Splay, bend, and mostly twist in a cylindrically symmetric medium.

indicate that they are cylindrically symmetric the director
is defined using polar coordinates. The coordinate system
consists of two subsystems, one located at the axis of sym-
metry of the droplet and the other at the position of the
director. The angle θ is the angle between the director
and the symmetry axis, while ϕ is the angle that the project-
ions of the molecules in a plane perpendicular to the axis
of symmetry make with the radial direction. The center of
the molecule is at a distance ρ from the axis of symmetry
and a height z above the $z = 0$ plane. This coordinate
system is shown in Fig.III.2 and in it the director can be
written as

$$\hat{n}(\rho,z) = \sin\theta(\rho,z)\ \cos\phi(\rho,z)\hat{\rho}$$
$$+ \sin\theta(\rho,z)\ \sin\phi(\rho,z)\hat{\phi} \qquad (III.2)$$
$$+ \cos\theta(\rho,z)\hat{z} \quad .$$

Because of the rotational symmetry, the angles θ and ϕ
are independent of the azimuthal position about the axis of
symmetry, i.e., they are independent of the angle ϕ.

The total volume energy can be obtained from Eqs. III.1
and III.2 by integrating throughout the region of interest.
Thus one has

$$E = 2\pi \int_{\rho=0}^{\rho=\rho_O} \int_{z=Z_{LS}(\rho)}^{z=Z_{US}(\rho)} d\rho \ dz \ \rho F \qquad (III.3)$$

where ρ_O is the largest radial distance of interest while
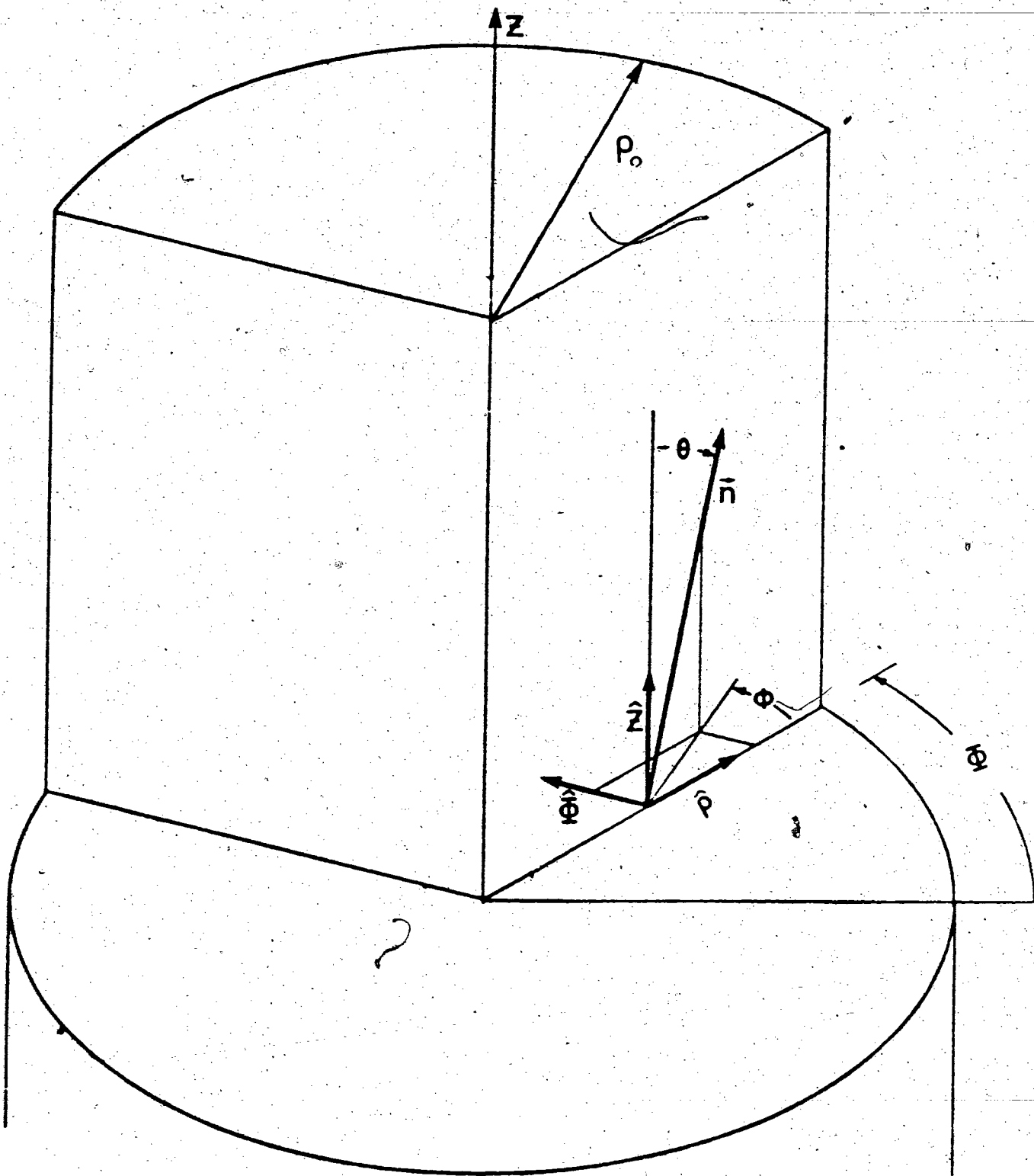
Figure III.2

The coordinate system showing the polar angles θ and ϕ and the unit vectors $\hat{\rho}$, $\hat{\Phi}$, and $\hat{z}$ at the point (ρ, z).

$Z_{LS}(\rho)$ and $Z_{US}(\rho)$ are the z-coordinates of the lower and upper surfaces of the region of interest, respectively. Both are possibly a function of the radial distance. The factor of 2π results from the integration in $d\phi$ having been carried out because of the symmetry present.

In App. I the appropriate manipulations have been performed and the expression one finds for the Helmholtz free energy is

$$E = \pi \int d\rho dz f(\rho, z, \theta(\rho,z), \phi(\rho,z), \theta_\rho(\rho,z), \theta_z(\rho,z), \phi_\rho(\rho,z), \phi_z(\rho,z), H)$$

(III.4a)

where

$$
\begin{aligned}
f = \quad & \frac{1}{\rho} \sin^2\theta \, [S \cos^2\phi + T \cos^2\theta \sin^2\phi + B \sin^2\theta \sin^2\phi] \\
& + \rho \, \theta_\rho^2 \, [S \cos^2\theta \cos^2\phi + T \sin^2\phi + B \sin^2\theta \cos^2\phi] \\
& + \rho \sin^2\theta \, \phi_\rho^2 \, [S \sin^2\phi + T \cos^2\theta \cos^2\phi + B \sin^2\theta \cos^2\phi] \\
& + \rho \, \theta_z^2 \, [S \sin^2\theta + B \cos^2\theta] \\
& + \rho \sin^2\theta \, \phi_z^2 \, [T \sin^2\theta + B \cos^2\theta] \\
& + 2 \sin\theta \, \cos\theta \, \theta_\rho \, [S \cos^2\phi + T \sin^2\phi] \\
& + 2 \sin^2\theta \, \sin\phi \cos\phi \, \phi_\rho \, [- S + T \cos^2\theta + B \sin^2\theta] \\
& - 2 \sin^2\theta \cos\phi \, \theta_z \, S \\
& + 2 \sin^3\theta \cos\theta \sin\phi \, \phi_z \, [B-T] \\
& + 2 \rho \sin\theta \cos\theta \sin\phi \cos\phi \, \theta_\rho \, \phi_\rho \, [T-S] \\
& + 2 \rho \sin\theta \cos\theta \cos\phi \, \theta_\rho \, \theta_z \, [B-S] \\
& + 2 \rho \sin^2\theta \sin\phi \, \theta_z \, \phi_\rho \, S \\
& - 2 \rho \sin^2\theta \sin\phi \, \theta_\rho \, \phi_z \, T \\
& + 2 \rho \sin^3\theta \cos\theta \cos\phi \, \phi_\rho \, \phi_z \, [B-T] \\
& + \rho \sin^2\theta \, \Delta\chi \, H^2
\end{aligned}
$$

(III.4b)

where the subscripts are partial derivatives and

where $\Delta\chi$ is the anisotropy in the magnetic susceptibility

$$\Delta\chi = \chi_{\|} - \chi_{\perp} \qquad \text{(III.5)}$$

where $\chi_{\|}$ and $\chi_{\perp}$ are the magnetic susceptibilities parallel and perpendicular to the director, respectively, while H is the magnetic field.

The minimization of the total energy of a droplet is a complicated problem and will be discussed in its entirety in App. II. For the present time it is desirable to simplify the problem by replacing the full droplet by a geometry which approximates the central region of the droplet. The approximation used is a cylinder with height Z_0 equal to the thickness of the droplet and where the radius ρ_0 is the region of the droplet in which the surfaces can still be thought of as being parallel to the supporting substrate. It will be shown that this approximation contains the main region of interest and can produce most of the features observed experimentally. This is justified from the experimental observation that pieces of dirt or irregularities near the outer regions of the drop have little effect on the central region.

The boundary conditions must also be considered. Dubois-Violette (Du-69) discusses in some detail the types of terms that appear at the interface of a nematic with an isotropic medium. She comes to the conclusion that the most important term is that which has been observed and commented on by many

others in a much simpler fashion, this is the presence of

a cone of easy pinning as described in Ch. I. To repeat,

this means that the molecules like to make a certain well-

defined angle with the normal to the interface. In terms of

the simplified problem to be solved because the top and bottom

surfaces are at $z = 0$ and $z = z_0$, independent of radius, the

cone of easy pinning means that the polar angle θ is deter-

mined at the top and bottom surfaces while the angle ϕ is free

to be determined by other considerations such as the minimi-

zation of the energy. For a real drop where the top and bottom

surfaces are not parallel to the substrate this constraint

becomes a more complicated function involving the angle ϕ and

the shape of the surface as well as the angle θ. This will

be discussed more fully in App. II.

At the outer surface, the assumption is made that there

is no pinning of any kind present. In this case both the

angles θ and ϕ are free to be determined by the minimization

of the bulk energy. In reality, the angles θ and ϕ at ρ_0

will be determined in part by the outer regions of the drop

and eventually by the outer surfaces of the drop. The

assumption of no pinning will turn out to give a good appro-

ximation to the true solution.

The problem to be solved involves minimizing the free

energy as given by Eq. III.4 subject to the boundary conditions

of hard pinning of the angle ϕ at the top and bottom surfaces.

To minimize the energy a variational calculation must be performed on Eq. III.4 with both the angles θ and ϕ to be varied independently. Formally one proceeds by equating the variation of the energy to zero. From Eq. III.4a one has

$$\delta E = 0 = \pi \int_0^{\rho_0} \int_0^{Z_0} d\rho\, dz\; \delta f(\rho, z, \theta, \theta_\rho, \theta_z, \phi, \phi_\rho, \phi_z, H)$$

<div align="right">(III.6a)</div>

which upon application of the chain rule becomes

$$0 = \pi \int_0^{\rho_0} \int_0^{Z_0} d\rho\, dz \left[\frac{\partial f}{\partial \theta} \delta\theta + \frac{\partial f}{\partial \theta_\rho} \delta\theta_\rho + \frac{\partial f}{\partial \theta_z} \delta\theta_z \right. \\ \left. + \frac{\partial f}{\partial \phi} \delta\phi + \frac{\partial f}{\partial \phi_\rho} \delta\phi_\rho + \frac{\partial f}{\partial \phi_z} \delta\phi_z \right].$$

<div align="right">(III.6b)</div>

Performing an integration by parts produces

$$0 = \pi \int_0^{\rho_0} \int_0^{Z_0} d\rho\, dz \left[\left(\frac{\partial f}{\partial \theta} - \frac{\partial}{\partial \rho} \frac{\partial f}{\partial \theta_\rho} - \frac{\partial}{\partial z} \frac{\partial f}{\partial \theta_z} \right) \delta\theta \right. \\ \left. + \left(\frac{\partial f}{\partial \phi} - \frac{\partial}{\partial \rho} \frac{\partial f}{\partial \phi_\rho} - \frac{\partial}{\partial z} \frac{\partial f}{\partial \phi_z} \right) \delta\phi \right] \\ + \pi \int_0^{Z_0} dz \left[\frac{\partial f}{\partial \theta_\rho} \delta\theta + \frac{\partial f}{\partial \phi_\rho} \delta\phi \right] \Bigg|_{\rho = 0}^{\rho = \rho_0} \\ + \pi \int_0^{\rho_0} d\rho \left[\frac{\partial f}{\partial \theta_z} \delta\theta + \frac{\partial f}{\partial \phi_z} \delta\phi \right] \Bigg|_{z = 0}^{z = Z_0}$$

<div align="right">(III.7)</div>

Since the variations of θ and ϕ are independent and arbitrary in the bulk one obtains two independent differential equations. Because $\delta\theta$ is arbitrary one has

$$\frac{\partial f}{\partial \theta} - \frac{\partial}{\partial \rho} \frac{\partial f}{\partial \theta_\rho} - \frac{\partial}{\partial z} \frac{\partial f}{\partial \theta_z} = 0.$$

<div align="right">(III.8)</div>

This is referred to as the θ-equation in the bulk. Similarly since $\delta\phi$ is arbitrary in the bulk one finds

$$\frac{\partial f}{\partial \phi} - \frac{\partial}{\partial \rho} \frac{\partial f}{\partial \phi_\rho} - \frac{\partial}{\partial z} \frac{\partial f}{\partial \phi_z} = 0. \qquad (III.9)$$

This is referred to as the ϕ-equation in the bulk.

These are the well-known Euler-Lagrange equations that appear whenever a minimization of energy is being attempted. In addition one also obtains some boundary equations. Since neither angle θ nor ϕ are determined apriori at $\rho=0$ or at $\rho=\rho_0$ and since the variations in θ and in ϕ are independent, two equations are produced:

$$\text{and} \qquad \left. \begin{array}{l} \dfrac{\partial f}{\partial \theta_\rho} = 0 \\[2em] \dfrac{\partial f}{\partial \phi_\rho} = 0 \end{array} \right\} \quad \text{for all } z \text{ at } \rho=0 \text{ and } \rho=\rho_0 \qquad \begin{array}{l} (III.10a) \\[2em] (III.10b) \end{array}$$

On the top and bottom surfaces, the assumption of hard pinning has been made, thus $\delta\theta \equiv 0$. However, the azimuthal angle ϕ is free and thus one gets

$$\frac{\partial f}{\partial \phi_\rho} = 0 \qquad \text{for all } \rho \text{ at } z=0 \text{ and } z=z_0. \qquad (III.11)$$

This is the system of equations that must be satisfied to produce an extremum, hopefully a minimum, and even a absolute minimum, in the energy.

The manipulations are performed in App. I. The results
of the calculation produces the following set of equations.

The θ-equation is

$$0 = \frac{1}{\rho^2} \sin\theta \cos\theta \ [S \cos^2\phi + T (\cos^2\theta - \sin^2\theta) \sin^2\phi + 2 B \sin^2\theta \sin^2\phi]$$

$$+ \sin\theta \cos\theta \cos^2\phi \ \theta_\rho^2 \ [S-B]$$

$$+ 2 \sin\phi \cos\phi \ \theta_\rho \phi_\rho \ [S \cos^2\theta - T + B \sin^2\theta]$$

$$- (\frac{1}{\rho} \theta_\rho + \theta_{\rho\rho}) \ [S \cos^2\theta \cos^2\phi + T \sin^2\phi + B \sin^2\theta \cos^2\phi]$$

$$+ \sin\theta \cos\theta \ \phi_\rho^2 \ [S \cos^2\phi + T (\sin^2\phi - 2 \sin^2\theta \cos^2\phi)$$

$$+ 2 B \sin^2\theta \cos^2\phi]$$

$$+ \sin\theta \cos\theta \ \theta_z^2 \ [B-S]$$

$$- \theta_{zz} \ [S \sin^2\theta + B \cos^2\theta]$$

$$+ \sin\theta \cos\theta \ \phi_z^2 \ [2 T \sin^2\theta + B(\cos^2\theta - \sin^2\theta)]$$

$$+ \frac{1}{\rho} \sin\theta \cos\theta \sin\phi \cos\phi \ \phi_\rho \ [S + T (4 \cos^2\theta - 5) + 4 B \sin^2\theta]$$

$$+ \frac{1}{\rho} \sin^2\theta \sin\phi \ \phi_z \ [- S + T (2 - 4 \cos^2\theta) + B (3 \cos^2\theta - \sin^2\theta)]$$

$$+ \sin\theta \cos\theta \sin\phi \cos\phi \ \phi_{\rho\rho} \ [S-T]$$

$$+ \frac{1}{\rho} \sin\theta \cos\theta \cos\phi \ \theta_z \ [S-B]$$

$$+ \sin\theta \cos\theta \sin\phi \ \theta_z \phi_\rho \ [B-S]$$

$$+ 2 \sin\theta \cos\theta \cos\phi \ \theta_{\rho z} \ [S-B]$$

$$+ [\cos^2\theta - \sin^2\theta] \cos\phi \ \theta_\rho \theta_z \ [S-B]$$

$$- \sin\theta \cos\theta \sin\phi \ \theta_\rho \phi_z \ [S-B]$$

$$+ \sin^2\theta \cos\phi \ \phi_\rho \phi_z \ [- S + 2 T (\sin^2\theta - \cos^2\theta) + B (3 \cos^2\theta - \sin^2\theta)]$$

$$+ \sin^2\theta \sin\phi \ \phi_{\rho z} \ [T-S]$$

$$+ \sin\theta \cos\theta \ \Delta\chi \ H^2 \ .$$

$$(III.12)$$

The ϕ-equation is

$$0 = \frac{1}{\rho^2} \sin\phi \cos\phi \, [-S + T \cos^2\theta + B \sin^2\theta]$$

$$+ \sin\phi \cos\phi \, \theta_\rho^2 \, [-S + 2T - B]$$

$$+ \sin\phi \cos\phi \, \phi_\rho^2 \, [-S + T \cos^2\theta + B \sin^2\theta]$$

$$- 2 \cot\theta \, \theta_\rho \, \phi_\rho \, [S \sin^2\phi - T (\sin^2\theta - \cos^2\theta) \cos^2\phi + 2 B \sin^2\theta \cos^2\phi]$$

$$- (\frac{1}{\rho} \phi_\rho + \phi_{\rho\rho}) \, [S \sin^2\phi + T \cos^2\theta \cos^2\phi + B \sin^2\theta \cos^2\phi]$$

$$- \cot\theta \, \theta_z \, \phi_z \, [4 T \sin^2\theta + 2 B (\cos^2\theta - \sin^2\theta)]$$

$$- \phi_{zz} \, [T \sin^2\theta + B \cos^2\theta]$$

$$+ \frac{1}{\rho} \cot\theta \sin\phi \cos\phi \, \theta_\rho \, [S + T(3 \sin^2\theta - \cos^2\theta) - 4 B \sin^2\theta]$$

$$+ \frac{1}{\rho} \sin\phi \, \theta_z \, [\sin^2\theta - 3 \cos^2\theta] \, [B-T]$$

$$+ \cot\theta \sin\phi \cos\phi \, \theta_{\rho\rho} \, [S-T]$$

$$+ \cot\theta \sin\phi \, \theta_\rho \, \theta_z \, (-S + 2T - B]$$

$$+ \sin\phi \, \theta_{\rho z} \, [T-S]$$

$$+ \sin\theta \cos\theta \sin\phi \, \phi_\rho \, \phi_z \, [B-T]$$

$$+ [3 \cos^2\theta - \sin^2\theta] \cos\phi \, [\theta_z \, \phi_\rho + \theta_\rho \, \phi_z] \, [T-B]$$

$$+ 2 \sin\theta \cos\theta \cos\phi \, \phi_{\rho z} \, [T-B]$$

$$+ \frac{1}{\rho} \sin\theta \cos\theta \cos\phi \, \phi_z \, [T-B].$$

$$(III.13)$$

The surface equations to be satisfied at $\rho = 0$ and $\rho = \rho_0$ are

$$0 = \rho \, \theta_\rho \, [S \cos^2\theta \cos^2\phi + T \sin^2\phi + B \sin^2\theta \cos^2\phi]$$

$$+ \sin\theta \cos\theta \, [S \cos^2\phi + T \sin^2\phi]$$

$$+ \rho \sin\theta \cos\theta \sin\phi \cos\phi \, \phi_\rho \, [T - S]$$

$$+ \rho \sin\theta \cos\theta \, \theta_z \, [B - S]$$

$$- \rho \sin^2\theta \sin\phi \, \phi_z \, T$$

$$(III.14)$$

and

$$0 = \rho \sin^2\theta \; \phi_\rho \; [S \sin^2\phi + T \cos^2\theta \cos^2\phi$$
$$+ B \sin^2\theta \cos^2\phi]$$
$$+ \sin^2\theta \sin\phi \cos\phi \; [- S + T \cos^2\theta + B \sin^2\theta]$$
$$+ \rho \sin\theta \cos\theta \sin\phi \cos\phi \; \theta_\rho \; [T - S]$$
$$+ \rho \sin^2\theta \sin\phi \; \theta_z \; S$$
$$+ \rho \sin^3\theta \cos\theta \cos\phi \; \phi_z \; [B - T].$$

(III.15)

At $\rho = 0$ Eq. III.14 implies that

$$\cos\theta \sin\theta = 0 \qquad\qquad (III.16)$$

which means that $\theta = 0$ or $\theta = 90°$. It is easy to show that $\theta = 90°$ corresponds to an infinite energy and therefore must be neglected. Thus one finds

$$\theta = 0 \quad \text{at } \rho = 0 \text{ for all } z. \qquad (III.17)$$

Eq. III.15 is identically satisfied at $\rho = 0$ with $\theta = 0$.

The requirement that θ equals zero for all z at $\rho = 0$ while θ is non-zero for all ρ at $z = 0$ and $z = Z_0$ leads to a contradiction at the points $\rho = 0$, $z = 0$ and $\rho = 0$, $z = Z_0$. To remove this singularity one must relax the surface pinning and/or distort the surface. This problem will be discussed in App. II. For now it is sufficient to say that the extent of the distortion region will be a few molecular lengths

which is much smaller than the region to which attention is being focused.

Along the top and bottom surfaces, the hard pinning has determined the value of θ to be used. Thus

$$\left.\begin{array}{ll} \theta = \theta_{US} & \text{at } z = Z_0 \\ \\ \text{and} \\ \\ \theta = \theta_{LS} & \text{at } z = 0 \end{array}\right\} \quad \text{for all } \rho. \qquad \text{(III.18)}$$

In addition the angle ϕ must satisfy the differential equation

$$0 = \phi_z [T \sin^2\theta + B \cos^2\theta] + \frac{1}{\rho} \sin\theta \cos\theta \sin\phi [B-T]$$

$$- \sin\phi \, \theta_\rho \, T + \sin\theta \cos\theta \cos\phi \, \phi_\rho \, [B-T]$$

$$\text{(III.19)}$$

valid at $z = 0$ and $z = Z_0$ for all ρ.

The problem demands the solution of the pair of coupled non-linear second order partial differential equations, Eqs. III.12 and III.13 everywhere in the bulk subject to Eq. III.17 at $\rho = 0$ and the pair of coupled non-linear first order partial differential equations, Eqs. III.14 and III.15 at $\rho = \rho_0$, as well as the hard pinning equations, Eq. III.18 and the non-linear first order partial differential equation, Eq. III.19 along the top and bottom surfaces. Since Eq. III.15 is satisfied identically at $\rho = 0$, there appears to be no

boundary equation from which ϕ along the axis of symmetry can be determined. This is rectified by requiring that ϕ be analytic at $\rho = 0$.

Two solutions to the ϕ-equation, Eq. III.13, are immediately obvious. These are where ϕ is identically equal to 0 or π everywhere. These satisfy the bulk equations as well as the surface equations, Eqs. III.15 and III.19. If one were to assume that ϕ is a constant, it would follow that only $\phi = 0$ or $\phi = \pi$ works. It is not obvious however, whether there are equilibrium solutions in which ϕ is not constant. It will be shown that for certain relative values of the elastic constants, stable non-zero solutions for ϕ are also possible. By examining Eqs. III.13, III.15, and III.19, it is easily shown that if a stable non-zero solution for ϕ is found, then replacing all ϕ's by $-\phi$ also produces a stable solution with the same set of θ values and the same energy. Thus the number of different equilibrium solutions will always be even. There will always be equilibrium solutions with $\phi = 0$ and $\phi = \pi$ and for a certain range of the elastic constants there might be additional stable pairs that are symmetrical about $\phi = 0$.

III.2 ONE CONSTANT APPROXIMATION

Before attempting to solve the whole problem as encompassed by the rather complicated system of equations given in the previous section, a simplification called the one constant approximation will be briefly discussed. This approximation, sometimes called the isotropic case, consists of assuming that the three elastic constants S, T, and B are equal. This produces a great deal of simplification and corresponds to isotropic exchange in magnetism. Now Eq. III.4b for the energy of the system simplifies to

$$\frac{f}{S} = \sin^2\theta\left[\frac{1}{\rho} + \rho\ \phi_\rho^2 + \rho\ \phi_z^2 - 2\cos\phi\ \theta_z \right.$$
$$\left. + 2\rho\sin\phi\ (\theta_z\ \phi_\rho - \theta_\rho\ \phi_z) + \rho\ \frac{\Delta\chi}{S}\ H^2\right]$$
$$+ \rho\ \theta_\rho^2 + \rho\ \theta_z^2 + 2\sin\theta\ \cos\theta\ \theta_\rho \ .$$

$$(III.20)$$

Is there any configuration of the molecules that might reduce the energy? Most of the terms cost energy since they are squares. For the time being the assumption will be made that ϕ is a constant or only slowly varying. This leaves two terms that are linear. Of these the term $2\sin\theta\cos\theta\ \theta_\rho$ will always be positive since θ will be shown to be a monotonically non-decreasing function of radius. The interesting term is $-2\sin^2\theta\cos\phi\ \theta_z$. This will increase the energy if $\cos\phi\ \theta_z$ is negative but will decrease it if this product is positive.

This procedure represents a technique for reducing the splay energy. It is most easily understood with the help of Fig. III.3. Fig. III.3a shows a top view of a situation in which the projections of the molecules in the horizontal plane are depicted as being in a radial direction. This configuration has a divergence and thus a splay energy associated with it. One can look upon this as a positive source density in any given region if one assigns a physical meaning to the choice of direction of $\hat{n}$. The number of arrows pointing out of a sector with sides along the radial directions is greater than the number pointing in, because of the greater arc length at the greater radius. Figs. III.3b and III.3c show two side views representing what the molecules can do in the z-direction. In Fig. III.3b the value of θ is increasing as one moves in the direction of increasing z while the angle ϕ is constant at 180°. The configuration of the molecules shows a divergence pattern which again corresponds to a positive source density inasmuch as there is a net outward directedness across planes of constant z. This source adds to that due to the splay component from the horizontal plane and the energy is increased. In Fig. III.3c the situation is reversed, the angle θ still increases as one moves to larger z-values but now the angle ϕ is 0 . In this configuration one sees that the apparent source of the splay is negative in that there
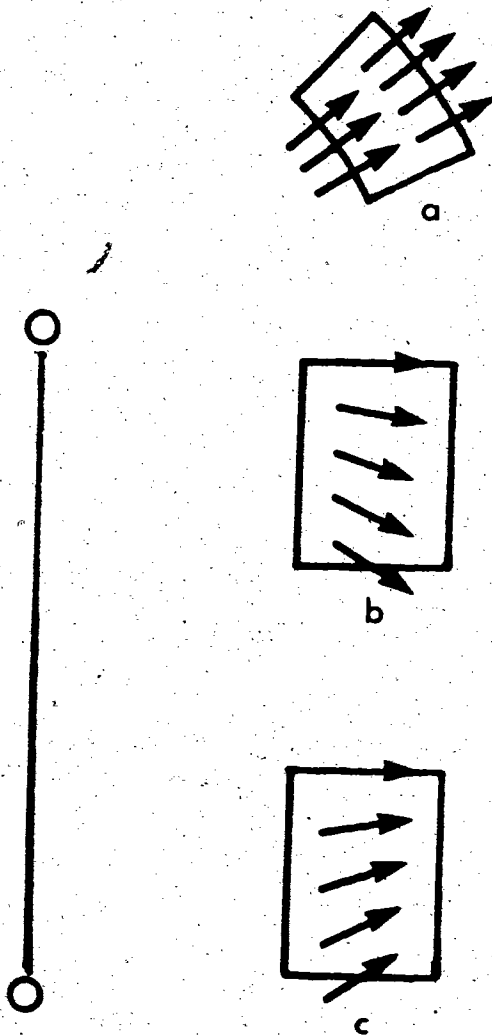
<u>Figure III.3</u>

(a)   Shows the top view of a region in which there is a
positive splay density in the horizontal plane.   In the
vertical plane of this region there can be a positive source
density (b) or   a negative source density (c).   OO is the
axis of symmetry.

is a net inward directedness across planes of constant z. In this case the divergences tend to cancel and the energy is reduced. The axis of symmetry breaks the symmetry between the two configurations, one increase the energy while the other decreases it.

In the one constant approximation the θ-equation in the bulk, Eq. III.12, reduces to

$$\theta_{\rho\rho} + \frac{1}{\rho}\,\theta_\rho + \theta_{zz} = \sin\theta\,\cos\theta\,\left(\frac{1}{\rho^2} + \phi_\rho^{\ 2} + \phi_z^{\ 2} + \frac{\Delta\chi H^2}{S}\right) \tag{III.21}$$

while the ϕ-equation, Eq. III.13, becomes

$$\phi_{\rho\rho} + \frac{1}{\rho}\,\phi_\rho + \phi_{zz} = -\,2\,\cot\theta\,(\theta_\rho\,\phi_\rho + \theta_z\,\phi_z). \tag{III.22}$$

The solutions of these equations must be obtained by computer. The only further simplification results in Eq. III.21 when θ is small. Then one has

$$\theta_{\rho\rho} + \frac{1}{\rho}\,\theta_\rho + \theta_{zz} = \theta\left(\frac{1}{\rho^2} + \phi_\rho^{\ 2} + \phi_z^{\ 2} + \frac{\Delta\chi H^2}{S}\right). \tag{III.23}$$

If the derivatives of ϕ can be neglected compared to $\frac{1}{\rho}$, this equation becomes uncoupled and the solution can be put in the form

$$\theta = \int_A dA\, J_1(A\rho)\left(\begin{array}{l} L_1(A)\,\sinh(\sqrt{A^2 + \Delta\chi\,H^2}\;z) \\ + L_2(A)\,\cosh(\sqrt{A^2 + \Delta\chi\,H^2}\;z) \end{array}\right) \tag{III.24}$$

where J_1 is a Bessel function of order one and the integration
is carried out over the constant of integration A to determine
$L_1(A)$ and $L_2(A)$ so that the boundary conditions are satisfied.
This, in itself, becomes a difficult job. Even with this
form of solution for small θ, the ϕ-equation, Eq. III.22, has
no obvious solutions other than the trivial ones previously
mentioned, namely $\phi \equiv 0$ or π everywhere. The solution for the one
constant approximation will be described in detail later as
a special case of the general solution where the elastic con-
stants can have different relative values.

III.3 THREE CONSTANT CASE

Experimentally it has been determined that the three
elastic constants S, T, and B are not necessarily equal. For
nematics liquids on which the constants have been measured
separately, it appears that generally the bend elastic con-
stant is larger than the splay constant, while the twist
constant is the smallest. Thus every term in Eqs. III.4,
III.12, and III.13 is important. Obviously, one would not
expect to be able to find any analytic solutions to the bulk
equations.

Particular attention will now be paid to the energy
equation to see if one can guess the nature of possible solu-
tions. First of all the case for large ρ will be considered.

One can write

$$\theta(\rho, z) = \theta_O(z) + \frac{a(z)}{\rho} + \frac{b(z)}{\rho^2} + \dots$$

$$\text{(III.25a)}$$

and

$$\phi(\rho, z) = \phi_O(z) + \frac{c(z)}{\rho} + \frac{d(z)}{\rho^2} + \dots$$

$$\text{(III.25b)}$$

where $\theta_O(z)$ and $\phi_O(z)$ are the values of θ and ϕ for infinite ρ and where the parameters a, b, c, d, etc., are functions of z but are independent of ρ. Differentiating Eqs. III.25 with respect to ρ produces the first and second derivatives of θ and ϕ which are then put into the energy expression, Eq. III.4b. Keeping only the highest two orders in ρ in the energy results in the expression

$$
\begin{aligned}
f = \rho &\left[\theta_{oz}^2 \ [S \sin^2\theta_O + B \cos^2\theta_O] \right. \\
&\left. + \ \sin^2\theta_O \ \phi_{oz}^2 \ [T \sin^2\theta_O + B \cos^2\theta_O] \right. \\
&\left. + \ \sin^2\theta_O \ \Delta\chi \ H^2 \right] \\
+ 2 &\left[\sin\theta_O \cos\theta_O \ \theta_{oz}^2 \ [S - B] \ a \right. \\
&\left. + \ \theta_{oz} \ a_z \ [S \sin^2\theta_O + B \cos^2\theta_O] \right. \\
&\left. + \ [\sin\theta_O \cos\theta_O \ a \ \phi_{oz}^2 + \ \sin^2\theta_O \ \phi_{oz} \ c_z] \right. \\
&\left. \qquad\qquad \times \ [T \sin^2\theta_O + B \cos^2\theta_O] \right. \\
&\left. + \ \sin^3\theta_O \ \cos\theta_O \ \phi_{oz}^2 [T - B] \ a \right. \\
&\left. - \ \sin^2\theta_O \ \cos\phi_O \ \theta_{oz} \ S \right. \\
&\left. + \ \sin^3\theta_O \ \cos\theta_O \ \sin\phi_O \ \phi_{oz} \ [B - T] \right. \\
&\left. + \ \sin\theta_O \ \cos\theta_O \ a \ \Delta\chi \ H^2 \right]
\end{aligned}
$$

$$\text{(III.26)}$$

The highest order term is independent of the angle ϕ_o. The energy could be reduced if θ_{oz}, ϕ_{oz}, and θ_o could all be reduced to zero, however, the boundary conditions requiring fixed values of θ on the top and bottom surfaces will generally not allow θ_o and θ_{oz} to be zero. However, since ϕ_o is undetermined one can minimize the energy by making ϕ_{oz} equal to zero for very large ρ.

The second highest order term in the energy then reduces to

$$2 \left[\begin{array}{l} \sin\theta_o \cos\theta_o \; \theta_{oz}^2 \; a \; [S - B] \\ + \; \theta_{oz} \; a_z \; [S \sin^2\theta_o + B \cos^2\theta_o] \\ - \sin^2\theta_o \; \cos\phi_o \; \theta_{oz} \; S \\ + \sin\theta_o \; \cos\theta_o \; a \; \Delta\chi \; H^2 \end{array} \right] .$$

$$(III.27)$$

In this expression the angle ϕ occurs only once, in the second to last term. ϕ_o will be picked so as to minimize the energy which is done by making $\cos\phi_o \; \theta_{oz}$ a positive quantity. If θ_{oz} is positive, the energy requires that ϕ should be 0 , while if θ_{oz} is negative, ϕ_o should be 180°. This produces a reduction in the splay energy as discussed in the previous section. Thus at large ρ, the molecules should be close to radial. For large ρ the θ-equation in the bulk, Eq. III.12, keeping only the highest order terms, becomes

$$\theta_{ozz} [S \sin^2\theta_o + B \cos^2\theta_o]$$
$$= \sin\theta_o \; \cos\theta_o \; [\theta_{oz}^2 \; [B - S] + \Delta\chi \; H^2] .$$

$$(III.28)$$

This equation is useful for describing the behavior of the droplet far from the axis of symmetry.

The ϕ-equation in the bulk, Eq. III.13, is satisfied identically. It produces the equation

$$\phi_{ozz} = 0 \qquad\qquad (III.29)$$

which is consistent with $\phi_{oz} = 0$ for all z.

Thus on energy considerations one expects to find that for large ρ the molecules have a θ-dependence described by Eq. III.28, and a value of ϕ around 0 or 180° depending on whether θ_z is a positive or negative number.

At the other extreme, for small ρ, the situation is much less clear. The behavior of a few terms from the energy expression, Eq. III.4, will be examined. The question to be posed is what value of ϕ would the energy prefer if ϕ were a constant or only slowly varying. The terms to be considered are those which are thought to be the most important and which lend themselves to analysis without too much difficulty. The object is to indicate a possible solution, the exact nature of which will be determined later. The terms are in the integrand of Eq. III.4. The analysis will first be done for large θ (~90°). The first term is

$$\frac{1}{\rho} \sin^2\theta [S \cos^2\phi + T \cos^2\theta \sin^2\phi + B \sin^2\theta \sin^2\phi] .$$

$$(III.30a)$$

When $\theta \sim 90°$ this becomes

$$\frac{1}{\rho} [S \cos^2\phi + B \sin^2\phi].$$

(III.30b)

The value of ϕ which lowers the energy depends on which of the elastic constants S or B is smaller. If $S < B$, ϕ should be 0 or 180° while if $S > B$, ϕ should be 90° or 270°.

The second term for $\theta \sim 90°$ becomes

$$\rho \theta_\rho^2 [T \sin^2\phi + B \cos^2\phi]$$

(III.31)

which prefers $\phi = 90°$ or 270° if $T < B$ and 0 or 180° if $T > B$.

The third and fifth terms are negligible since it was assumed that the derivatives of ϕ are small. The fourth term has no ϕ preference.

The sixth term for $\theta = 90°$ vanishes but for θ slightly less than 90° becomes

$$2 \cos\theta \; \theta_\rho [S \cos^2\phi + T \sin^2\phi]$$

(III.32)

which, since θ_ρ will be shown to be positive, prefers $\phi = 0$ or 180° for $T > S$ and $\phi = 90°$ or 270° for $T < S$.

The seventh term will be neglected. The eighth term

$$- 2 \sin^2\theta \cos\phi \; \theta_z S$$

(III.33)

depends on the value of θ_z before the preferred angle ϕ can be determined. If θ_z is positive, ϕ should be 0 while if θ_z is negative, ϕ should be 180°.

The remaining terms are more complicated, involving the products of too many functions to be analyzed in such a crude fashion.

What has been found for large θ (~90°) is that if the twist elastic constant is smaller than the splay and bend constants, the second and sixth terms of the energy prefer ϕ to be 90° or 270° while if T is greater than S and B ϕ should be 0 or 180°. The preference of the first term depends on the relative size of S and B while the seventh term wants ϕ to be 0 or 180° depending on the sign of θ_z. Because of the contradictory demands of the terms examined no general conclusion can be reached as to a preferred value for ϕ.

The nature of the energy equation at small ρ for small θ will now be examined. From Eq. III.4b when θ is small the first, second, and sixth terms can be combined to give

$$\frac{1}{\rho}(\theta + \rho\,\theta_0)^2\,[S\cos^2\phi + T\sin^2\phi].$$

(III.34)

These terms all prefer $\phi = 90°$ or 270° if T < S and $\phi = 0$ or 180° if T > S.

The third, fifth, and seventh terms are assumed to be small since they contain derivatives of ϕ while the eighth term has to wait until θ_z is determined before a value of ϕ can be picked. Again the rest of the terms are too complicated to be analyzed in this fashion. However, if θ, when small, still has some of the Bessel function character found in the one constant approximation for small ρ one can write

$$\theta = A\rho.$$

(III.35)

In this case, the terms in Eq. III.34 are of order ρ while the last seven terms in Eq. III.4 are of order ρ^2 or smaller and thus can be neglected. This argument would also apply to the third, fifth, and seventh terms which were neglected previously on the assumption that ϕ was only slowly varying.

From this rather simple-minded analysis one can see the possibility of an interesting situation arising if the twist elastic constant is less than the splay and bend constants since then there is reason to suspect the preference for having $\phi = 90°$ or $270°$ for small ρ while for large ρ it was shown that ϕ should be 0 or $180°$ depending on the way in which θ varies with z. This configuration would be one in which the projections of the molecules in the horizontal plane rotates from being circumferential for small radii to being radial for large radii.

Analysis of this fashion on the θ- and ϕ-bulk equations for small ρ are uninstructive and will not be attempted here.

The handling of the equations by computer will be described in App. III. The results of the calculations will be presented and discussed in Ch. IV.

CHAPTER IV

IV.1 CHOICE OF PARAMETERS

The first set of calculations were carried out using appropriate parameters for MBBA. The values of S, T, and B show large uncertainties because of the extrapolation procedures required to obtain them and because of variations in the purity of the material used. The elastic constants also show strong dependences on temperature.

The computations to be presented in Ch. IV.2 were done using Haller's (Ha-72a) measurements since his values are typical and he measured all three elastic constants. He has found that S/B = .8 and T/B = .5 at room temperature. In Ch. IV.3 the effect of different relative values of the elastic constants will be discussed.

The hard pinning angle of MBBA molecules at an air interface has been measured by Prost (Pr-71) who found $\theta_{SUR}^{air} = 12°$ by fitting the data found from birefringence measurements, and by Bouchiat (Bo-71) who observed $\theta_{SUR}^{air} = 10°-20°$ depending on the temperature. His measurements were made by determining the amount of light reflected from the liquid crystal-air interface. For the purposes of this calculation the value of 15° was assumed to be the hard pinning angle at the air interface.

The MBBA molecule has the polarizable CH = N bond located
at the center of the molecule. Because water is a highly
polarizable medium the MBBA should like to get its dipole
as close to the water as possible which suggests that the
molecules would like to lie parallel to a water substrate,
i.e. θ_{SUR}^{water} should be 90°. This condition is confirmed
by comparison of the observed optical fringe patterns with
the computer calculations particularly in magnetic fields.

IV.2   RESULTS FOR S/B = .8 AND T/B = .5

Haller's (Ha-72a) values for the elastic constants at
room temperature were used to calculate the equilibrium con-
figurations of the molecules in the cylindrically symmetric
region described in Ch. III. The height of the cylinder,
Z_o, was taken to be 19 units, while three values for the
radius ρ_o were used: 40, 80, and 160 units. As will be
shown in App. III, the important parameter is the aspect
ratio, ρ_o/Z_o, rather than the absolute size since solutions
of different sized cylinders with the same aspect ratio
scale linearly. The reason for using the cylinders with
different aspect ratios is to find a solution in which the
central region of the droplet, the region of the rotated
cross, is independent of the radius of the cylinder. It
is found that for ρ_o equal 80 and 160 units the configura-
tions for radii less than 40 units agree within 1% while

for ρ_o equal 40 units the agreement for radii less than 20 units is a few percent.

With $\theta_{LS} = 15°$ and $\theta_{US} = 90°$, corresponding to having the air at the lower surface and the water at the upper surface of the liquid crystal droplet, as in Fig. II.1a, the two twisted solutions and that normal solution with $\phi = 0$ everywhere were found to be close in energy while the normal solution with $\phi = \pi$ everywhere was found to be much higher in energy (a factor of 2 for $\rho_o = 80$ units) and to be an unstable equilibrium. The reason the $\phi = 0$ normal configuration is lower in energy than the $\phi = \pi$ configuration is because with $\theta_{LS} = 15°$ and $\theta_{US} = 90°$ for all but small radii θ_z is a positive number. After Eq. III.27 it was shown that for large radii the energy would be reduced if the quantity $\cos\phi \; \theta_z$ is positive. With a positive θ_z this requires that the angle ϕ be zero. If the water and air surfaces were interchanged, as in Fig. II.1b, the $\phi = \pi$ solution would have been lower in energy than the $\phi = 0$ one and the twisted solutions would have their azimuthal angles augmented by π. The following discussion will apply to the geometry of Fig. II.1a and therefore the high energy $\phi = \pi$ solution will generally be ignored. The normal configuration will refer to the $\phi = 0$ solution.

The computer outputs for $\rho_o = 80$ units are contained in App. IV. In Fig. IV.1 are shown some representative slices of the stable twisted configuration ($\phi \neq 0$). Fig. IV.2 shows some representative slices of the normal or untwisted equilibrium configuration (ϕ is zero everywhere). Fig. IV.1 really represents two solutions because as explained in Ch. III replacing ϕ by $-\phi$ also produces a stable configuration. The molecules in the view about the axis of symmetry that are within 7° of the cross of the crossed polarizers are indicated with crosses. One can see a brush pattern very close to that observed in the droplets between crossed polarizers.

The θ solutions in the various configurations differ by only a few percent, the largest discrepancy being for small radii. θ monotonically increases from the bottom to the top surfaces over the whole drop except for radii less than six units where θ decreases from both surfaces towards the interior. Along the axis of symmetry the average value of ϕ for the twisted configuration is about 1.7 while at the outer edge of the 80 unit cylinder ϕ has decreased to .06 radians. This has the features predicted in Ch. III for the case when T is less than S and B: for small radii ϕ is of the order of 90° while for larger radii ϕ approaches zero. The energy of
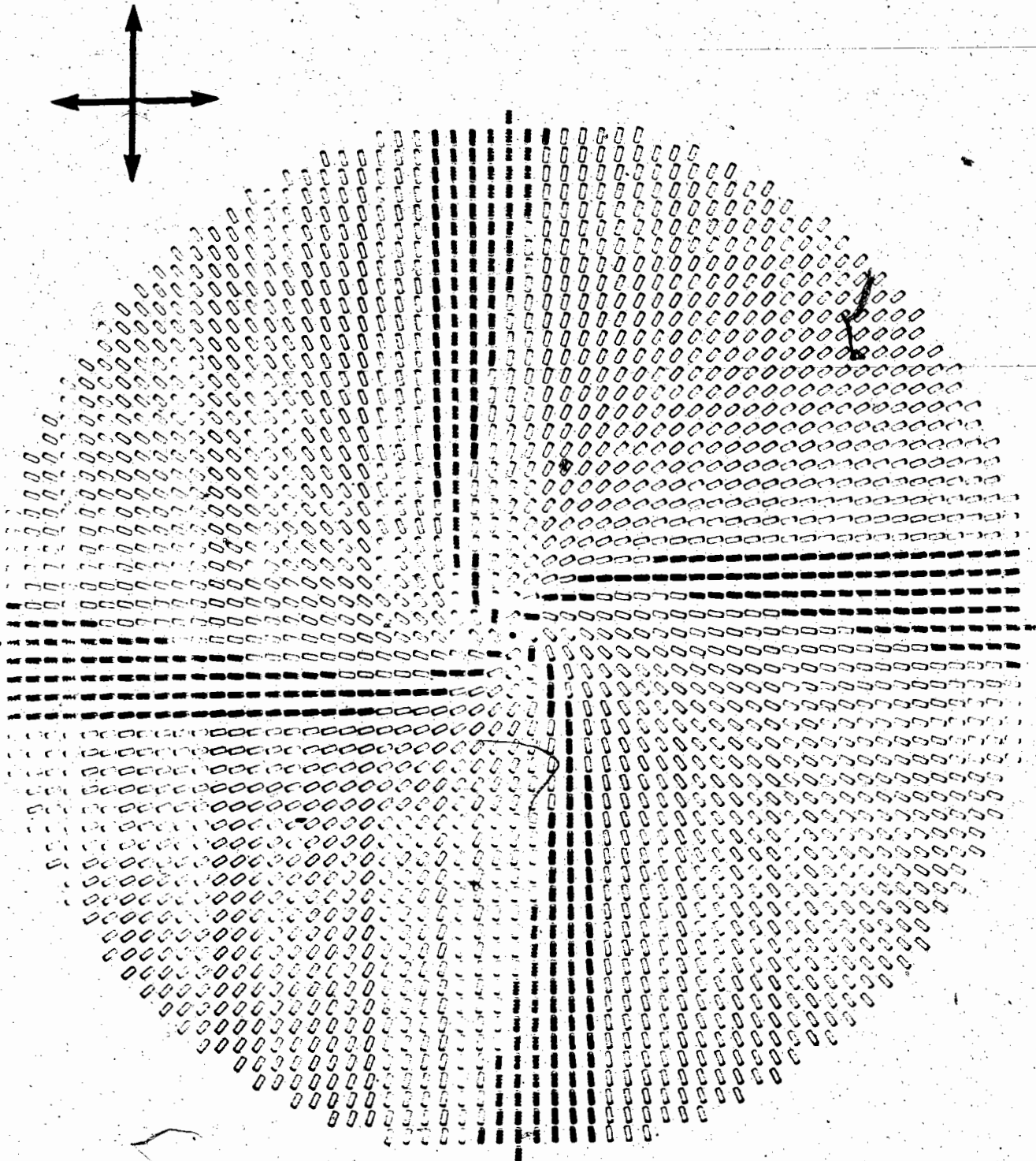
Figure IV.1a

Top view of a layer 2 units from the water surface of a
19 unit thick MBBA droplet for the twisted configuration
with S/B = .8 and T/B = .5 from ρ = 0 to ρ = 112 units.
The inserted crosses indicate those molecules whose pro-
jections in a plane perpendicular to the axis of symmetry
lie within 7° of either the polarizer of the analyzer axis.
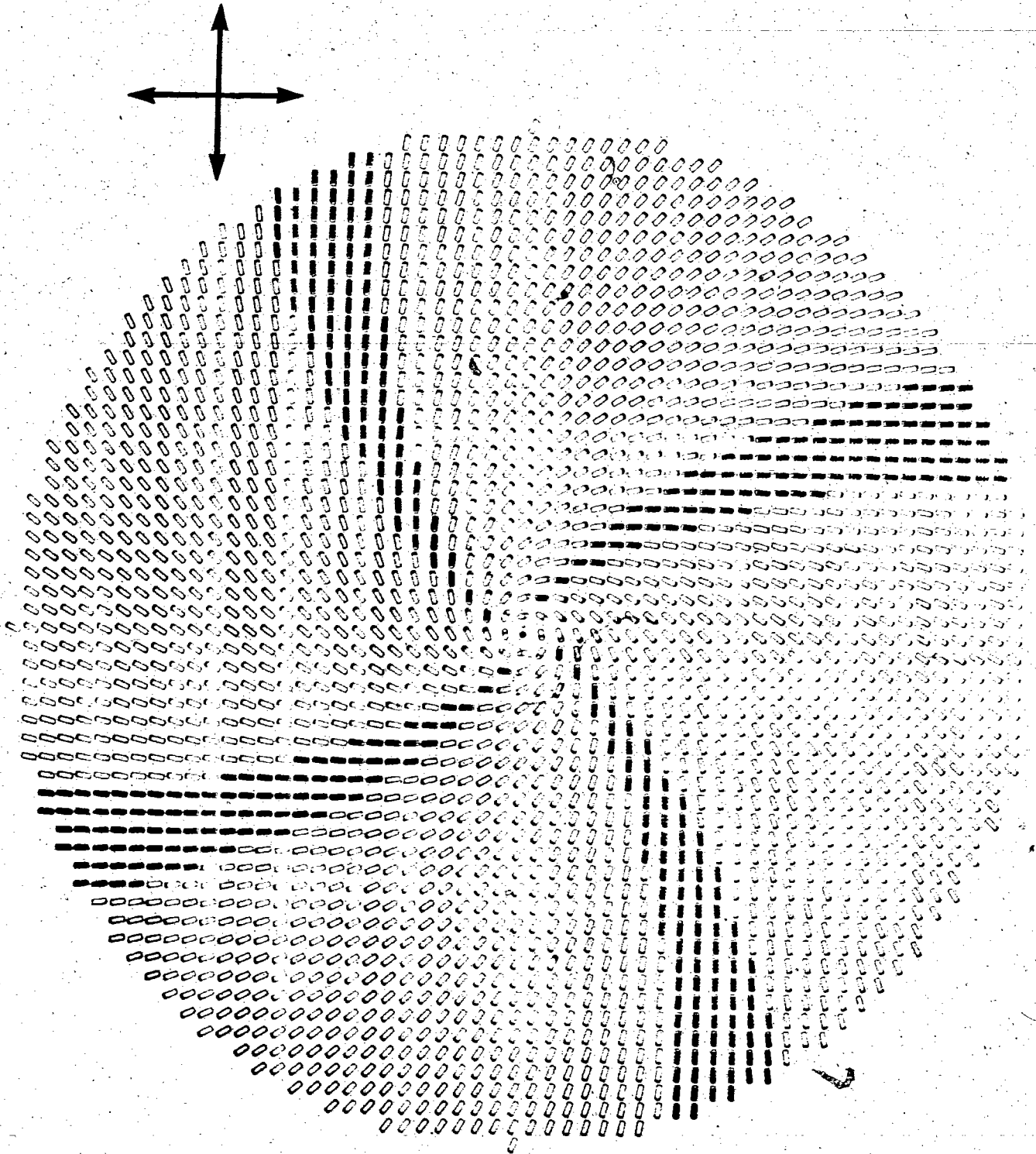
Figure IV.1b

Magnification of the central region of (a) from $\rho = 0$
to $\rho = 28$ units.
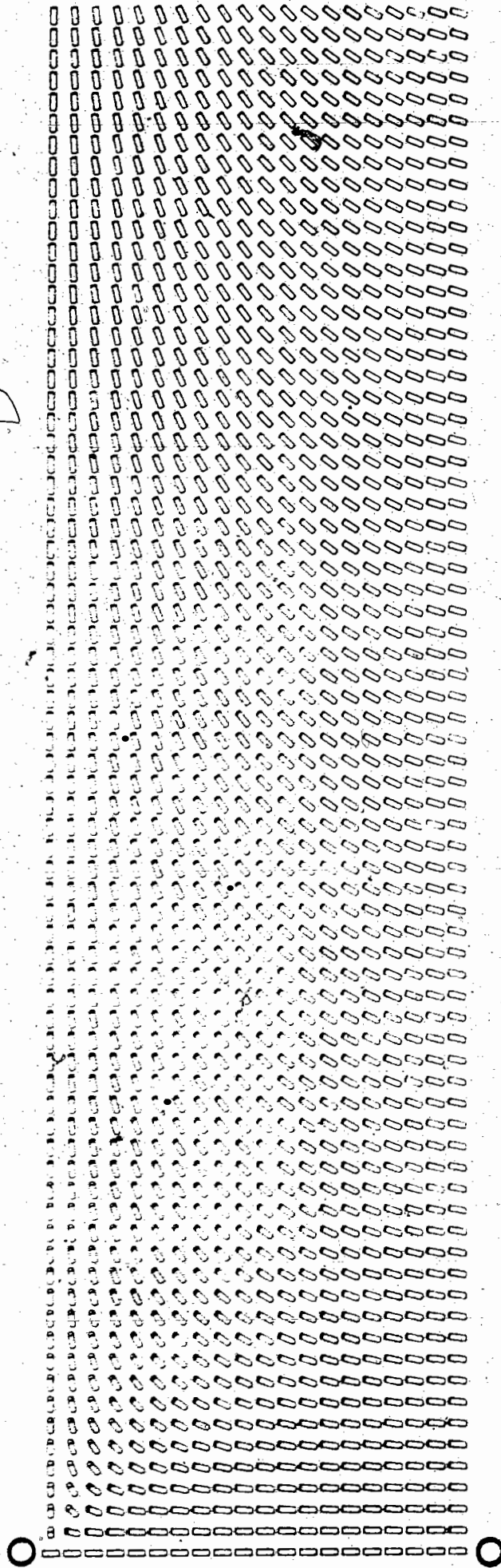
Figure IV.1c

Side view of the twisted solution of a 19 unit thick MBBA droplet
with S/B = .8 and T/B = .5 from ρ= 0 to ρ= 80 units. The water
surface is at the top and the air surface is at the bottom.
OO is the axis of symmetry.
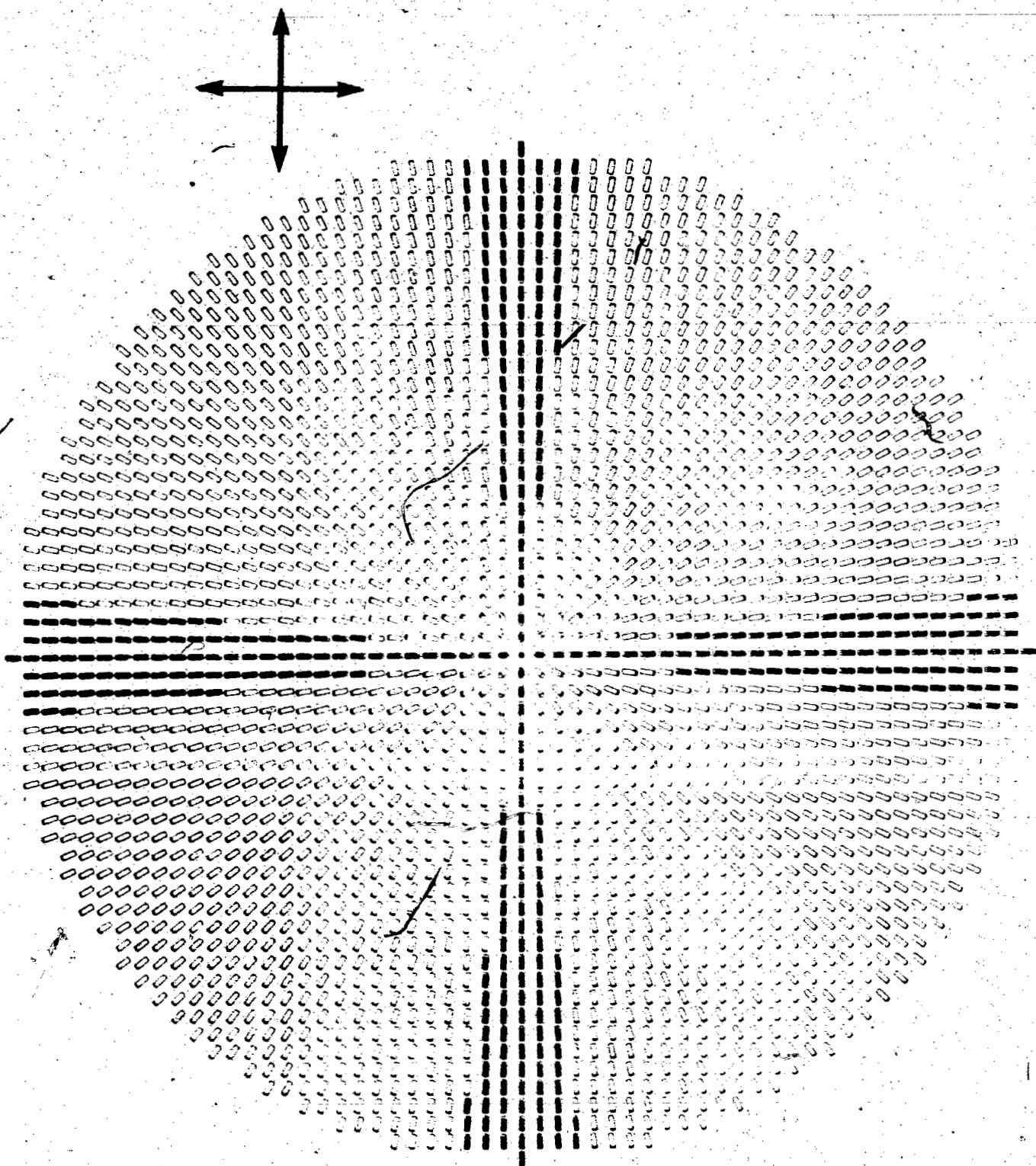
Figure IV.2a

Top view of a layer 2 units from the water surface of a
19 unit thick MBBA droplet for the normal configuration
with S/B = .8 and T/B = .5 from ρ = 0 to ρ = 28 units.
The inserted crosses indicate those molecules whose pro-
jections in a plane perpendicular to the symmetry axis
lie within 7° of either the polarizer or the analyzer axis.
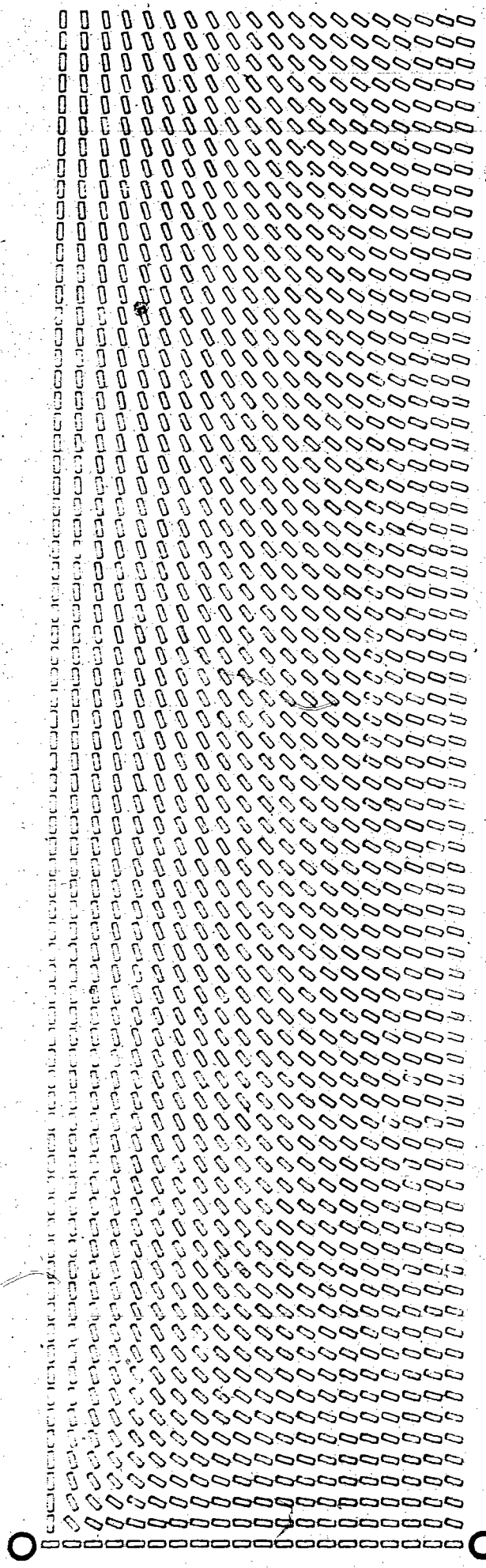
Figure IV.2b

Side view of the normal solution of a 19 unit thick MBBA droplet with S/B = .8 and T/B = .5 from ρ = 0 to ρ = 80 units. The water surface is at the top and the air surface is at the bottom. OO is the axis of symmetry.

the twisted configuration is slightly smaller than the energy of the normal configuration.

The energy differences between the twisted and the normal configurations as a function of ρ_0 for a 19 unit high cylinder in units $\pi B \times$ the unit of length are:

$$
\begin{aligned}
\Delta E &= 1.8 && \text{for } \rho_0 = 40 \\
&= 3.1 && \text{for } \rho_0 = 80 && \text{(IV.1)} \\
&= 3.8 && \text{for } \rho_0 = 160 \ .
\end{aligned}
$$

This is changing approximately exponentially so that for an infinite drop ΔE would be about 4.2. If the unit of length is microns and if $B = .8$ dynes, the energy difference for an infinite drop would be 10^{-9} ergs. The question of whether the normal configuration is truly stable has not been answered. However, considering the small difference in energy and the observed existence of the normal configuration, this state must be at least a metastable solution.

Examination of the computer outputs in App. IV shows that θ increases as the radius increases until one gets within 30 or 40 units of ρ_0 where θ peaks and then starts to slowly decrease. This decrease is an artifact caused by the application of the θ-boundary condition. In an infinite cylinder θ should increase and level off at the values of θ predicted by the solution of

the one-dimensional equation, Eq. III.28. These values have been calculated and agree within 1% with the values of θ at $\rho = 40$ obtained in the solution with $\rho_0 = 80$. This is further evidence that $\rho_0 = 80$ is equivalent to an infinite drop at least as far as the central region of the droplet is concerned.

Examination of the computer outputs for $\rho_0 = 80$ units, Tables 3 and 4 in App. IV, shows that the twisted solution saves energy for small ρ everywhere except along the top surface where θ is large. This can be explained by looking at the energy expressions presented in Ch. III. Of the terms considered, only those in Eq. III.30a and III.33 indicate a higher energy when ϕ is 90° for the relative values of the elastic constants used. Eq. III.33 is always unhappy about having $\phi = 90°$. However, since for small radii θ_z changes sign from the bottom to the top surfaces, this term prefers to have $\phi \sim 180°$ near the bottom surface and $\phi \sim 0$ near the top surface. If changes in ϕ with height were too expensive some intermediate values of ϕ might be preferred. Eq. III.30a shows a cross-over point which favors $\phi = 90°$ if θ is small enough as indicated in Eq. III.34. The value of θ at which Eq. III.30a starts to favor the twisted configuration can be found by equating its value for $\phi = 0$ and for $\phi = 90°$.

This gives

$$S = T \cos^2\theta + B \sin^2\theta \qquad\qquad \text{(IV.2a)}$$

which reduces to

$$\sin^2\theta = \frac{(S-T)}{(B-T)} \qquad\qquad \text{(IV.2b)}$$

which for the elastic constants used gives a critical angle
of 50° for θ. Examination of the computer outputs verify
that near the axis of symmetry for θ less than about 50°
the energy density of the twisted configuration is less
than the normal one while for θ larger than about 50° it is
larger. The reason that ϕ stays around 90° would seem to be
because for most of the droplet at small radii, θ is less
than 50°, which favors $\phi \sim 90°$, and changing ϕ with z costs
too much energy. This can be seen by examining those terms
in the energy equation, Eq. III.4b, which contain ϕ_z. The
fifth term contains ϕ_z^2 and is always positive. The ninth
term could save energy with a negative ϕ_z but it contains
$\cos\theta$ which is small for θ around 90° and so the saving is
small. The same applies to the fourteenth term while the
thirteenth term costs energy for a negative ϕ_z. The result
of this is that ϕ should show little variation with z,
a fact that is verified by the computer outputs.

The importance of the splay cancellation is seen most clearly from the doubling of the energy of the $\phi = \pi$ normal configuration compared to the $\phi = 0$ configuration in the geometry of Fig.II.1a for $\rho_o = 80$. The saving in energy can be seen also by comparing the drops with cylindrical symmetry to equal areas of the outer regions of an infinitely large drop. For a 19 unit high cylinder the average energies per unit area in units of $\pi B/$unit of length as a function of the radius of the cylinder are:

$$E/\text{area} = .063 \qquad \text{for} \quad \rho_o = 40$$
$$= .062 \qquad\qquad\qquad = 80$$
$$= .068 \qquad\qquad\qquad = 160$$
$$= .071 \qquad\qquad\qquad = \infty$$

$$(IV.3)$$

This saving is large compared to the additional saving arising from the handedness of the solutions ($\Delta E/\text{area} \sim .0005$ in the same units for $\rho_o = 80$). That there is a mininum at $\rho_o/Z_o \sim 4$ can be seen as a direct result of the splay cancellation.

The splay energy is derived in App. I and is given by Eq. A I.3. Neglecting the radial derivatives, the splay energy is

$$\sin^2\theta \; (\frac{\cos\phi}{\rho} - \theta_z)^2 \; .$$

$$(IV.4)$$

This can be made zero by requiring

$$\frac{\cos\phi}{\rho} = \theta_z \quad .$$

$$(IV.5)$$

Away from the center of the drop θ changes approximately

uniformly from θ_{LS} at the lower surface to θ_{US} at the upper

surface. θ_z is then approximated by

$$\theta_z = \frac{\theta_{US} - \theta_{LS}}{Z_0}$$

which becomes $\sim .07$ for the values used in these calcula-

tions. As $\cos\phi$ cannot exceed unity the radius beyond which

splay cancellation can no longer be fully effective is

about 15 units. Examination of the energy densities in

the computer outputs show that for radii around 15-20 units,

the energy density does go through a minimum. This suggests

that in a large medium it might be possible to reduce the

total energy by producing many small regions in which there

is cylindrical symmetry. For MBBA between air and water

the centers of these regions would be separated by distances

of the order of $8Z_0$. Thus a sample with a regular array of

disclinations might have a lower energy than one with trans-

lational invariance. These regions would be +1 point dis-

clinations. They must be accompanied by the appropriate

number of -1 point disclinations. The calculation given

here is probably an excellent guide for estimating the energy

of the +1 point disclination in an array, but for the accom-

panying -1 point diclination the present calculation is

only roughly applicable inasmuch as the latter lack cy-

lindrical symmetry.

- It is well known that liquid crystal samples usually

contain many disclinations. These are usually blamed on

impurities and imperfections, but maybe disclinations

are an intrinsic property of the liquid crystal itself

when subjected to conflicting boundary conditions.

IV.3 EFFECTS OF DIFFERENT ELASTIC CONSTANTS

Using Haller's (Ha-72a) values for the elastic constants

of MBBA, the variational calculation performed in Ch.III has

predicted the existence of the three equilibrium configura-

tions of almost equal energy discussed in the previous sec-

tion. The effect on these configurations of varying the elastic

constants will now be discussed.

The important criterion for getting the twisted configu-

ration is believed to be the fact that the twist elastic

constant is smaller than the splay elastic constant. This

is shown by first using the one constant approximation,

discussed in Ch. III.2, in which all the elastic constants

are put equal. In this case, the only stable configuration

is the normal one. Then different sets of values for

S/B and T/B were assumed, as indicated in Fig. IV.3. Those

which have a stable twisted configuration are indicated by

crosses while circles show those in which only the normal

configuration is stable. These results prove that the
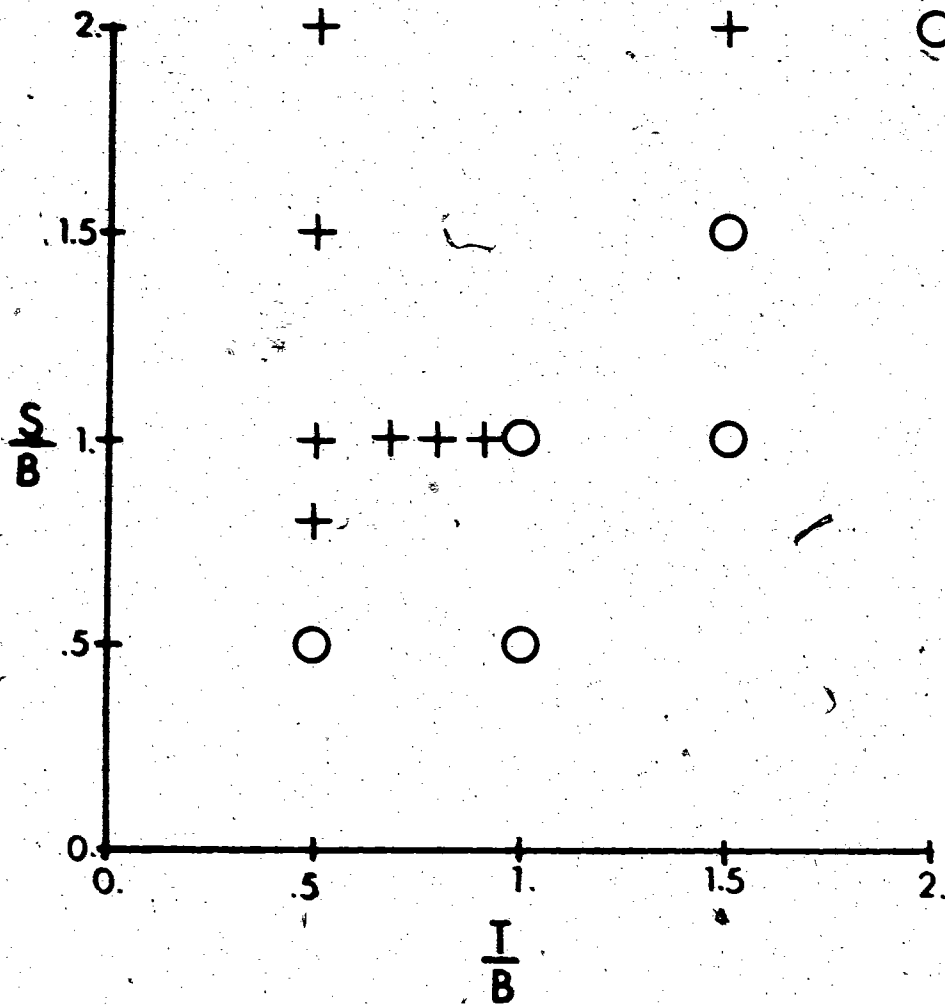
Figure IV.3

Phase diagram for the twisted configuration. A stable
twisted phase (x) occurs for T/S < 1.   For T/S > 1 only
the normal phase (o) is stable.

twisted configuration is stable only when the twist elastic
constant is less than the splay elastic constant. The calcu-
lations indicate that the transition is likely second order.
The twist-like configurations for $S/B = 1$ and $T/B = .5$, $.7$,
$.8$, and $.9$, are shown in Figs. IV.4. The variation of φ at
$\rho = 4$ units goes as $(T - .93S)^{1/3}$ for these four configurations.

As the liquid crystal becomes less pure, its transition
temperature to the isotropic state decreases. Haller (Ha-72a)
has shown experimentally, that as the temperature of the sample
approaches the transition temperature, the ratio T/S approaches
unity. Therefore differences in purity between droplets might
explain the fact that not all twisted configurations observed
in the microscope display the same amount of rotation of the
central cross. This is further confirmed by the observation
that as time goes on, and the droplets presumably become less
pure, the twisted crosses become less rotated. After a long
time on a water substrate, the crosses become almost straight.
The drops also show less optical retardation which is another
indication that the impurities are suppressing the nematic
ordering.

IV.4 EFFECTS OF A MAGNETIC FIELD

A magnetic field applied along the axis of symmetry of
the droplets generally does not distort the symmetry. Because
the molecules show a preference to align with the magnetic
field (anisotropic diamagnetism) the equilibrium configuration
should vary with the strength of the applied field. This
effect is most easily seen by the change of the fringe pattern

T/B = .5

T/B = .7

T/B = .8

T/B = .9
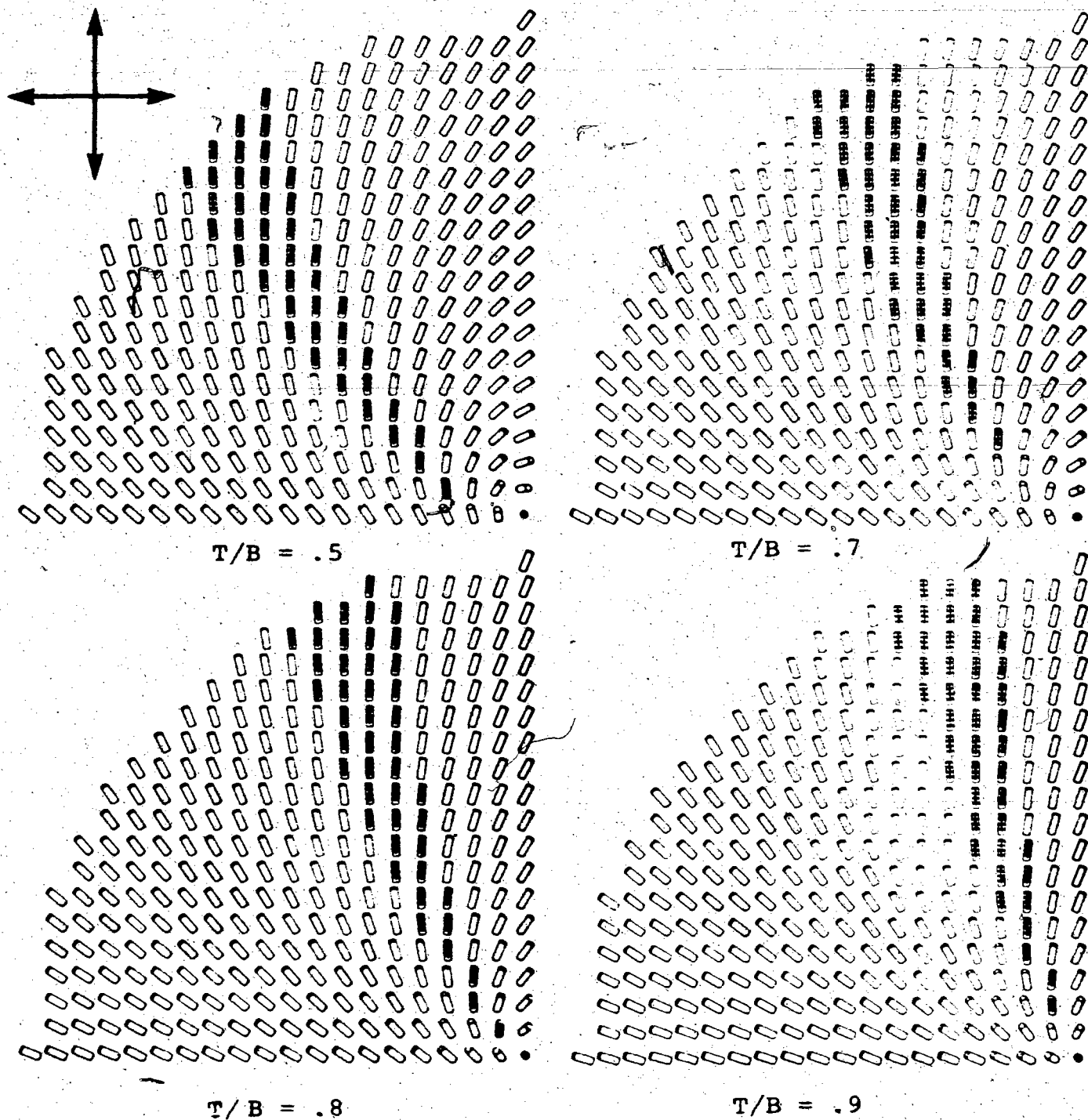
Figure IV.4

Top view of a layer 2 units from the water surface of a 19
unit thick MBBA droplet for the twisted configuration with
S/B = 1 and T/B = .5, .7, .8, and .9 from ∂ = 0 to ∂ = 28
units. The inserted crosses indicate those molecules whose
projections in a plane perpendicular to the symmetry axis
lie within 7° of the polarizer of the analyzer axis.

as described in Ch. II.

Haller (Ha-72a) has measured the diamagnetic anisotropy
for MBBA at room temperature obtaining the value $\Delta\chi/B = .0015$
$\mu m^{-2} kG^{-2}$. As this introduces a unit of length one must now
assume a definite size for the droplets. Thus each unit
of length previously mentioned now becomes a micron.

With the magnetic field applied parallel to the axis of
symmetry of the 19 micron high cylinder the equilibrium con-
figurations for H < 3 kG are easily obtained from the H = 0
solutions. There is a general decrease in the θ values and
in the twisted solution there is an increase in the ϕ values.
The decrease in θ is caused by the desire of the molecules
to become more parallel to the magnetic field because of the
anisotropic diamagnetism. The increase in ϕ is brought about
because the large θ region, which is unhappy with $\phi \sim 90°$,
has become smaller.

When the magnetic field is increased above 3 kG , the
nature of the twisted solutions change. This is a result of
the fact that for large radii θ is no longer a monotonically
increasing function from the bottom to the top surfaces.
For H = 10 kG one finds a solution that is almost stable
in which the values of θ far from the surfaces are close to
zero while the ϕ values are somewhat larger than in the zero
field case. Letting the computer run longer produces a second
solution that is considerably different. The most radical
change is that at large radii near the bottom surface of the

drop ϕ has rotated from being close to 0 to being close to 180°. In effect the magnetic field has divided the droplet into two almost independent regions. In the top part of the droplet the θ values decrease from the top surface and ϕ varies from being of the order of 90° for small radii to about 0 for larger radii. In the bottom region θ decreases from the bottom surface and ϕ varies from being of the order of 90° for small radii to 180° for larger radii. The two regions are joined by a narrow layer in which for large radii ϕ changes very rapidly from around 180° to around 0 with θ very close to zero. The fact that the large changes in ϕ occur at small values of θ means that not much energy is involved in the transition region despite the large ϕ_z.

The reason for the changeover is once again to save splay energy. It was shown after Eq. III.27 that for large radii the angle ϕ was picked so as to ensure that the quantity $\cos\phi \ \theta_z$ was positive. With an applied magnetic field, near the bottom surface θ_z has become negative which implies that ϕ should be 180° while in the upper region of the droplet θ_z is still positive which wants ϕ to be 0 . The two regions must be connected by a region in which ϕ changes rapidly which is most economically done when θ is small. The driving force for the $\phi = 180°$ configuration over the $\phi = 0$ configuration along the bottom surface is very small, in fact the computer calculation suggests that the solutions

are probably separated by a very small energy barrier. Thus the easiest way for the 180° configuration to develop from the 0 configuration may be through the nucleation of small regions. The bubbles that are sometimes formed might be regions of the 180° configuration in the 0 configuration. What one observes may be the domain walls separating these two regions. If the magnetic field were left on long enough the bubbles should merge to produce the uniform 180° region. There was an indication of this happening in the droplets observed, but unfortunately this could not be followed to its conclusion because of the magnet overheating in spite of the water cooling. When the magnetic field is reduced, the $\phi = 180°$ solution becomes unstable and the bubbles shrink producing the low field $\phi = 0$ configuration. The characteristic time for the growth or shrinking of these regions is of the order of minutes which is an indication of how small the difference in energy is between these two solutions.

The large radius one-dimensional equation derived in Ch. III, Eq. III.28, can be solved in regions in which ϕ is not changing and predicts the values of $\theta(z)$ as a function of magnetic field. These values agree within .1% with those obtained for large radii for the full two-dimensional calculations for the solutions when $\rho_0 = 160$ microns and $\phi \sim 0$. This simplified calculation will be used in Ch.V in determining the dependence of the fringe pattern on the magnetic field.

CHAPTER V

V.1 INTRODUCTION TO THE OPTICS CALCULATION

In Ch. IV the molecular configurations obtained by
minimizing the energy of a cylindrically symmetric region
of a nematic liquid crystal were presented in Figs. IV.1
and IV.2. Also indicated in these figures by the inserted
crosses are those molecules which lie within a small angle
($\sim 7°$) of the polarizer or the analyzer axis. If this one
layer was representative of the whole sample, the light
passing through the region of the "crossed" molecules would
be either pure e- or pure o-rays and therefore the polariza-
tion would not change and the light would be absorbed by the
analyzer as explained in Ch. II. These patterns have a
close resemblance to those observed in MBBA droplets. Since
ϕ is virtually independent of z, this cross-section is repre-
sentative of the whole sample. It is mainly the optical
thickness which is affected by the z-dependence of θ. The
nature of the fringe pattern would depend on the thickness
of the droplet, the wavelength of the incident light, and
the birefringence of the light produced by the material com-
posing the droplet. The nature of the brush pattern, however,
is approximately independent of these effects, but not com-
pletely.

To find the exact optical pattern that would be produced
by these molecular configurations requires the solution of

Maxwell's equations in a medium with a continually varying optic axis. Chou (Ch-72) has presented the solution of Maxwell's equations in a region with translational invariance in the horizontal plane and where the molecules were constrained to lie in the horizontal plane. His calculation will be expanded to allow the molecules complete freedom in their orientations. It would be desirable to relax the constraint of translational invariance in the plane perpendicular to the light path since this is not satisfied in the droplet geometry. This would make Maxwell's equations very tedious and time consuming to solve, if not impossible with present computers. The assumption to be made is that the drops have local translational invariance. For large radii, where the rate of change of the molecular configuration with distance is small, the geometry is close to being locally translationally invariant, but near the axis of symmetry this approximation is less accurate. Maxwell's equations will be applied to the molecular configurations of Ch. IV with full knowledge that the optical patterns predicted for small radii will not be quite right.

The presence of the polarizer in front of the cylindrically symmetric droplet results in two regions in which the light propagates as an o-ray and two regions where it propagates as an e-ray. (This is assuming that the azimuthal angle is constant with height. If it is not, then this

argument can be applied to each layer.) Since the effect of the medium on the e- and o-rays are different, one would expect to observe two-fold symmetry in the optical pattern of a liquid crystal droplet between crossed polarizers.

The main feature that is neglected in the assumption of local translational invariance is the displacement of the e- and o-rays relative to one another. The amount of this displacement is proportional to the thickness of the sample. For a typical MBBA droplet, 20 microns thick, the shift of the e-ray with respect to the o-ray can be a few microns. This will have relatively little effect on the optical pattern at large radii. However, for smaller radii, a 2 or 3 micron shift can completely distort the image. The distortion should be larger for large drops since they are thicker and the relative displacements should therefore be greater. The optical patterns that one would expect if the approximation of local translational invariance were correct will be presented in the fourth section of this chapter after the solution of Maxwell's equations has been discussed. These will show two-fold symmetry at all radii.

V.2 MAXWELL'S EQUATIONS IN A TRANSLATIONALLY INVARIANT MEDIUM

The dielectric tensor of a uniaxial crystal in a coordinate system with the z-axis parallel to the optic axis is

$$\overset{\leftrightarrow}{\varepsilon}{}' = \begin{pmatrix} \varepsilon_{11} & 0 & 0 \\ 0 & \varepsilon_{11} & 0 \\ 0 & 0 & \varepsilon_{33} \end{pmatrix}$$

(V.1)

where ε_{11} and ε_{33} are the dielectric constants for the ordinary and extraordinary waves respectively. The dielectric tensor in a coordinate system in which the optic axis makes an angle θ with respect to the z-axis and ϕ with respect to the x-axis, can be obtained by applying the well known tensor operation

$$\overset{\leftrightarrow}{\varepsilon} = \overset{\leftrightarrow}{A}^{-1} \; \overset{\leftrightarrow}{\varepsilon}{}' \; \overset{\leftrightarrow}{A}$$

(V.2)

where $\overset{\leftrightarrow}{A}$ is the rotation matrix from the fixed coordinate system to the coordinate system attached to the local director. $\overset{\leftrightarrow}{A}$ can be obtained by applying two consecutive rotations, first about the z-axis by the angle ϕ, and then about the y-axis through the angle $-\theta$. After combining the two rotations one has

$$\overset{\leftrightarrow}{A} = \begin{pmatrix} \cos\theta \cos\phi & \cos\theta \sin\phi & -\sin\theta \\ -\sin\phi & \cos\phi & 0 \\ \sin\theta \cos\phi & \sin\theta \sin\phi & \cos\theta \end{pmatrix} .$$

(V.3)

Performing the operation indicated by Eq. V.2 one finds that the dielectric tensor can be written as

$$\overset{\leftrightarrow}{\varepsilon} = \varepsilon_0 \begin{pmatrix} 1 - \alpha(1 - 2\sin^2\theta \cos^2\phi) & \alpha\sin^2\theta\sin^2\phi & \alpha\sin2\theta\cos\phi \\ \alpha\sin^2\theta\sin^2\phi & 1-\alpha(1-2\sin^2\theta\sin^2\phi) & \alpha\sin2\theta\sin\phi \\ \alpha\sin2\theta\cos\phi & \alpha\sin2\theta\sin\phi & 1 + \alpha\cos2\theta \end{pmatrix}$$

(V.4)

where α is called the birefringence ratio and ϵ_o is the mean dielectric constant. These quantities are defined from

$$\epsilon_{33} = (1 + \alpha)\epsilon_o$$

and

$$\epsilon_{11} = (1 - \alpha)\epsilon_o \quad .$$

$$(V.5)$$

Maxwell's equations in a source-free non-magnetic region are

$$\nabla \cdot \vec{H} = 0 \qquad\qquad (V.6a)$$

$$\nabla \cdot \vec{D} = 0 \qquad\qquad (V.6b)$$

$$\nabla \times \vec{H} = \frac{1}{c}\frac{\partial \vec{D}}{\partial t} \qquad\qquad (V.6c)$$

$$\nabla \times \vec{E} = -\frac{1}{c}\frac{\partial \vec{H}}{\partial t} \qquad\qquad (V.6d)$$

where $\vec{H}$ is the magnetic induction, $\vec{D}$ is the electric displacement, and $\vec{E}$ is the electric field. To obtain a more useful form for the purpose at hand the curl is applied to both sides of Eq. V.6d producing

$$
\begin{aligned}
0 &= \nabla \times (\nabla \times \vec{E}) + \frac{1}{c}\ \nabla \times \frac{\partial \vec{H}}{\partial t} \\
&= \nabla \times (\nabla \times \vec{E}) + \frac{i\omega}{c}\ \nabla \times \vec{H} \\
&= \nabla \times (\nabla \times \vec{E}) - \frac{\omega^2}{c^2}\ \overleftrightarrow{\epsilon}\ \vec{E}
\end{aligned}
$$

$$(V.7)$$

where both $\vec{H}$ and $\vec{D}$ have been assumed to be harmonic functions
of time with angular frequency ω and use has been made of
Eq. V.6c and of the tensor relationship between the electric
displacement and electric field

$$\vec{D} = \overleftrightarrow{\varepsilon} \, \vec{E}$$

(V.8)

The curl curl term in Eq. V.7 contains derivatives of the
electric field with respect to all three coordinates. It is
at this point that the assumption of local translational
invariance is made: all derivatives with respect to x and y
are set equal to zero. Eq. V.7 then reduces to the three
equations

$$0 = \frac{\partial^2 E_x}{\partial z^2} + \frac{\omega^2}{c^2} \, [\varepsilon(11)E_x + \varepsilon(12)E_y + \varepsilon(13)E_z] \quad \text{(V.9a)}$$

$$0 = \frac{\partial^2 E_y}{\partial z^2} + \frac{\omega^2}{c^2} \, [\varepsilon(21)E_x + \varepsilon(22)E_y + \varepsilon(23)E_z] \quad \text{(V.9b)}$$

$$0 = \varepsilon(31)E_x + \varepsilon(32)E_y + \varepsilon(33)E_z \quad . \quad \text{(V.9c)}$$

Eq. V.9c can be solved for E_z and this can be used to elimi-
nate E_z from Eqs. V.9a and V.9b.

In addition to the volume equations one must consider
what happens at the boundaries. From the continuity of the
tangential components of the magnetic induction and Eq. V.6d
one has that the tangential component of the curl of $\vec{E}$ must be

continuous. With translational invariance in the x-y plane
this becomes

$$\frac{\partial \vec{E}_t}{\partial z} = \frac{\partial \vec{E}_i}{\partial z} + \frac{\partial \vec{E}_r}{\partial z} \qquad \text{in x-y plane}$$

(V.10)

where t, i, and r refer to the transmitted, incident, and
reflected light respectively. "In the x-y plane" means that
only the x and y components of the vector relation are to
be considered. At the bottom interface (z = 0) the inci-
dent and reflected light (which propagate parallel to the
axis of symmetry) are in an isotropic medium, with index
of refraction n_{ext}, and thus the electric fields can be
written as

and
$$\vec{E}_i(z) = \vec{E}_i \exp\left[-\frac{i\omega n_{ext} z}{c}\right]$$

(V.11a)

$$\vec{E}_r(z) = \vec{E}_r \exp\left[\frac{i\omega n_{ext} z}{c}\right] .$$

(V.11b)

Combining these with Eq. V.10 gives

$$\frac{\partial E_t(z\to 0^+)}{\partial z} = \frac{i\omega n_{ext}}{c} \left[\vec{E}_r(z\to 0^-) - \vec{E}_i(z\to 0^-)\right] \text{in x-y plane}$$

(V.12)

where 0^- and 0^+ mean just below and just above the bottom
surface, respectively.

In addition the tangential components of the electric
fields are continuous, i.e.

$$\vec{E}_t(z\to 0^+) = \vec{E}_i(z\to 0^-) + \vec{E}_r(z\to 0^-) \qquad \text{in x-y plane} .$$

(V.13)

Adding this and Eq. V.12 gives as the boundary condition at the bottom surface

$$2\vec{E}_i(z \to 0^-) = \vec{E}_t(z \to 0^+) - \frac{c}{i\omega n_{ext}} \frac{\partial \vec{E}_t(z \to 0^+)}{\partial z} \quad \text{in x-y plane.}$$

(V.14)

At the top surface, the continuity of the tangential components of the electric field and the magnetic induction give

$$\vec{E}_t(z \to L^-) = \vec{E}_1(z \to L^+) \qquad \qquad \text{(V.15a)}$$

and

$$\frac{\partial \vec{E}_t(z \to L^-)}{\partial z} = \frac{\partial \vec{E}_1(z \to L^+)}{\partial z}$$

in x-y plane

(V.15b)

where E_1 is the electric field of the light in the isotropic medium that has been transmitted by the sample of thickness L and where L^- and L^+ mean just below and just above the top surface. Combining Eqs. V.15a and V.15b and using a harmonic spacial variation for the transmitted field as in Eq. V.11 gives

$$\vec{E}_t(z \to L^-) = - \frac{c}{i\omega n_{ext}} \frac{\partial \vec{E}_t(z \to L^-)}{\partial z} \quad \text{in x-y plane}$$

(V.16)

for the boundary condition at the top surface.
The solution of these equations on the computer will be discussed in App. V.

V.3 APPLICATION TO DROPS

In practice since the drops have cylindrical symmetry if one can solve for the behavior of light rays polarized in two different directions at a particular radius, then by the proper linear combination of the two rays, the effect of the medium on light at any azimuthal position at that radius can be determined directly. Maxwell's equations were therefore solved at each radius for light that was polarized parallel to the x-axis and then for light polarized parallel to the y-axis. When the ρ- and Φ- axes coincide with the x- and y-axes respectively the result of the calculations can be formally written as

$$\begin{pmatrix} E_{xOUT} \\ E_{yOUT} \end{pmatrix} = \begin{pmatrix} E_{\rho OUT} \\ E_{\Phi OUT} \end{pmatrix} = \overset{\leftrightarrow}{T} \begin{pmatrix} E_{\rho IN} \\ E_{\Phi IN} \end{pmatrix} = \overset{\leftrightarrow}{T} \begin{pmatrix} E_{xIN} \\ E_{yIN} \end{pmatrix}$$

(V.17)

where IN and OUT refer to the electric fields that are incident to the medium and that leave the medium respectively, while $\overset{\leftrightarrow}{T}$ is the transmission matrix that represents the effect of the medium on the light. When the ρ-Φ axes are rotated by an angle Φ with respect to the x-y system one has

$$\begin{pmatrix} E_{\rho IN} \\ E_{\Phi IN} \end{pmatrix} = \overset{\leftrightarrow}{R} \begin{pmatrix} E_{xIN} \\ E_{yIN} \end{pmatrix}$$

(V.18a)

where

$$\overset{\leftrightarrow}{R} = \begin{pmatrix} \cos\phi & \sin\phi \\ \\ -\sin\phi & \cos\phi \end{pmatrix}$$

(V.18b)

with a similar expression for the outgoing waves. Therefore Eq. V.17 becomes

$$\begin{pmatrix} E_{xOUT} \\ E_{yOUT} \end{pmatrix} = \overset{\leftrightarrow}{R}^{-1} \overset{\leftrightarrow}{T} \overset{\leftrightarrow}{R} \begin{pmatrix} E_{xIN} \\ E_{yIN} \end{pmatrix} .$$

(V.19)

If the y-axis is parallel to the polarizer axis and the incident light has unit amplitude then

$$\vec{E}_{IN} = \begin{pmatrix} 0 \\ 1 \end{pmatrix}$$

(V.20)

If the analyzer is parallel to the x-axis then the only component of the electric field of interest is

$$E_{xOUT} = (1,0) \overset{\leftrightarrow}{R}^{-1} \overset{\leftrightarrow}{T} \overset{\leftrightarrow}{R} \begin{pmatrix} 0 \\ 1 \end{pmatrix}$$

(V.21a)

$$= (\cos\phi, -\sin\phi) \overset{\leftrightarrow}{T} \begin{pmatrix} \sin\phi \\ \cos\phi \end{pmatrix} .$$

(V.21b)

where use has been made of the definition of $\overset{\leftrightarrow}{R}$, Eq. V.18b.

Thus once the matrix $\overset{\leftrightarrow}{T}$ is known for any two polarizations at a given radius, the amplitude of the light transmitted

through the crossed polarizers and the drop for all azimuthal angles at this radius can be found by application of Eq.V.21. This was carried out in the computer calculation OPT5 contained in App.V.

V.4 THE BRUSH PATTERNS

The results of the optics calculation on the molecular pattern of the twisted configuration presented in Fig. IV.1 between crossed polarizers is shown in Fig. V.1. In this pattern the effect of the fringes has been suppressed by making the birefringence, Δn, smaller. This effect could also be achieved by using longer wavelengths or thinner samples. The main features of the brush pattern are unaffected by these changes which were done to avoid distortions of the extinction cross that the presence of fringes can cause. These distortions can be seen in Figs. I.1 and II.3.

The optical pattern is characterized by having the brushes in the outer regions roughly parallel to the cross of the polarizers as described in Ch.II. Towards the center of symmetry the brushes rotate producing what looks like a rotated cross. However, the arms never get straight, they continue to slowly spiral all the way into the center. The tangent to the brushes near the center of symmetry is at approximately 45°. This is the part of the pattern that produces the rotated 45° cross.
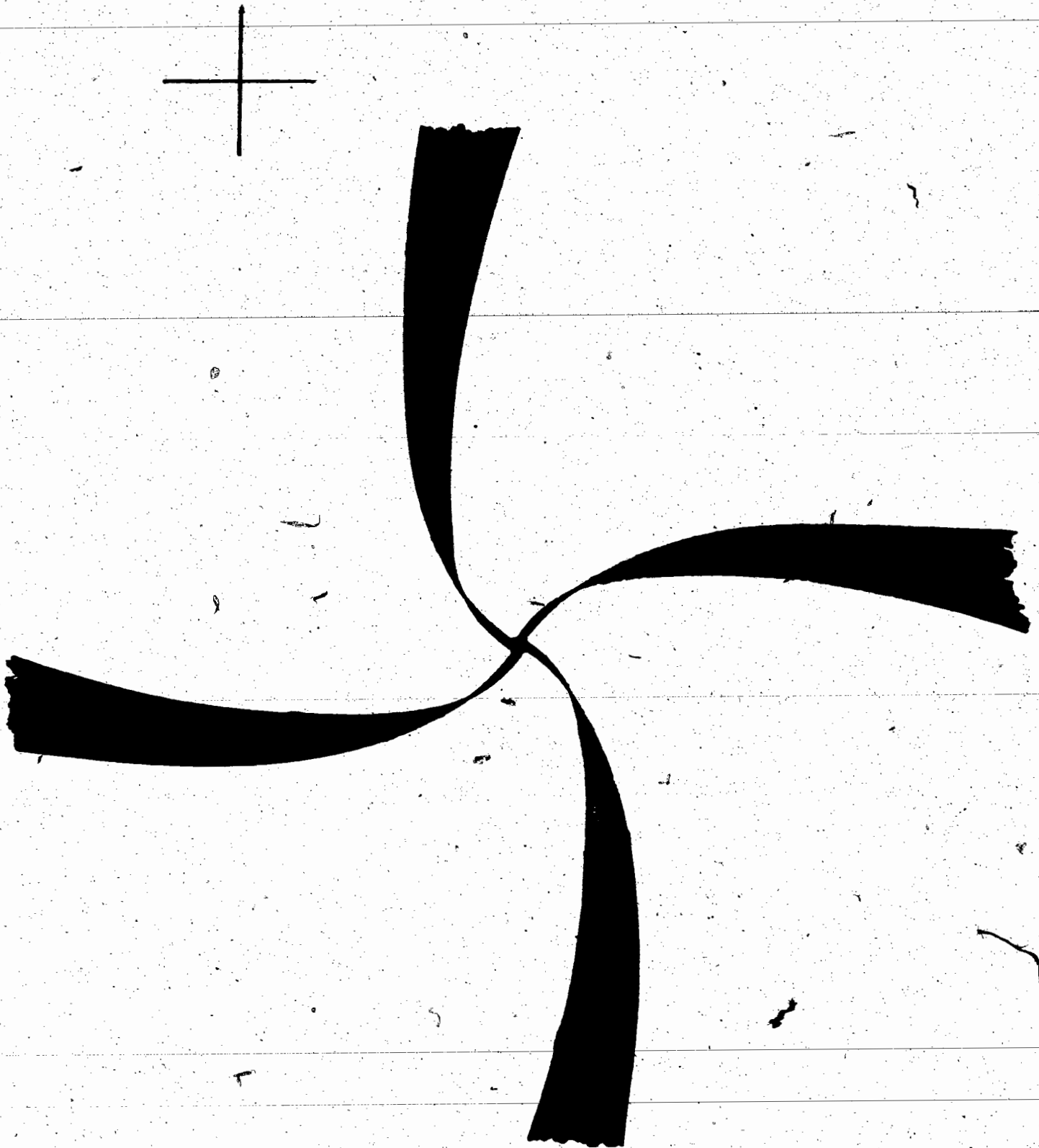
Figure V.1

The extinction cross predicted by the solution of Maxwell's
equations for the twisted configuration of an MBBA droplet with
S/B = .8 and T/B = .5 between crossed polarizers. The fringe
pattern has been suppressed. The shading indicates where the
transmission coefficient is less than 3%.

The pattern displays two-fold symmetry as discussed in the first section of this chapter. However, the deviations from four-fold symmetry, especially for larger radii, are very small. This is a result of ϕ being approximately independent of z. The light incident on the droplet produces the e- and o-rays which are polarized parallel and perpendicular to the principal plane, respectively. If ϕ were completely independent of z the principal plane would also be independent of z. In this case since there is no mixing between the two different polarizations the amplitudes of the e- and o-rays remain constant as they propagate through the droplet. If in Eq. V.21b the angle ϕ now refers to the angle between the x-axis and the principal plane (ϕ is now equal to the old value of $\phi+\phi$) then the off-diagonal elements of the transmission matrix $\overleftrightarrow{T}$ are zero. In this case the amplitude of the light through the analyzer is given by

$$F_{xOUT} = \sin\phi \, \cos\phi \, (T(11) - T(22)). \qquad (V.22)$$

The intensity of the transmitted light, equal to the product of E_{xOUT} and its complex conjugate, produces four-fold symmetry in the optical pattern.

As explained in the introduction to this chapter, the computer calculation should be modified to allow for the differences in displacement between the e- and o-rays which become most important when the approximation of local

translational invariance is strongly violated. This relative displacement is responsible for the lack of perfect agreement of the observed droplets with the computer calculations, especially for small radii. Though the concept of refraction of the rays is qualitatively understood, an attempt to obtain quantitative answers in a cylindrically symmetric region to compare with observations would require vast amounts of computer space and time and has not been attempted.

The distortion of the brush pattern when it encounters a fringe is in agreement with the calculations that have been performed. The exact structure of a brush pattern can vary from drop to drop. Since smaller drops have fewer fringes and less distortion due to the relative displacement of the o- and e-ray images they generally present nicer looking crosses than do the larger drops as can be seen in Fig. II.3.

As the ratio of T/S approaches unity the twisted configuration becomes less rotated as shown in Fig. IV.4. The pattern of the inserted crosses in these figures suggest that as T/S approaches unity the extinction brushes should approach more closely to that of the normal configuration. This is verified by the optics calculation.

The optics calculation predicts that the twisted central cross should become more rotated and larger in extent as the magnetic field is increased. This is due to the increase in the ϕ-values, with magnetic field as mentioned in Ch. IV. This effect is observed, however, quantitative comparisons are difficult to make because the changes in the magnetic field also cause large changes in the fringe pattern which affects the way in which the brush patterns are distorted. The response of the fringe pattern to the magnetic field will be discussed after some simplifications in the optics equations, applicable for large radii, are made.

V.5   OPTICS FOR Φ INDEPENDENT OF Z

A simplification of the equations of Ch. V.2 can be made if the azimuthal angle ϕ is independent of z. One can always make $\phi = 0$ in this case by performing a rotation by ϕ about the z-axis. This simplification is useful because for radial distances greater than about the thickness of the drop the z-dependence of ϕ is small.

When $\phi = 0$, the dielectric tensor, Eq. V.4, becomes

$$\overset{\leftrightarrow}{\varepsilon} = \varepsilon_0 \begin{pmatrix} 1 - \alpha\cos2\theta & 0 & \alpha\sin2\theta \\ 0 & 1 - \alpha & 0 \\ \alpha\sin2\theta & 0 & 1 + \alpha\cos2\theta \end{pmatrix}$$

$$(V.23)$$

and Eqs. V.9 become

$$0 = \frac{\partial^2 E_x}{\partial z^2} + \frac{\omega^2}{c^2} [\varepsilon(11)E_x + \varepsilon(13)E_z]$$ (V.24a)

$$0 = \frac{\partial^2 E_y}{\partial z^2} + \frac{\omega^2}{c^2} \varepsilon(22)E_y$$ (V.24b)

$$0 = \varepsilon(31)E_x + \varepsilon(33)E_z \quad .$$ (V.24c)

Eqs. V.24a and V.24c describe the propagation of the e-ray while Eq. V.24b describes the propagation of the o-ray.

Substituting the dielectric tensor matrix elements from Eq. V.23 into Eqs. V.24 gives

$$\frac{\partial^2 E_x}{\partial z^2} = -\frac{\omega^2}{c^2} \varepsilon_0 \left(\frac{1 - \alpha^2}{1+\alpha\cos2\theta} \right) E_x$$ (V.25a)

and

$$\frac{\partial^2 E_y}{\partial z^2} = -\frac{\omega^2}{c^2} \varepsilon_0 (1 - \alpha) E_y .$$ (V.25b)

The solutions of these equations are the harmonic functions

$$E_x = E_{xo} e^{\pm\frac{i\omega nz}{c}}$$ (V.26a)

and

$$E_y = E_{yo} e^{\pm\frac{i\omega n_o z}{c}}$$ (V.26b)

where E_{xo} and E_{yo} are the amplitudes of the electric fields

and n_o and n are the indices of refraction for the ordinary
and extraordinary waves, respectively, and are defined as

$$n_o = \sqrt{(1 - \alpha)\varepsilon_o} = \varepsilon_{11} \qquad \text{(V.27a)}$$

and

$$n = \sqrt{\frac{(1-\alpha^2)\varepsilon_o}{1+\alpha\cos 2\theta}}$$

$$= \left(\frac{\cos^2\theta}{n_o^2} + \frac{\sin^2\theta}{n_e^2}\right)^{-\frac{1}{2}} \qquad \text{(V.27b)}$$

where

$$n_e = \sqrt{\varepsilon_o(1+\alpha)} = \sqrt{\varepsilon_{33}} \qquad \text{(V.27c)}$$

is the maximum index of refraction possible for the e-ray. In
doing the integration it was assumed that the spatial varia-
tions in θ are small compared to the wavelength of light.

Eqs. V.26 and V.27 can be applied point by point through
the material and the contribution to the phase difference between
the e- and o-rays can be calculated. When the phase difference

$$\Delta P = \frac{\omega}{c} \int_0^L dz \, |n(\theta) - n_o| \qquad \text{(V.28a)}$$

$$= \frac{2\pi}{\lambda_v} \int_0^L dz \, |n(\theta) - n_o| \qquad \text{(V.28b)}$$

is a multiple of 2π an extinction fringe of frequency $\omega/2\pi$
or vacuum wavelength λ_v will occur.

V.6 COMPARISON OF FRINGE PATTERN WITH OBSERVATION

A quantitative comparison of the observed fringes with theory will be made for an MBBA droplet about 250 microns in diameter. The comparison will be made by observing the variation of the optical path length with magnetic field at a radius of about 25 microns. The reason for using this radius is that the surfaces of the droplet are still almost horizontal, yet the behavior at this radius corresponds to the large ρ limit. Further out, because the surfaces are more sloped one could no longer assume that the θ's at the surfaces are the hard pinning angles. One would also need to consider the slopes of the surfaces and the azimuthal angles as shown in App. II. In addition, θ would once again become a function of radius because of the change in thickness and therefore the large ρ limit of the θ-equation, Eq. III.28, would not be applicable.

The experiments were performed by selecting the desired wavelength with the monochromator and then varying the magnetic field directed along the droplet's axis of symmetry until the desired extinction fringe coincided with a crosshair in the eyepiece. The uncertainty in the positioning of the fringes was estimated to be about $\pm 20\%$ of a fringe.

The data will be presented after the method of analysis is discussed. The radial dependence of θ and ϕ are assumed to be small which is a good assumption for distances away from the axis of symmetry equal to the thickness of the drop.

This allows one to make use of Eq. III.28 to evaluate the variation of θ with vertical position in the droplet. A first integration of Eq. III.28 can be performed to give

$$\theta_z^2 [S \sin^2\theta + B \cos^2\theta] = \sin^2\theta \, \Delta\chi \, H^2 + K \tag{V.29}$$

where K is a constant of integration picked to satisfy the boundary conditions.

Eqs. V.29 or III.28 can be solved for θ and then Eq. V.28 can be used to evaluate the optical phase difference, ΔP, for the droplet as a function of wavelength and the magnetic field.

Eq. V.28b can be expanded for $\Delta n/n_o \ll 1$ to give

$$\Delta P = \frac{2\pi}{\lambda_v} \Delta n \int_C^{Z_o} dz \, \sin^2\theta \tag{V.30}$$

where

$$\Delta n = n_e - n_o \tag{V.31}$$

and where use has been made of Eq. V.27. Upon rewriting this becomes

$$\frac{\Delta P \lambda_v}{2\pi \Delta n} = \int_0^{Z_o} dz \, \sin^2\theta = F(H). \tag{V.32}$$

The quantity $\dfrac{\Delta P \lambda_v}{2\pi \Delta n}$ for all wavelengths should fall on the line given by the function $F(H)$. To facilitate the analysis for different wavelengths both sides of Eq. V.32 are multiplied by $\Delta n(6000)$, the birefringence at 6000Å. The function $\dfrac{\Delta P \lambda_v \, \Delta n(6000)}{2\pi \Delta n(\lambda)}$ can be made independent of wavelength as shown

in Fig. V.2 if the variation of the birefringence with wave-length is assumed to be

$$\frac{\Delta n(\lambda)}{\Delta n(6000)} = 1 + .8\left(\frac{\lambda(\overset{o}{A}) - 6000}{6000}\right).$$ (V.33)

From Eq. V.32, the line given by the locus of these points should be equal to $F(H)\Delta n(6000)$. The best fit to the data is shown by the solid curve which agrees well with most of the points. The largest discrepancy is at high magnetic fields where the positions of the fringes were most difficult to determine because of their width. The fit was done by varying the parameters $\Delta n, S/B, \Delta\chi/B$, the hard pinning angles θ_{LS} and θ_{US}, and the thickness of the drop, z_O. In order to get agreement with the data for reasonable values of $\Delta n(6000)$ θ_{US} must be around 90°. Since Eq. V.30 indicates that the phase difference is proportional to $\sin^2\theta$, most of the optical effect comes from near the upper interface where θ is large. The phase difference is therefore insensitive to the pinning angle θ_{LS} (~15°) at the air interface. Computer calculations indicate that the shape of the curve is approximately indepen-dent of S/B and $\Delta\chi/B$ and that for magnetic fields larger than 2 kG the thickness of the drop plays no role. These can be understood by examining Eq. V.29 when there is a magnetic field sufficiently strong (~2 kG) to ensure that θ decreases
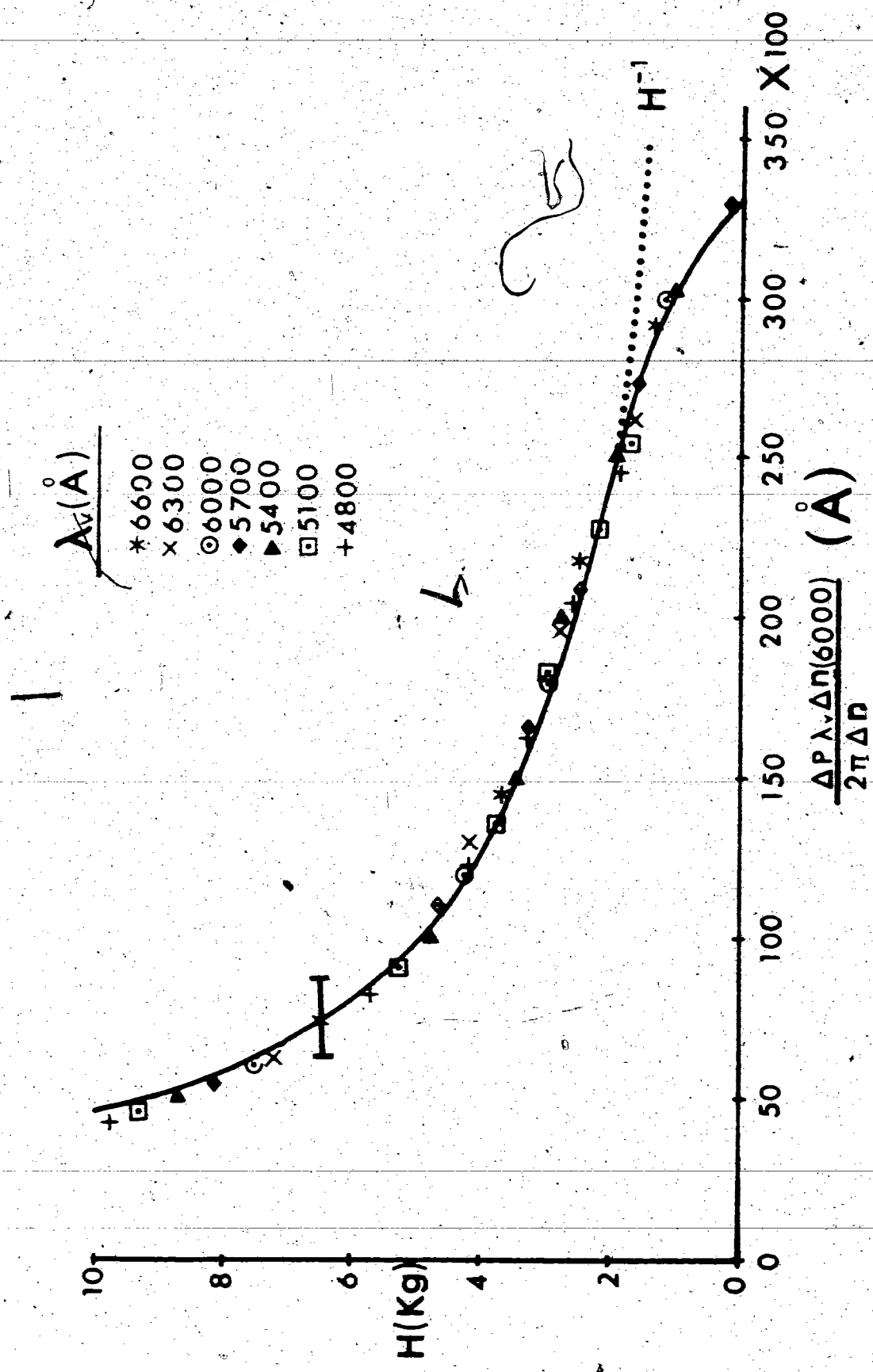
Figure V.2

The magnetic field at which an extinction fringe at the vacuum
wavelength coincided with a crosshair at a radius of 25 microns
in an MBBA droplet 250 microns in diameter as a function of

$$\frac{\Delta P \lambda \cdot \Delta n (6000)}{2 \pi \Delta n}$$

from both surfaces, reaching a minimum value θ_{min} at which point $\theta_z = 0$. This allows the evaluation of K and Eq. V.29 becomes

$$\theta_z^2 = \frac{\Delta\chi H^2 (\sin^2\theta - \sin^2\theta_{min})}{(S \sin^2\theta + B \cos^2\theta)} \quad . \qquad (V.34)$$

Making a change in variable in Eq. V.32 from z to θ and using Eq. V.34 gives

$$\frac{\Delta P \lambda_v \Delta n(6000)}{2\pi \Delta n(\lambda)} = \frac{\Delta n(6000)}{(\Delta\chi)^{1/2} H} \left[\int_{\theta_{LS}}^{\theta_{min}} d\theta \frac{(S \sin^2\theta + B\cos^2\theta)^{1/2} \sin^2\theta}{(\sin^2\theta - \sin^2\theta_{min})^{1/2}} + \int_{\theta_{min}}^{\theta_{US}} d\theta \frac{(S \sin^2\theta + B\cos^2\theta)^{1/2} \sin^2\theta}{(\sin^2\theta - \sin^2\theta_{min})^{1/2}} \right] \quad .$$

$$(V.35)$$

For large magnetic fields θ_{min} is of the order of zero and the integrals become independent of the magnetic field. Therefore the phase difference should vary inversely with the magnetic field which is shown as the dotted line in Fig. V.2 normalized to 5 kG. This 1/H region is good for magnetic fields larger than about 2 kG for the particular drop studied. From Eq. V.3 one finds that the ratio of the phase differences at two magnetic fields that are sufficiently large should be inversely proportional to the ratio of the magnetic fields, independent of Δn, S, B, θ_{min}, θ_{LS}, or θ_{US}. Therefore ΔP at 10 kG should be half of ΔP at 5 kG with no

adjustable parameters. The experimentally observed ratio is .43 which is considerably lower. This difference can result from an error of 10 percent in the measurement of the center of the fringe which is easy to make when the fringe occupies most of the drop as is the case for the 1st order fringe.

Evaluation of the integrals of Eq. V.35 and comparison with Fig. V.2 produces a value for $\frac{\Delta n(6000)}{(\Delta\chi/B)^{\frac{1}{2}}}$ of 5.7 micron kG which agrees with the ratio of the values Haller (Ha-72b) has found for Δn and $\Delta\chi/B$ at room temperature. (S/B was taken to be .8).

When the magnetic field is small, θ increases uniformly from the bottom to the top surfaces. Eq. V.32 can then be used to estimate the thickness of the drop, Z_o, which for this drop was found to be 28 microns.

The interpretation of the fringe pattern of this droplet allows one to experimentally measure the dispersion in the birefringence of MBBA as well as the hard pinning angle at a water interface. Neither of these measurements have been previously reported in the literature.

DISCUSSION

The purpose of this thesis is to obtain descriptions of the minimum energy configurations of the molecular alignment in nematic liquid crystal droplets, and to compare the predicted optical patterns resulting from these configurations with those one observes experimentally. The system used for comparison was the room temperature nematic liquid crystal Methoxybenzylidene-Butyalaniline at the interface between air and water. The optical patterns observed between crossed polarizers were of three types which have been called the left-handed, right-handed, and normal configurations in which the extinction cross, whose arms are roughly parallel to the axes of the polarizer and the analyzer for large radii, spiral counterclockwise, clockwise, or remain unrotated, respectively, as the center of the optical pattern is approached. The droplets have complete cylindrical symmetry as shown by the invariance of the optical patterns as they are rotated between the polarizers.

The energy of a droplet depends upon the surface tension, the angle the molecular alignment makes with the surfaces, and the Frank (Fr-58) elastic energy in the volume which is composed of three types of distortions, called splay, twist, and bend. The expression for the total free energy of this system is shown in App. II. Because the surface energies are much larger than the volume energies (except possibly at a few singularities) the

problem can be broken up into two parts: the surface energies determine the shape of the droplet independent of the volume effects; then the volume configuration is determined subject to the droplet surface. This results in a lens-shaped droplet with a well-defined axis of symmetry. Where the axis of symmetry cuts the surfaces the volume energy becomes large. This can produce surface distortions and/or the molecular alignment at the surface, the hard-pinning angles, can be relaxed. In App. II the distortions are shown to be of molecular size based on the relative strengths of the surface tensions and the volume elastic constants. This order of magnitude argument is made more fully in App. VI using the results of the full calculation. The small size of these distortions justify their neglect when considering the molecular alignment on the scale of microns and larger.

Minimizing the volume energy produces a pair of second order non-linear coupled partial differential equations in cylindrical coordinates to be satisfied at every point in the droplet as well as four first order coupled partial differential equations to be satisfied at the appropriate surfaces of the droplet. Because of the complexity of these equations the only method of solution is by computer which requires an appropriate grid system to be established. This is difficult for a lens-shaped droplet because the surfaces are not rectangular and therefore do not fit the rectangular set of grid points that one obtains from a cylindrical coordinate system with cylindrical symmetry (the ρ-z plane). One could set the problem up using a parabolic coordinate

system to match the shape of the droplet surfaces but then the torque and energy equations become much more difficult. Thus, even though the solution to the full droplet doesn't present any conceptual difficulties it remains to be done because of these computational problems.

At this point the outer regions of the droplets are forgotten and attention is focused on the central region which has become a cylinder with flat surfaces. This has the advantage that it can be fit perfectly to a rectangular grid. This approximation appears to be justified on the grounds that pieces of dirt or irregularities in the outer regions of the droplet, or the size of the droplets do not seem to affect the central configuration either theoretically or experimentally.

The equations are then solved using a relaxation technique. Depending on the elastic constants (in particular the ratio of the twist elastic constant T to the splay constant S) either 2 or 4 equilibrium solutions are found. When $T/S > 1$ two solutions are found. In one the molecules the in $\rho - z$ plane appear to follow hyperbolae about the point singularity at the water surface as shown in Fig. IV.2b while in the other case the molecules in the $\rho - z$ plane appear to surround the point singularity at the water surface radially. Such a configuration can be obtained from Fig. IV.2b by reflecting each molecule about an axis parallel to the symmetry axis. Away from the air surface these solutions mathematically can be approximated by two solutions of the one constant equation, Eq. III.21 with ϕ constant and no magnetic

field. These solutions are

$$\tan\theta = \pm\frac{\rho}{z-Z_o} \qquad \text{(VI.1)}$$

where Z_o is the z-coordinate of the water surface. The + solution is the radial case while the - solution corresponds to the hyperbolic configuration. While both solutions have been recognized by others (Kleman (Kl-72), Meyer (Me-72)) it has not been recognized that the energy of the two is different. In fact Meyer (Me-72) shows the molecular configuration in a drop- let to be the one that is radial in the ρ-z plane whereas the present calculations show that it is the solution which is hyperbolic in the ρ-z plane that is significantly lower in ener- gy (~a factor of 2). This factor of 2 is derived explicitly in App. VI. This great reduction in energy is due to the process of splay cancellation in which a contribution to the splay (a divergence) which appears in the ρ-z plane can be cancelled to a large extent by a splay which appears in the ρ-ϕ plane. This cancellation can take place only if the molecules are hyperbolic about the singularity in the ρ-z plane. This ensures that the projections of the molecules in the ρ-ϕ plane are radial and is called the normal configuration. The necessary radial configuration in the ρ-ϕ plane is in agreement with the observations presented in Ch. II and with the conclusions of Meyer (Me-72) and Le Roy (Le-72) who studied droplets under similar conditions.

When T/S<1, which is called weak twist, there are two additional solutions of equal energy possible in which for small

radii the projections of the molecules in the ρ-ϕ plane rotate away from the radial configuration in either the clock- or counterclock-wise directions producing the right- and left-handed configurations ,respectively. The energy of the two twisted solutions is only slightly less than the normal configuration with the result that all three are seen experimentally.

The two concepts discovered in this thesis, splay cancellation and weak twist should have been anticipated. The reason they remained unknown was that the complexity of the mathematics forced people to make many simplifying approximations. In the one constant approximation the twisted configurations do not occur except for large magnetic field. Another usual approximation is to assume translational invariance in the z-direction and to fix the azimuthal angle ϕ (Saupe (Sa-73)). Under these conditions splay cancellation cannot occur. Thus neither splay cancellation nor the twisted configurations were recoverable from these less generalized treatments of the problem.

To obtain the optical patterns corresponding to the calculated configurations requires the solution of Maxwell's equations for the propagation of light in a birefringent medium in which the optic axis has non-zero spatial derivatives. However, the system of equations that are produced are too complicated even for present day computers. The present calculations are made with the assumption of local translational invariance. This approximation works well except very near the cylinder axis and is susceptible to computer analysis. The optical patterns

that are produced are in close agreement with those observed experimentally, consisting of an extinction cross rougly parallel to the crossed polarizer and analyzer, rotated for small radii for the twisted configurations, and concentric colored fringes.

The transmitted light is generally elliptically polarized, but when the light emerges with the long axis of the ellipse parallel to the initial polarization it also results that the ellipse is very narrow, that is, the transmitted light at the extinction cross is linearly polarized and the absorption by the analyzer is highly effective. In addition the conditions for the extinction cross are independent of wavelength for droplets with thicknesses large compared to the wavelength. Thus the extinction crosses are black. The fringe pattern, on the other hand is very sensitive to the wavelength of the light.

In addition to translational invariance it is assumed that the light is parallel to the axis of symmetry and perpendicular to the two surfaces. To relax any of these assumptions would make the optical calculation much more demanding than the program shown in App. V. Yet none of these assumptions is really true and it is difficult to judge how important these effects are theoretically. Experimentally one can vary the degree of convergence or divergence of the light and show that the position of the cross is not affected except in the central region where the focusing conditions to produce a clear cross are more strin-gent.

The appearance of the central cross does depend upon the focusing of the objective lens. In thicker drops this is much more noticeable, the central cross is distorted substantially from the almost four-fold symmetry predicted by the translationally invariant calculation. The e-rays undergo considerable refraction on passing throug the drops. This can be seen by focusing on little bubbles which can be produced on the surface. When viewed through the droplets the images are displaced radially depending upon whether they are viewed with the e-rays or the o-rays. Thus while one observes patterns close to those calculated, there are details for which the present calculation are not adequate.

The molecular configuration of a given droplet can be changed in response to three stimuli:magnetic field, temperature, and purity of the material. The molecules, being diamagnetic, can lower their energies by aligning parallel to a magnetic field. The magnetic field can be applied easily either perpendicular or parallel to the axis of symmetry. Applying it perpendicular to the symmetry axis destroys the cylindrical symmetry and causes a molecular pattern with a disclination line as shown by Le Roy (Le-72). Applying the magnetic field parallel to the symmetry axis usually maintains the cylindrical symmetry and therefore can be easily handled mathematically by the addition of a term to the energy proportional to the square of the field. As the field is increased the extinction cross is only slightly affected (there is a small enhancement in the amount of the central rota-

tion for the twisted solutions), but the fringe pattern under-
goes large changes, because the optical retardation of the drop-
let is becoming smaller as the molecules align with their optic
axis parallel to the applied field and the transmitted light.
There is good quantitative agreement between the predicted and
observed optical patterns in the presence of a magnetic field.

When the magnetic field is increased above a threshold
field, about 3 kG for MBBA between air and water, the molecules
near the air interface find themselves incorrectly aligned to
benefit from splay cancellation and they rotate by π . This
occurs when the magnetic field is sufficiently strong that the
polar angles of the molecules far from the surfaces are close
to zero resulting in a decoupling between the region of the
droplet near the air surface and the region near the water sur-
face. The computer calculations indicate that there is possibly
a small energy barrier that must be overcome in order for this
transition to take place. Experimentally one sometimes observes
bubbles forming when a large enough magnetic field is applied.
These bubbles could be regions of the nucleation of the rotated
configuration in the unrotated bulk. These bubbles grow as the
field is maintained or increased and eventually disappear after
the magnetic field is removed. This transition will have to be
studied in more detail, both theoretically and experimentally,
to learn more about how the nucleation is accomplished.

In the twisted configurations the equilibrium position of
the molecules and the resulting rotated cross depends on the

ratio of the twist and splay elastic constants. As T/S approaches
unity (for T/S<1) the amount of rotation decreases until at some
value of the order of .93 the twisted configuration goes over to
the normal configuration (apparently continuously). The ratio
of the elastic constants can be changed by varying the tempera-
ture or the purity of the material. Haller (Ha-72a) has shown
that the ratio of T/S approaches unity as the temperature
approaches the transition with most of the change taking place
close to the clearing point. The dependence of the rotated
cross on temperature has not been studied quantitatively for MBBA
on water inasmuch as the change in temperatue changes the amount
of water absorbed with a resultant change in the purity and in
the elastic constants of the material. The temperature dependence
of the rotated cross of MBBA droplets in air on a glass substrate
treated to ensure the homeotropic alignment of the molecules has
been examined. The cross appears to be roughly independent of
temperature until just below the clearing point when it straight-
ens out, in agreement with prediction.These measurements will
have to be done more carefully to find the exact functional
dependence.

The dependence of the rotated cross on the purity can be
determined by deliberately doping the MBBA with water. This
remains to be attempted.

It would be interesting to consider the case where the
bend (and twist) elastic constants vary strongly with temperature,
becoming much larger than the splay constant near a transition

temperature (Cladis (Cl-73)). In this limit the molecules should
arrange themselves so that there are no bend-like distortions.
In the configurations described by Eq. VI.1, the configuration
that is purely radial in the ρ-z plane is completely splay-like
and thus its energy is independent of the bend elastic constant.
However, the solution which is hyperbolic in the ρ-z plane
contains both splay and bend. When the elastic constants are
equal the hyperbolic solution is lower in energy than the radial
one because of splay cancellation (see App. VI), but when the
bend elastic constant becomes large this is no longer true and
one should have a transition between these as the temperature is
lowered. The ratio of B to S required to make the transtion
take place has not yet been calculated nor has an experiment
been performed for comparison.

CHAPTER VII

CONCLUSIONS

The orientation of the molecules in the central region of a nematic liquid crystal droplet with cylindrical symmetry has been discovered. The minimization of the energy subject to the condition of hard pinning of the molecules in an easy cone at the surfaces predicts the existence of at least one stable equilibrium solution, the normal configuration. In addition, when the twist elastic constant is less than the splay elastic constant two other stable equilibrium states are found which are mirror images of each other. These have been called the left- and right-handed configurations and are of slightly lower energy ($\sim 10^{-9}$ ergs for MBBA at room temperature) than the normal configuration.

The optical patterns that result from light propagating parallel to the symmetry axis in these different arrangements has been determined through the solution by computer of Maxwell's equations. The features of the predicted patterns between crossed polarizers are in close agreement with those observed, explaining the coexistence of droplets with straight-through crosses and with the central crosses that are rotated in either direction. The observed variation in the angle of rotation of the central crosses has been shown to be consistent with differing relative values of the elastic constants. This can arise from variations in the purity of the liquid crystalline material from one drop to another and with time.

An explanation for the formation of "bubbles" in some of the large drops when a magnetic field is applied has been suggested in terms of the nucleation of regions in which the azimuthal angles of the molecules have changed by $180°$ to reduce the splay energy.

Quantitative agreement has been found between the changes in the molecular configuration and the optical fringe pattern in response to a variable magnetic field. This comparison allows one to measure the dispersion in the birefringence of MBBA and the angle of pinning at the water interface.

Finally, a possible explanation of the existence of large numbers of disclinations in nematic films as a means of reducing the energy, in particular the splay energy, has been postulated.

APPENDIX I

ENERGY AND TORQUE EQUATIONS

The director as defined by Eq. III.2 is

$$\hat{n} = \sin\theta\cos\varphi\,\hat{\rho} + \sin\theta\sin\varphi\,\hat{\varphi} + \cos\theta\,\hat{z} \tag{AI.1}$$

The energy density as defined by Eq. III.1 contains the three terms

$$F = \tfrac{1}{2}S\,|\nabla\cdot\hat{n}|^2 + \tfrac{1}{2}T\,|\hat{n}\cdot(\nabla\times\hat{n})|^2 + \tfrac{1}{2}B\,|\hat{n}\times(\nabla\times\hat{n})|^2 \tag{AI.2}$$

which are the splay, twist, and bend energies respectively.

The splay energy involves

$$\begin{aligned}
\nabla\cdot\hat{n} \cdot \ &\frac{1}{\rho}\frac{\partial}{\partial\rho}(\rho\,n_\rho) + \frac{\partial}{\partial z}n_z \\
&= \frac{1}{\rho}\frac{\partial}{\partial\rho}(\rho\sin\theta\cos\varphi) + \frac{\partial}{\partial z}(\cos\theta) \\
&= \frac{1}{\rho}\sin\theta\cos\varphi + \cos\theta\cos\varphi\,\theta_\rho \\
&\quad - \sin\theta\sin\varphi\,\varphi_\rho - \sin\theta\,\theta_z \tag{AI.3}
\end{aligned}$$

The bend and twist energies involve the quantity

$$\nabla\times\hat{n} = \begin{vmatrix} \dfrac{1}{\rho}\hat{\rho} & \hat{\varphi} & \dfrac{1}{\rho}\hat{z} \\[2mm] \dfrac{\partial}{\partial\rho} & - & \dfrac{\partial}{\partial z} \\[2mm] n_\rho & \rho\,n_\varphi & n_z \end{vmatrix}$$

$$\begin{aligned}
= &-\hat{\rho}\left(\cos\theta\sin\varphi\,\theta_z + \sin\theta\cos\varphi\,\varphi_z\right) \\
&+\hat{\varphi}\left(\cos\theta\cos\varphi\,\theta_z - \sin\theta\sin\varphi\,\varphi_z\right. \\
&\qquad\left. + \sin\theta\,\theta_\rho\right) \\
&+\hat{z}\left(\frac{1}{\rho}\sin\theta\sin\varphi + \cos\theta\sin\varphi\,\theta_\rho\right. \\
&\qquad\left. + \sin\theta\cos\varphi\,\varphi_\rho\right) \tag{AI.4}
\end{aligned}$$

The twist energy depends on the component of $\nabla \times \hat{n}$ parallel to the director which after doing the multiplication and collecting terms becomes

$$\hat{n} \cdot (\nabla \times \hat{n}) = -\sin^2\theta \, \varphi_z + \sin\varphi \, \theta_g$$
$$+ \frac{1}{g} \sin\theta \cos\theta \sin\varphi$$
$$+ \sin\theta \cos\theta \cos\varphi \, \varphi_g \quad . \qquad (AI.5)$$

The bend energy depends on the component of $\nabla \times \hat{n}$ perpendicular to the director which after doing the multiplication and collecting terms becomes

$$\hat{n} \times (\nabla \times \hat{n}) = \hat{g} \left[\frac{1}{g} \sin^2\theta \sin^2\varphi - \sin\theta \cos\theta \cos^2\varphi \, \theta_g \right.$$
$$+ \sin^2\theta \sin\varphi \cos\varphi \, \varphi_g - \cos^2\theta \cos\varphi \, \theta_z$$
$$\left. + \sin\theta \cos\theta \sin\varphi \, \varphi_z \right]$$

$$- \hat{\phi} \left[\frac{1}{g} \sin^2\theta \sin\varphi \cos\varphi + \cos^2\theta \sin\varphi \, \theta_z \right.$$
$$+ \sin\theta \cos\theta \cos\varphi \, \varphi_z + \sin^2\theta \cos^2\varphi \, \varphi_g$$
$$\left. + \sin\theta \cos\theta \sin\varphi \cos\varphi \, \theta_g \right]$$

$$+ \hat{z} \left[\sin\theta \cos\theta \, \theta_z + \sin^2\theta \cos\varphi \, \theta_g \right]. \qquad (AI.6)$$

The energy density is the sum of the squares of these quantities weighted with the appropriate elastic constants. In addition the term

$$\sin^2\theta \, \Delta \chi \, H^2 \qquad (AI.7)$$

is added to take account of the presence of a magnetic field.

After collecting and rearranging the terms the energy density for a nematic liquid crystal can be written as

$$F = \frac{1}{\rho^2} \sin^2\theta \left[S \cos^2\varphi + T \cos^2\theta \sin^2\varphi + B \sin^2\theta \sin^2\varphi \right]$$

$$+ \theta_\rho^2 \left[S \cos^2\theta \cos^2\varphi + T \sin^2\varphi + B \sin^2\theta \cos^2\varphi \right]$$

$$+ \sin^2\theta \, \varphi_\rho^2 \left[S \sin^2\varphi + T \cos^2\theta \cos^2\varphi + B \sin^2\theta \cos^2\varphi \right]$$

$$+ \theta_z^2 \left[S \sin^2\theta + B \cos^2\theta \right]$$

$$+ \sin^2\theta \, \varphi_z^2 \left[T \sin^2\theta + B \cos^2\theta \right]$$

$$+ \frac{2}{\rho} \sin\theta \cos\theta \, \theta_\rho \left[S \cos^2\varphi + T \sin^2\varphi \right]$$

$$+ \frac{2}{\rho} \sin^2\theta \sin\varphi \cos\varphi \, \varphi_\rho \left[-S + T \cos^2\theta + B \sin^2\theta \right]$$

$$- \frac{2}{\rho} \sin^2\theta \cos\varphi \, \theta_z S$$

$$+ \frac{2}{\rho} \sin^3\theta \cos\theta \sin\varphi \, \varphi_z \left[B - T \right]$$

$$+ 2 \sin\theta \cos\theta \sin\varphi \cos\varphi \, \theta_\rho \varphi_\rho \left[T - S \right]$$

$$+ 2 \sin\theta \cos\theta \cos\varphi \, \theta_\rho \theta_z \left[B - S \right]$$

$$+ 2 \sin^2\theta \sin\varphi \, \theta_z \varphi_\rho S$$

$$- 2 \sin^2\theta \sin\varphi \, \theta_\rho \varphi_z T$$

$$+ 2 \sin^3\theta \cos\theta \cos\varphi \, \varphi_\rho \varphi_z \left[B - T \right]$$

$$+ \sin^2\theta \cdot \Delta\chi \, H^2 \, .$$

$$\text{(AI.8)}$$

To find the energy minimum requires the application

of the Euler-Lagrange relations derived in Eqs. III.8-III.11

to the energy

$$E = 2\pi \int_{g=0}^{g_0} \int_{z=0}^{z_0} dg\, dz\, g\, F. \tag{AI.9}$$

The energy expression consists of the two independent

variables Θ and φ. The Θ-equations is obtained by applying

the function

$$T = \delta\Theta\left(\frac{\partial}{\partial\Theta} - \frac{\partial}{\partial g}\left(\frac{\partial}{\partial\Theta_g}\right) - \frac{\partial}{\partial z}\left(\frac{\partial}{\partial\Theta_z}\right)\right) \tag{AI.10}$$

to the integrand of Eq. AI.9 while the φ-equation

comes from applying the operator

$$P = \delta\varphi\left(\frac{\partial}{\partial\varphi} - \frac{\partial}{\partial g}\left(\frac{\partial}{\partial\varphi_g}\right) - \frac{\partial}{\partial z}\left(\frac{\partial}{\partial\varphi_z}\right)\right) \tag{AI.11}$$

to the integrand. This will be carried out term by term

to the integrand of Eq. AI.9 where F is defined by Eq. AI.8.

Applying the operator

$$Q = T + P \tag{AI.12}$$

to the first term produces

$$2\delta\Theta\left[\frac{1}{g}\sin\Theta\cos\Theta\left[S\cos^2\varphi + T\cos^2\Theta\sin^2\varphi\right.\right.$$
$$\left.+ B\sin^2\Theta\sin^2\varphi\right]$$
$$\left.+ \frac{1}{g}\sin^3\Theta\cos\Theta\sin^2\varphi\left[B-T\right]\right]$$
$$+ 2\delta\varphi\left[\frac{1}{g}\sin^2\Theta\sin\varphi\cos\varphi\left[-S+T\cos^2\Theta+B\sin^2\Theta\right]\right]$$

$$= 2\delta\Theta\left[\frac{1}{g}\sin\Theta\cos\Theta\left[S\cos^2\varphi + T(\cos^2\Theta-\sin^2\Theta)\sin^2\varphi\right.\right.$$
$$\left.+ 2B\sin^2\Theta\sin^2\varphi\right]$$
$$+ 2\delta\varphi\left[\frac{1}{g}\sin^2\Theta\sin\varphi\cos\varphi\left[-S+T\cos^2\Theta+B\sin^2\Theta\right].\right.$$

$$\tag{AI.13}$$

Applying Q to the second term gives

$$2\delta\theta\left[\rho\,\Theta_\rho^2\sin\theta\cos\theta\cos^2\varphi\,[B-S]\right.$$
$$\left.-\frac{\partial}{\partial\rho}\left[\rho\,\Theta_\rho\,[S\cos^2\theta\cos^2\varphi+T\sin^2\varphi+B\sin^2\theta\cos^2\varphi]\right]\right]$$
$$+2\delta\varphi\left[\rho\,\Theta_\rho^2\sin\varphi\cos\varphi\,[-S\cos^2\theta+T-B\sin^2\theta]\right]$$

$$=2\delta\theta\left[\rho\,\Theta_\rho^2\sin\theta\cos\theta\cos^2\varphi\,[S-B]\right.$$
$$+2\rho\,\Theta_\rho\,\Theta_\rho\sin\varphi\cos\varphi\,[S\cos^2\theta-T+B\sin^2\theta]$$
$$\left.-(\Theta_\rho+\rho\,\Theta_{\rho\rho})\,[S\cos^2\theta\cos^2\varphi+T\sin^2\varphi+B\sin^2\theta\cos^2\varphi]\right]$$
$$+2\delta\varphi\left[\sin\varphi\cos\varphi\,\rho\,\Theta_\rho^2\,[-S\cos^2\theta+T-B\sin^2\theta]\right]$$

(AI.14)

Applying Q to the third term gives

$$2\delta\theta\left[\rho\sin\theta\cos\theta\,\varphi_\rho^2\,[S\sin^2\varphi+T\cos^2\theta\cos^2\varphi+B\sin^2\theta\cos^2\varphi]\right.$$
$$\left.+\rho\sin^3\theta\cos\theta\,\varphi_\rho^2\cos^2\varphi\,[B-T]\right]$$
$$+2\delta\varphi\left[\rho\sin^2\theta\sin\varphi\cos\varphi\,\varphi_\rho^2\,[S-T\cos^2\theta-B\sin^2\theta]\right.$$
$$\left.-\frac{\partial}{\partial\rho}\left[\rho\sin^2\theta\,\varphi_\rho\,[S\sin^2\varphi+T\cos^2\theta\cos^2\varphi+B\sin^2\theta\cos^2\varphi]\right]\right]$$

$$=2\delta\theta\left[\rho\sin\theta\cos\theta\,\varphi_\rho^2\,[S\sin^2\varphi+2B\sin^2\theta\cos^2\varphi+T(\cos^2\theta-\sin^2\theta)\cos^2\varphi]\right.$$

$$+ 2\delta\varphi \left[g \sin^2\theta \sin\varphi \cos\varphi \, \varphi_g^2 \left[-S + T\cos^2\theta + B\sin^2\theta \right] \right.$$
$$- 2g \sin\theta \cos\theta \, \theta_g \varphi_g \left[S \sin^2\varphi + 2B \sin^2\theta \cos^2\varphi \right.$$
$$\left. - T(\sin^2\theta - \cos^2\theta)\cos^2\varphi \right]$$
$$- \sin^2\varphi (\varphi_g + g\varphi_{gg}) \left[S \sin^2\varphi + T \cos^2\theta \cos^2\varphi \right.$$
$$\left. \left. + B \sin^2\theta \cos^2\varphi \right] \right].$$

(AI.15)

Applying Q to the fourth term produces

$$2\delta\theta \left[g \theta_g^2 \sin\theta \cos\theta \, [S-B] \right.$$
$$\left. - \frac{\partial}{\partial g} \left[g \theta_g [S \sin^2\theta + B \cos^2\theta] \right] \right]$$

$$= 2\delta\theta \left[g \sin\theta \cos\theta \, \theta_g^2 \, [B-S] \right.$$
$$\left. - g \theta_{gg} [S \sin^2\theta + B \cos^2\theta] \right].$$

(AI.16)

Applying Q to the fifth term gives

$$2\delta\theta \left[g \sin\theta \cos\theta \, \varphi_g^2 \, [T\sin^2\theta + B\cos^2\theta] \right.$$
$$\left. + g \sin^3\theta \cos\theta \, \varphi_g^2 \, [T-B] \right]$$
$$+ 2\delta\varphi \left[-\frac{\partial}{\partial g} \left[g \sin^2\theta \, \varphi_g [T\sin^2\theta + B\cos^2\theta] \right] \right]$$

$$= 2\delta\theta \left[g \sin\theta \cos\theta \, \varphi_g^2 \, [2T\sin^2\theta + B(\cos^2\theta - \sin^2\theta)] \right]$$
$$+ 2\delta\varphi \left[-g \sin\theta \cos\theta \, \theta_g \varphi_g \, [4T\sin^2\theta \right.$$
$$+ 2B(\cos^2\theta - \sin^2\theta)]$$
$$\left. - g \sin^2\theta \, \varphi_{gg} \, [T\sin^2\theta + B\cos^2\theta] \right].$$

(AI.17)

Applying Q to the sixth term gives

$$2\delta\theta\left[(\cos^2\theta-\sin^2\theta)\,\theta_g\,[S\cos^2\varphi+T\sin^2\varphi]\right.$$
$$\left.-\frac{\partial}{\partial g}[\sin\theta\cos\theta\,[S\cos^2\varphi+T\sin^2\varphi]]\right]$$
$$+2\delta\varphi\left[2\sin\theta\cos\theta\sin\varphi\cos\varphi\,\theta_g\,[T-S]\right]$$

$$=2\delta\theta\left[2\sin\theta\cos\theta\sin\varphi\cos\varphi\,\varphi_g\,[S-T]\right]$$
$$+2\delta\varphi\left[2\sin\theta\cos\theta\sin\varphi\cos\varphi\,\theta_g\,[T-S]\right].$$

$$\text{(AI.18)}$$

Applying Q to the seventh term produces

$$2\delta\theta\left[2\sin\theta\cos\theta\sin\varphi\cos\varphi\,\varphi_g\,[-S+T\cos^2\theta\right.$$
$$+B\sin^2\theta]$$
$$\left.+2\sin^3\theta\cos\theta\sin\varphi\cos\varphi\,\varphi_g\,[B-T]\right]$$
$$+2\delta\varphi\left[\sin^2\theta\,(\cos^2\varphi-\sin^2\varphi)\,\varphi_g\,[-S+T\cos^2\theta\right.$$
$$+B\sin^2\theta]$$
$$\left.-\frac{\partial}{\partial g}[\sin^2\theta\sin\varphi\cos\varphi\,[-S+T\cos^2\theta+B\sin^2\theta]]\right]$$

$$=2\delta\theta\left[2\sin\theta\cos\theta\sin\varphi\cos\varphi\,\varphi_g\,[-S+2B\sin^2\theta\right.$$
$$\left.+T(\cos^2\theta-\sin^2\theta)]\right]$$
$$+2\delta\varphi\left[2\sin\theta\cos\theta\sin\varphi\cos\varphi\,\theta_g\,[S-2B\sin^2\theta\right.$$
$$\left.+T(\sin^2\theta-\cos^2\theta)]\right].$$

$$\text{(AI.19)}$$

Applying Q to the eighth term gives

$$2\delta\theta\left[-2\sin\theta\cos\theta\cos\varphi\,\theta_g\,S\right.$$
$$\left.+\frac{\partial}{\partial g}[\sin^2\theta\cos\varphi\,S]\right]$$

$$+ 2\delta\varphi\left[\sin^2\theta \sin\varphi\, \theta_z S\right]$$

$$= 2\delta\theta\left[-\sin^2\theta \sin\varphi\, \varphi_z S\right]$$
$$+ 2\delta\varphi\left[\sin^2\theta \sin\varphi\, \theta_z S\right].$$

(AI.20)

Applying Q to the ninth term produces

$$2\delta\theta\left[(3\sin^2\theta\cos^2\theta - \sin^4\theta)\sin\varphi\, \varphi_z [B-T]\right]$$
$$+ 2\delta\varphi\left[\sin^3\theta\cos\theta\cos\varphi\, \varphi_z [B-T]\right.$$
$$\left. - \frac{\partial}{\partial z}\left[\sin^3\theta\cos\theta\sin\varphi[B-T]\right]\right]$$

$$= 2\delta\theta\left[\sin^2\theta\,(3\cos^2\theta - \sin^2\theta)\sin\varphi\, \varphi_z [B-T]\right]$$
$$+ 2\delta\varphi\left[-\sin^2\theta\,(3\cos^2\theta - \sin^2\theta)\sin\varphi\, \theta_z [B-T]\right].$$

(AI.21)

Applying Q to the tenth term produces

$$2\delta\theta\left[\rho(\cos^2\theta - \sin^2\theta)\sin\varphi\cos\varphi\, \theta_\rho\, \varphi_\rho [T-S]\right.$$
$$\left. - \frac{\partial}{\partial\rho}\left[\rho\sin\theta\cos\theta\sin\varphi\cos\varphi\, \varphi_\rho [T-S]\right]\right]$$
$$+ 2\delta\varphi\left[\rho\sin\theta\cos\theta\,(\cos^2\varphi - \sin^2\varphi)\theta_\rho\, \varphi_\rho [T-S]\right.$$
$$\left. - \frac{\partial}{\partial\rho}\left[\rho\sin\theta\cos\theta\sin\varphi\cos\varphi\, \theta_\rho [T-S]\right]\right].$$

$$= 2\delta\theta\left[-\sin\theta\cos\theta[T-S]\left(\sin\varphi\cos\varphi(\varphi_\rho + \rho\,\varphi_{\rho\rho})\right)\right.$$
$$\left. + \rho(\cos^2\varphi - \sin^2\varphi)\varphi_\rho\right]$$

$$+ 2\delta\varphi\left[-\sin\varphi\cos\varphi[T-S]\left(\begin{array}{l}\sin\theta\cos\theta(\theta_\rho + \rho\,\theta_{\rho\rho})\\ + \rho(\cos^2\theta - \sin^2\theta)\theta_\rho^2\end{array}\right)\right].$$

$$(AI.22)$$

Applying Q to the eleventh term gives

$$2\delta\theta\left[\begin{array}{l}\rho(\cos^2\theta - \sin^2\theta)\cos\varphi\,\theta_\rho\,\theta_z\,[B-S]\\ -\dfrac{\partial}{\partial\varphi}[\rho\sin\theta\cos\theta\cos\varphi\,\theta_z\,[B-S]]\\ -\dfrac{\partial}{\partial z}[\rho\sin\theta\cos\theta\cos\varphi\,\theta_\rho\,[B-S]]\end{array}\right]$$
$$+2\delta\varphi[\rho\sin\theta\cos\theta\sin\varphi\,\theta_\rho\,\theta_z\,[S-B]]$$

$$= 2\delta\theta\left[[B-S]\left(\begin{array}{l}-\sin\theta\cos\theta\cos\varphi(\theta_z + 2\rho\,\theta_{zz})\\ +\rho\sin\theta\cos\theta\sin\varphi(\theta_z\,\varphi_\rho + \theta_\rho\,\varphi_z)\\ -\rho(\cos^2\theta - \sin^2\theta)\cos\varphi\,\theta_\rho\,\theta_z\end{array}\right)\right]$$
$$+2\delta\varphi[\rho\sin\theta\cos\theta\sin\varphi\,\theta_\rho\,\theta_z\,[S-B]].$$

$$(AI.23)$$

Applying Q to the twelfth term gives

$$2\delta\theta\left[\begin{array}{l}2\rho\sin\theta\cos\theta\sin\varphi\,\theta_z\,\varphi_z\,S\\ -\dfrac{\partial}{\partial z}[\rho\sin^2\theta\sin\varphi\,\varphi_z\,S]\end{array}\right]$$
$$+2\delta\varphi\left[\begin{array}{l}\rho\sin^2\theta\cos\varphi\,\theta_z\,\varphi_z\,S\\ -\dfrac{\partial}{\partial\varphi}[\rho\sin^2\theta\sin\varphi\,\theta_z\,S]\end{array}\right]$$

$$= 2\delta\theta[-\rho\sin^2\theta(\cos\varphi\,\varphi_\rho\,\varphi_z + \sin\varphi\,\varphi_{\rho z})S]$$
$$+2\delta\varphi[-(\sin\theta(\theta_z + \rho\,\theta_{\rho z}) + 2\rho\cos\theta\,\theta_\rho\,\theta_z)\sin\theta\sin\varphi\,T].$$

$$(AI.24)$$

Applying Q to the thirteenth term produces

$$2\delta\Theta\left[-2\rho\sin\Theta\cos\Theta\sin\varphi\,\Theta_z\varphi_z T \atop +\frac{\partial}{\partial\varphi}[\rho\sin^2\Theta\sin\varphi\,\varphi_z T]\right]$$

$$+2\delta\varphi\left[-\rho\sin^2\Theta\cos\varphi\,\Theta_z\varphi_z T \atop +\frac{\partial}{\partial z}[\rho\sin^2\Theta\sin\varphi\,\Theta_z T]\right]$$

$$=2\delta\Theta\left[\sin^2\Theta\left(\sin\varphi(\varphi_z+\rho\varphi_{zz})+\rho\cos\varphi\,\varphi_z\varphi_z\right)T\right]$$
$$+2\delta\varphi\left[\rho\sin\Theta\sin\varphi\left(2\cos\Theta\,\Theta_z\Theta_z+\sin\Theta\,\Theta_{zz}\right)T\right].$$

$$(AI.25)$$

Applying Q to the fourteenth term produces

$$2\delta\Theta\left[\rho(3\sin^2\Theta\cos^2\Theta-\sin^4\Theta)\cos\varphi\,\varphi_z\varphi_z[B-T]\right]$$

$$+2\delta\varphi\left[-\rho\sin^3\Theta\cos\Theta\sin\varphi\,\varphi_z\varphi_z[B-T] \atop {=\frac{\partial}{\partial\varphi}[\rho\sin^3\Theta\cos\Theta\cos\varphi\,\varphi_z[B-T]] \atop -\frac{\partial}{\partial z}[\rho\sin^3\Theta\cos\Theta\cos\varphi\,\varphi_z[B-T]]}\right]$$

$$=2\delta\Theta\left[\rho\sin^2\Theta(3\cos^2\Theta-\sin^2\Theta)\cos\varphi\,\varphi_z\varphi_z[B-T]\right]$$
$$=2\delta\varphi\left[\sin^2\Theta\left(\rho\sin\Theta\cos\Theta\sin\varphi\,\varphi_z\varphi_z\right.\right.$$
$$-\rho(3\cos^2\Theta-\sin^2\Theta)\cos\varphi(\Theta_z\varphi_\varphi+\Theta_\varphi\varphi_z)$$
$$-\sin\Theta\cos\Theta\cos\varphi(2\rho\varphi_{\varphi z}+\varphi_z)$$
$$\left.\left.\times[B-T]\right)\right]$$

$$(AI.26)$$

Applying Q to the fifteenth term gives

$$2 \, \delta\Theta \left[\sin\Theta \cos\Theta \, \Delta\chi \, H^2 \right] . \tag{AI.27}$$

The variations of Θ and φ are independent. Collecting the terms in $\delta\Theta$, dividing by ρ and setting the sum equal to zero produces the Θ-equation, Eq. III.12. Similarly, collecting the terms in $\delta\varphi$, dividing by $\rho \sin^2\Theta$ and setting the sum equal to zero gives the φ-equation, Eq. III.13.

To produce the boundary conditions along the top and bottom surfaces requires the application of the operator

$$U = \delta\Theta \frac{\partial}{\partial\Theta_z} + \delta\varphi \frac{\partial}{\partial\varphi_z} \tag{AI.28}$$

to the integrand of the energy. The variations in Θ and φ are independent (for a horizontal surface) and thus Eq. AI.28 produces two separate equations. The Θ-boundary equation on the top and bottom surfaces after dividing by ρ is

$$0 = \Theta_z \left[S \sin^2\Theta + B \cos^2\Theta \right] - \frac{1}{\rho} \sin^2\Theta \cos\varphi \, S$$
$$+ \sin\Theta \cos\Theta \cos\varphi \, \Theta_z [B-S] + \sin^2\Theta \sin\varphi \, \varphi_z S \tag{AI.29}$$

while the φ-boundary equation after dividing by $\rho \sin^2\Theta$ is

$$0 = \varphi_z \left[T \sin^2\Theta + B \cos^2\Theta \right] + \frac{1}{\rho} \sin\Theta \cos\Theta \sin\varphi [B-T]$$
$$- \sin\varphi \, \Theta_z T + \sin\Theta \cos\Theta \cos\varphi \, \varphi_z [B-T] . \tag{AI.30}$$

To produce the boundary conditions along the inner surface at $\rho = 0$ and the outer surface (vertical surface of

the cylinder) requires the application of the operator

$$R = \delta\Theta \frac{\partial}{\partial\Theta_{\mathfrak{z}}} + \delta\varphi \frac{\partial}{\partial\varphi_{\mathfrak{z}}}$$

(AI.31)

to the integrand of the energy. The variations in Θ and φ are independent and so two equations are produced. The Θ -boundary equation on the inner and outer surfaces is

$$0 = \rho \,\Theta_{\mathfrak{z}} \left[S \cos^2\Theta \cos^2\varphi + T \sin^2\varphi + B \sin^2\Theta \cos^2\varphi \right]$$
$$+ \sin\Theta \cos\Theta \left[S \cos^2\varphi + T \sin^2\varphi \right]$$
$$+ \rho \sin\Theta \cos\Theta \sin\varphi \cos\varphi \, \varphi_{\rho} \left[T-S \right]$$
$$+ \rho \sin\Theta \cos\Theta \cos\varphi \, \Theta_{\mathfrak{z}} \left[B-S \right]$$
$$- \rho \sin^2\Theta \sin\varphi \, \varphi_{\mathfrak{z}} T$$

(AI.32)

while the φ -boundary equation is

$$0 = \rho \sin^2\Theta \,\varphi_{\mathfrak{z}} \left[S \sin^2\varphi + T \cos^2\Theta \cos^2\varphi \right.$$
$$\left. + B \sin^2\Theta \cos^2\varphi \right]$$
$$+ \sin^2\Theta \sin\varphi \cos\varphi \left[-S + T \cos^2\Theta + B \sin^2\Theta \right]$$
$$+ \rho \sin\Theta \cos\Theta \sin\varphi \cos\varphi \left[T-S \right]$$
$$+ \rho \sin^2\Theta \sin\varphi \, \Theta_{\mathfrak{z}} S$$
$$+ \rho \sin^3\Theta \cos\Theta \cos\varphi \, \varphi_{\mathfrak{z}} \left[B-T \right].$$

(AI.33)

APPENDIX II

THE FULL DROPLET

When discussing the droplet in Ch. III the assumption was made that the central section of the droplet could be replaced by a cylinder. This approximation overlooked many of the more complex features that occur in real droplets. The main topological feature brushed aside is the presence of point disclinations or surface distortions called nipples, which occur where the axis of symmetry cuts the surfaces. The reason for having such features is to avoid the contradictory requirement of having $\theta=\theta_{SUR}$ at the surface for all radii while also having $\theta=0$ on the axis of symmetry for all z. Within the confines of the continuum theory used here one can avoid this dilemma by allowing the surface to distort by taking into account the finite value of the surface tension or by relaxing the hard pinning condition through a finite coefficient of pinning, or to do both. Beyond this one can appeal to behavior on a molecular level to treat the difficulty.

On a surface parallel to the ρ-ϕ plane, the hard pinning condition is

$$\theta(Z_{SUR}) = \theta_{SUR} \qquad (AII.1)$$

where Z_{SUR} refers to the z-coordinate of the surface.

When the surface is inclined by the angle

- 118 -

$$\psi = \tan^{-1}\left(\frac{dz_{SUR}}{d\rho}\right) \qquad \text{(AII.2)}$$

to the horizontal plane, Eq. AII.1 is incorrect since the cone of easy pinning is no longer parallel to the axis of symmetry. The hard pinning condition then becomes

$$(\hat{n} \cdot \hat{\imath})^2 = \cos^2\theta_{SUR} \qquad \text{(AII.3)}$$

where

$$\hat{\imath} = -\hat{\rho}\,\sin\psi + \hat{z}\,\cos\psi \qquad \text{(AII.4)}$$

is the perpendicular to the surface. The quadratic dependence is due to the indistinguishability of $\hat{n}$ and $-\hat{n}$.

From Eqs. AII.3, AII.4, and the definition of the director, Eq. III.2, one has

$$0 = (\cos\theta\,\cos\psi - \sin\theta\,\cos\phi\,\sin\psi)^2 - \cos^2\theta_{SUR} \qquad \text{(AII.5a)}$$

$$= q(\theta, \phi, \psi, \theta_{SUR}) \qquad \text{(AII.5b)}$$

as the relationship between the various angles required to satisfy the condition of hard pinning.

The energy density involved in the deviations from hard pinning can be written as

$$h = K\,q^2 \qquad \text{(AII.6)}$$

where K is the pinning elastic constant. The quadratic depen-zero when the surface is flat ($\psi = 0$) and $\theta = \theta_{SUR}$, 0, or $\pi/2$ since these are all possible equilibrium configurations.

the equilibrium configuration.

The size of the region in which these distortions

are important can be estimated by comparing the relative
strengths of the appropriate physical constants. For example,
the characteristic length of the surface distortions should
be of the order of B/σ where B is the bend elastic constant,
typically 10^{-6} dynes, while σ is the interfacial surface tension,
typically 10 dynes/cm. This gives a characteristic fall-off
length of 10 Å. Similarly the characteristic length for the
relaxation from hard pinning should be B/K which again is of
the order of 10 Å for reasonable values of K. Thus the distor-
tion region is of molecular size in extent.

The energy of the total system consisting of a droplet,
medium 1, at the interface between two isotropic media, 2 and
3, can be written as

$$E = 2\pi \int_{\rho=0}^{\rho_0} \int_{z_{LS}(\rho)}^{z_{US}(\rho)} d\rho \, dz \, \rho \, F$$
$$+ 2\pi \int_{\rho=0}^{\rho_0} d\rho \, \rho \left[\sigma_{12} \sec \psi_{US}(z_{US}) + \sigma_{13} \sec \psi_{LS}(z_{LS}) \right]$$
$$+ 2\pi \int_{\rho=\rho_0}^{\infty} d\rho \, \rho \, \sigma_{23}$$
$$+ 2\pi \int_{\rho=0}^{\rho_0} \left[K_{US} \, q_{US}^2 + K_{LS} \, q_{LS}^2 \right]$$

$$(AII.7)$$

where ρ_0 is the radius of the drop, $z_{US}(\rho)$ is the z-coordinate
of the upper surface, F is the energy density as defined in

Eq. AI.8, σ_{ij} is the interfacial surface tension between medium i and medium j, and the other quantities are as previously defined. The subscript LS refers to the same quantities on the lower surface.

The four terms in Eq. AII.7 refer to the energy associated with the volume, the top and bottom surfaces of the droplet, the interface outside the droplet, and the relaxation in the pinning, respectively.

In addition there is one constraint, namely that the volume of the droplet

$$V = 2\pi \int_{\rho=0}^{\rho_0} \int_{z_{LS}(\rho)}^{z_{US}(\rho)} d\rho \, dz \, \rho$$

(AII.8)

is a fixed quantity. The radius of the droplet, ρ_0, must be solved as part of the variational problem that minimizes the energy. The quantity upon which the variation is performed is

$$E^* = E + \lambda V \qquad (AII.9)$$

where λ is a Lagrange undetermined multiplier. The whole procedure can be formally carried out but is too complicated to be useful. The volume equations that would be produced are the same as Eqs. III.12 and III.13. The four surface equations of App. I get combined into one larger equation related by the angle of inclination ψ and the relation between the variations in θ and ϕ on the surface which can be found from Eq. AII.5. In addition, the shape and position of the surface

becomes part of the problem to be solved which requires the
use of a continually variable grid system. Such problems have
never been successfully solved. The best that can be done is
to guess an answer and then to try to determine how to correct the
guess. This technique has been discussed by Garabedian (Ga-64)
who tried to apply it with only limited success.

In view of the small size of the expected surface
distortions one can consider the droplet to be a lens whose
shape is determined by minimizing the surface energy neglecting
the volume effects. This procedure has been discussed fully
by Princen (Pr-69). The lens will have small distortions at
the poles and at the equator which are of molecular size in
extent.

APPENDIX III

COMPUTER CALCULATION FOR THE TORQUE EQUATIONS

Because of the cylindrical symmetry observed in the
nematic liquid crystal droplets, the problem of the orientation
of the molecules has been reduced from a three-dimensional to
a two-dimensional exercise. The calculation will be performed
in the rectangular region bounded by the horizontal lines
$z=0$ and $z=Z_0$ and the vertical lines $\rho=0$ and $\rho=\rho_0$.

The problem will be solved by simple relaxation techniques,
that is, a trial solution will be guessed and the computer
will keep correcting the intermediate answers until it has
reached a stable solution satisfying all the necessary equations.

Rather than trying to solve all the equations applicable
at a point simultaneously it was found advantageous to define
a particular equation as being the θ-equation which would
generate a value of θ or the ϕ-equation which would produce
a value of ϕ at the point of interest.

A further simplification was made by breaking each equat-
ion into two parts. The iterative part contains two terms that
will generate the new value for the variable being used. In
the bulk equations this term would consist of the two second
derivatives, $\dfrac{\partial^2}{\partial\rho^2}$ and $\dfrac{\partial^2}{\partial z^2}$ of the variable being iterated by
that equation, either θ or ϕ. All other terms get lumped together

in what is called the source term. The source term gets calculated using the old values for the variables at the point.

The surface terms get handled in the same fashion except that now the iterative term picks out one first derivative and all other terms become source terms evaluated using the old values of the variables at the point. This process will be made more explicit as each term is handled.

The handling of the derivatives will be discussed first. The derivatives are determined using a central-difference scheme obtainable from a Taylor series expansion about the point of interest. For example, to obtain the first and second derivatives of θ in the radial direction one can write for the point at larger radius

$$\theta(\rho+\Delta\rho,z) = \theta(\rho,z) + (\Delta\rho)\,\theta_\rho(\rho,z) + \tfrac{1}{2}(\Delta\rho)^2\,\theta_{\rho\rho}(\rho,z)$$

(AIII.1a)

while for the point at smaller radius one has

$$\theta(\rho-\Delta\rho,z) = \theta(\rho,z) - (\Delta\rho)\,\theta_\rho(\rho,z) + \tfrac{1}{2}(\Delta\rho)^2\,\theta_{\rho\rho}(\rho,z).$$

(AIII.1b)

Subtracting these two equations produces

$$\theta_\rho(\rho,z) = \frac{\theta(\rho+\Delta\rho,z) - \theta(\rho-\Delta\rho,z)}{2(\Delta\rho)}$$

(AIII.2)

while adding gives

$$\Theta_{\rho\rho}(\rho,z) = \frac{\Theta(\rho+\Delta\rho,z) + \Theta(\rho-\Delta\rho,z) - 2\Theta(\rho,z)}{(\Delta\rho)^2}$$

(AIII.3)

In a similar fashion one can show that

$$\Theta_z(\rho,z) = \frac{\Theta(\rho,z+\Delta z) - \Theta(\rho,z-\Delta z)}{2(\Delta z)}$$

(AIII.4)

and

$$\Theta_{zz}(\rho,z) = \frac{\Theta(\rho,z+\Delta z) + \Theta(\rho,z-\Delta z) - 2\Theta(\rho,z)}{(\Delta z)^2}$$

(AIII.5)

Writing the Taylor series with both $\Delta\rho$ and Δz non-zero for the four points given by $\rho\pm\Delta\rho$, $z\pm\Delta z$ allow one to determine the cross second derivatives as

$$\Theta_{\rho z}(\rho,z) = \frac{\begin{pmatrix}\Theta(\rho+\Delta\rho,z+\Delta z) + \Theta(\rho-\Delta\rho,z-\Delta z) \\ -\Theta(\rho+\Delta\rho,z-\Delta z) - \Theta(\rho-\Delta\rho,z+\Delta z)\end{pmatrix}}{4(\Delta\rho)(\Delta z)}$$

(AIII.6)

An analogous set of equations exists for the various derivatives of ϕ.

With the above definitions the bulk equations can now be handled.

The θ-equation, Eq. III.12, can be written as

$$\theta_{\rho\rho} K(\theta,\varphi) + \theta_{zz} L(\theta,\varphi)$$
$$= TSR (\rho, \theta, \varphi, \theta_\rho, \theta_{\rho z}, \varphi_\rho, \varphi_{\rho\rho}, \varphi_{\rho z})$$

(AIII.7)

where $K(\theta,\phi)$ and $L(\theta,\phi)$ are the coefficients of $\theta_{\rho\rho}$ and θ_{zz} respectively, while TSR, the source term, contains all the remaining terms of the equation . Using the expansions derived for $\theta_{\rho\rho}$ and θ_{zz} one can now write

$$\left(\frac{\theta(\rho+\Delta\rho, z) + \theta(\rho-\Delta\rho, z) - 2\theta(\rho, z)}{(\Delta\rho)^2} \right) K(\theta,\varphi)$$
$$+ \left(\frac{\theta(\rho, z+\Delta z) + \theta(\rho, z-\Delta z) - 2\theta(\rho, z)}{(\Delta z)^2} \right) L(\theta,\varphi)$$
$$= TSR$$

(AIII.8)

This equation can be solved for $\theta_{new}(\rho, z)$, the new value of θ at the point (ρ, z), in terms of the values of θ at the nearest neighbour points and the old values of θ and ϕ at (ρ, z) which get used in K, L, and TSR. Rearranging the terms results in

$$\Theta_{new}(\rho,z) = \frac{\left[\begin{array}{l}\left(\dfrac{\Theta(\rho+\Delta\rho,z)+\Theta(\rho-\Delta\rho,z)}{(\Delta\rho)^2}\right)K(\Theta,\varphi) \\[4mm] +\left(\dfrac{\Theta(\rho,z+\Delta z)+\Theta(\rho,z-\Delta z)}{(\Delta z)^2}\right)L(\Theta,\varphi) \\[4mm] -TSR\end{array}\right]}{\left[\dfrac{2K(\Theta,\varphi)}{(\Delta\rho)^2}+\dfrac{2L(\Theta,\varphi)}{(\Delta z)^2}\right]}$$

(AIII.9)

Similarly from the ϕ-equation, Eq. III.13, one can solve for a new value of ϕ at the point (ρ,z). One finds

$$\varphi_{new}(\rho,z) = \frac{\left[\begin{array}{l}\left(\dfrac{\varphi(\rho+\Delta\rho,z)+\varphi(\rho-\Delta\rho,z)}{(\Delta\rho)^2}\right)M(\Theta,\varphi) \\[4mm] +\left(\dfrac{\varphi(\rho,z+\Delta z)+\varphi(\rho,z-\Delta z)}{(\Delta z)^2}\right)N(\Theta,\varphi) \\[4mm] -PSR\end{array}\right]}{\left[\dfrac{2M(\Theta,\varphi)}{(\Delta\rho)^2}+\dfrac{2N(\Theta,\varphi)}{(\Delta z)^2}\right]}$$

(AIII.10)

where $M(\theta,\phi)$ and $N(\theta,\phi)$ are the coefficients of $\phi_{\rho\rho}$ and ϕ_{zz}, respectively, while PSR contains all the remaining terms of the equation.

These algorithms get applied at all grid points in the

interior of the region of interest.

The boundary terms will now be considered. The first thing one finds is that some of the derivatives at the boundary must be changed since it is not possible to define a central-difference for them. For example, along the outer surface, the expansion of $\theta(\rho, z)$ would require a value for $\theta(\rho_0 - \Delta\rho, z)$ and $\theta(\rho_0 + \Delta\rho, z)$ as in Eq. AIII.2. However, $\theta(\rho_0 + \Delta\rho, z)$ does not exist since ρ_0 is the largest radius under consideration. One must therefore make a special case here, defining the backward-difference as

$$\theta_\rho(\rho_0, z) = \frac{\theta(\rho_0, z) - \theta(\rho_0 - \Delta\rho, z)}{\Delta\rho}$$

(AIII.11)

with an analogous expression for $\phi_\rho(\rho_0, z)$.

Along the top and bottom surfaces similar problems arise with the z-derivatives. Therefore along the bottom surface one uses a forward-difference for ϕ_z:

$$\phi_z(\rho, 0) = \frac{\phi(\rho, \Delta z) - \phi(\rho, 0)}{\Delta z}$$

(AIII.12a)

while along the top surface the backwards-difference

$$\phi_z(\rho, z_0) = \frac{\phi(\rho, z_0) - \phi(\rho, z_0 - \Delta z)}{\Delta z}$$

(AIII.12b)

- 129 -

is required.

Analogous expressions exist for the derivatives of θ with respect to z along the top and bottom surfaces.

The boundary equations were derived in App. I and discussed in Ch. III. In the situation of interest, the angle θ is assumed to be pinned at some well-known values along the top and bottom surfaces. The equation from which ϕ will be determined is Eq. III.19 which can be written as

$$P(\theta,\varphi)\, \varphi_z(\zeta, z_{sur}) = PSRB(\zeta, \theta, \theta_\zeta, \varphi, \varphi_\zeta)$$

(AIII.13)

where $P(\theta,\phi)$ is the coefficient of ϕ_z and PSRB is the source term containing all the remaining terms of the equation. Again the technique is to use the old value for ϕ in PSRB and then calculate a new value for ϕ on the surface. Along the bottom surface, using Eq. AIII.12a, one has

$$\left(\frac{\varphi(\zeta,\Delta z) - \varphi(\zeta,0)}{\Delta z}\right) P(\theta,\varphi) = PSRB .$$

(AIII.14)

Therefore one finds for the new value of ϕ along the bottom surface the expression

$$\varphi_{new}(\zeta,0) = \varphi(\zeta,\Delta z) - PSRB\left(\frac{\Delta z}{P(\theta,\varphi)}\right) .$$

(AIII.15a)

Similarly along the top surface one finds

$$\varphi_{new}(g, Z_o) = \varphi(g, Z_o - \Delta z) + PSRB\left(\frac{\Delta z}{P(\Theta, \varphi)}\right).$$

<div align="right">(AIII.15b)</div>

This technique can be applied to all points along the top and bottom surfaces except the four corner points $(0, 0)$, $(0, z_o)$, $(\rho_o, 0)$, and (ρ_o, z_o) because the values of θ_ρ and ϕ_ρ are required to evaluate PSRB. These derivatives cannot be obtained with a central-difference approximation at the end points. Though one could use a forward- or backward-difference to define them, it was decided to treat them differently. They will be discussed later.

The outer surface is handled in much the same fashion. From Eq. III.14 one can write

$$\Theta_g \; Q(\Theta, \varphi) = TSRO(g, \Theta, \Theta_z, \varphi, \varphi_g, \varphi_z)$$

<div align="right">(AIII.16)</div>

where $Q(\theta, \phi)$ is the coefficient of θ_ρ and TSRO contains all the remaining terms of the equation. Using the backward-difference defined by Eq. AIII.11 one finds

$$\Theta_{new}(g_o, z) = \Theta(g_o - \Delta g, z) + \left(\frac{\Delta g}{Q(\Theta, \varphi)}\right) TSRO.$$

<div align="right">(AIII.17)</div>

Similarly from Eq. III.15 one has

$$\varphi_{new}(g_o, z) = \varphi(g_o - \Delta g, z) + \left(\frac{\Delta g}{R(\Theta, \varphi)}\right) PSRO$$

<div align="right">(AIII.18)</div>

where $R(\theta,\phi)$ is the coefficient of ϕ_ρ while PSRO contains all the remaining terms of the equation.

Again one cannot determine ϕ at the points $(\rho_o,0)$ and (ρ_o,Z_o) since PSRO requires the derivatives θ_z and ϕ_z which cannot be determined with a central-difference formula on the boundary. They will be treated after the axis of symmetry has been discussed.

As shown by Eq. III.16 along the axis of symmetry θ must be zero. Eq. III.15 was satisfied identically at $\rho=0$. Thus there is no boundary condition that has to be satisfied by ϕ along the axis of symmetry. The fact that ϕ must be an analytic function was made use of to perform the iteration. This was done by making a Taylor expansion about a point $2\Delta\rho$ away from the origin. One can show that

$$\varphi(0,z) = 3(\varphi(\Delta\rho,z) - \varphi(2\Delta\rho,z)) + \varphi(3\Delta\rho,z).$$

$$(AIII.19)$$

This process is valid for all points on the axis of symmetry including the points $(0,0)$ and $(0,Z_o)$.

The values for ϕ at the two points $(\rho_o,0)$ and (ρ_o,Z_o) on the outside surface which could not be previously determined can be found in a similar fashion. One can show that

$$\varphi(\rho_o,0) = 3(\varphi(\rho_o-\Delta\rho,0) - \varphi(\rho_o-2\Delta\rho,0)) + \varphi(\rho_o-3\Delta\rho,0)$$

$$(AIII.20a)$$

and similarly

$$\varphi(\rho_0, z_0) = 3\left(\varphi(\rho_0 - \Delta\rho, z_0) - \varphi(\rho_0 - 2\Delta\rho, z_0)\right) + \varphi(\rho_0 - 3\Delta\rho, z_0).$$

(AIII.20b)

Therefore every point in the system is either defined outright (θ values at the top and bottom surfaces), or else it has an equation from which it can be determined in the iteration scheme.

The only computational problem remaining is the size of the grid to be used. One wants to keep the number of grid points as small as possible because of the time required by the computer. On the other hand, to ensure accuracy and stability one requires a high density of points. In particular one needs a high density of points near the axis of symmetry close to the surfaces since in these regions θ is changing very rapidly. One also wants a high density of points near the surfaces so that the effects of the surface equations don't propagate too deeply into the bulk.

All these requirements can be met by having a variable grid with a high density of points near the surfaces and a lower density as one proceeds into the interior of the region. A typical grid system used is indicated in App. IV for a rectangle 19 units high and 80 units in radius. This system contains 30 grid points in the z-direction and 39 grid points in the ρ-direction.

In any iterative pass first θ and then φ is calculated

at each point starting at the smallest radius, sweeping through the height of the rectangle and then going on to the next radius. Then the boundary conditions are applied. For a grid size of 30x39 points each pass took about 2 seconds. Starting from a reasonable guess it would take about 1500 passes or 60 minutes of computer time for the solution to become stable. For the equilibrium solutions in which ϕ is zero everywhere, part of the program could be bypassed and the convergence could be reached in less than 10 minutes of computer time.

After stability had been reached, the energy density given by Eq. AI.8 was calculated, multiplied by the appropriate volume elements and summed.

The calculations are performed in the computer program B3C5 shown at the end of this appendix.

There are two further points that deserve mention. The first was hinted at when the rectangular region was said to be 19 units high and 80 units in radius. The reason for this is that the solution obtained is the solution for all cylinders with this particular aspect ratio. No absolute length entered the problem and so the solutions of different sized rectangles with the same aspect ratio will scale linearly with the absolute size picked. In practice an absolute size is picked only once one decides to do the optics of the resultant configuration.

The second feature is that the equilibrium configurations depend on the relative values of the elastic constants rather than their absolute magnitudes. All the torque equations were divided by the bend elastic constant and thus the configurations are functions of S/B and T/B (and $\bot$/B if a magnetic field is present). The total energy of these configurations scale linearly with the magnitude of the bend elastic constant.

The computer program in which these steps are performed, B3C5, follows.

```
//A122P3C5 JOB (****,*****),'PRESS',TIME=10                                  JOB  3
//*JCPPARM FCRMS=6819
// EXEC FORTGCLG,TIME.GC=10,NEPUNCH=
//FORT.SYSIN DC *
C  ALL LENGTHS IN MICRCNS
C  WORKING ON DROP WITH ZSUR=15, RAD=10
       CIMENSICN T(39,30),P(39,30),NPR(30),RAD(39),F(39,30),FTI(39),DR(39
      1),NDR(39),FP(15),NPZ(30),DZA(30),NDZ(30),Z(30),XT(30),XP(30)
C  INITIALIZE BCUNDARY CONDITIONS
       TLS=3.14159*90./180.
       TLS=3.14159*15./180.
       FKS=1.
       H=0.
       H2=H*H
       SK=.8
       TK=.5
       DST=SK-TK
       CSF=SK-1.
       DTR=TK-1.
       NPW=40
       TPFS=2.5
       TTF=FLOAT(NPW)*TPPS+10.
       JM=30
       IM=39
       JM1=JM-1
       IM1=IM-1
C  RAD MATRIX IS ACTUAL RADIAL DISTANCE CF POINT
       READ(5,4)RAD
    4  FCRMAT(10F6.2)
       WRITE(6,17)RAD
    6  FCRMAT(1X,22F6.2)
   17  FCRMAT(5X,'RADII TO BE USED ARE',/1X,20F6.2,/1X,19F6.2)
       DO 70 I=1,IM1
   70  DR(I)=RAD(I+1)-RAD(I)
       DO 71 I=2,IM1
       IF(DR(I)-DR(I-1))72,73,74
   72  NDR(I)=-1
       GC TC 71
   73  NDR(I)=0
       GC TC 71
   74  NDR(I)=1
   71  CCNTINUE
       WRITE(6,16)(NDR(I),I=2,IM1)
   16  FCRMAT(7X,19I6,/2X,19I6)
       READ(5,18)Z
   18  FCRMAT(10F6.2)
       DO 870 J=1,JM1
  870  DZA(J)=Z(J+1)-Z(J)
       DO 871 J=2,JM1
       IF(DZA(J)-DZA(J-1))872,873,874
  872  NDZ(J)=-1
       GO TO 871
  873  NDZ(J)=0
       GC TO 871
  874  NDZ(J)=1
  871  CCNTINUE
       WRITE(6,19)Z
   19  FORMAT(5X,'Z VALUES TO BE USED ARE',2(/2X,15F6.2))
       WRITE(6,20)(NDZ(J),J=2,JM1)
   20  FCRMAT(7X,14I6,/1X,14I6)
```

```
      WRITE(6,22)(RAD(I),I=1,IM,2)
   22 FORMAT(//1X,22F6.2)
C IJK=1 FOR DECK INPUT,=-1 FOR GENERATED INPUT,=C FOR MODIFIED INPUT
      IJK=1
      IF(IJK)961,963,962
  962 DO 960 I=1,IM
      READ(5,8)(T(I,J),J=1,JM)
      READ(5,8)(P(I,J),J=1,JM)
  960 CONTINUE
      GO TO 85
  961 DO 820 I=1,IM
      DO 820 J=1,JM
      P(I,J)=C.
  820 CONTINUE
      DO 821 I=1,IM
      T(I,1)=TLS
  821 T(I,JM)=TUS
      GO TO 85
C NCOPR=NO. OF RADII CARRIED OVER FROM PREVICUS PROGRAM
  963 NCCPR=24
C NPR=I VALUES CORRESPONDING TO PREVICUS PROGRAM
      READ(5,15)(NPR(I),I=1,NCOPR)
   15 FORMAT(10I5)
C NCOPZ =NO OF Z VALUES CARRIED OVER FROM PREVICUS PROGRAM
      NCOPZ=30
      READ(5,15)(NPZ(I),I=1,NCOPZ)
      WRITE(6,15)(NPR(I),I=1,NCOPR)
      WRITE(6,15)(NPZ(I),I=1,NCOPZ)
      DO 970 N=1,NCCPR
      I=NPR(N)
      READ(5,8)(XT(J),J=1,NCOPZ)
      READ(5,8)(XP(J),J=1,NCOPZ)
      DO 950 M=1,NCOPZ
      J=NPZ(M)
      T(I,J)=XT(M)
      P(I,J)=XP(M)
      IF(M-2)990,991,991
  991 JP=NPZ(M-1)
      IF(J-JP-1)990,990,992
  992 DT=(T(I,J)-T(I,JP))/(Z(J)-Z(JP))
      DP=(P(I,J)-P(I,JP))/(Z(J)-Z(JP))
      JL=JP+1
      JU=J-1
      DO 993 K=JL,JU
      T(I,K)=(Z(K)-Z(JP))*DT+T(I,JP)
  993 P(I,K)=(Z(K)-Z(JP))*DP+P(I,JP)
  990 CONTINUE
      IF(N-2)970,971,971
  971 IP=NPR(N-1)
      IF(I-IP-1)970,970,972
  972 DO 973 J=1,JM
      DT=(T(I,J)-T(IP,J))/(RAD(I)-RAD(IP))
      DP=(P(I,J)-P(IP,J))/(RAD(I)-RAD(IP))
      II=IP+1
      IU=I-1
      DO 973 K=II,IU
      T(K,J)=(RAD(K)-RAD(IP))*DT+T(IP,J)
  973 P(K,J)=(RAD(K)-RAD(IP))*DP+P(IP,J)
  970 CONTINUE
      DO 974 J=2,JM1
```

```
974  T(1.J)=0.
 85  DO 60 J=1.JM
     K=JM-J+1
     WRITE(6.2)7(K).(T(I.K).I=1.IM.2)
  2  FORMAT(1X.F6.3/1X.22F6.3)
     WRITE(6.3)(P(I.K).I=1.IM.2)
  3  FORMAT(1X.22F6.3)
 60  CONTINUE
     T55=T(5.5)
     P55=P(5.5)
     NPASS=0
150  NPASS=NPASS+1
C ITERATION OF THE AND PHI FOR I>1
180  DO 100 I=2.IM1
     RR=1./RAD(I)
     RR2=RR*RR
     IF(NDR(I))80.81.82
 80  II=I-1
     IR=I+2
     DRI=DR(I-1)
     GO TO 182
 81  II=I-1
     IR=I+1
     DRI=DR(I)
     GO TO 182
 82  II=I-2
     IR=I+1
     DRI=DR(I)
182  DRR2=DRI*DRI
     D2R=2.*DRI
181  DO 100 J=2.JM1
     IF(NDZ(J))680.681.682
680  JA=J+2
     JB=J-1
     DZ=DZA(J-1)
     GO TO 183
681  JA=J+1
     JB=J-1
     DZ=DZA(J)
     GO TO 183
682  JA=J+1
     JB=J-2
     DZ=DZA(J)
183  DZ2=DZ*DZ
     D2Z=2.*DZ
     DRN=D2R*D2Z
     CT=COS(T(I.J))
     ST=SIN(T(I.J))
     CT2=CT*CT
     ST2=ST*ST
     CP=COS(P(I.J))
     SP=SIN(P(I.J))
     CP2=CP*CP
     SP2=SP*SP
     TA=T(I.JA)
     TB=T(I.JB)
     TZ=(TA-TB)/D2Z
     PA=P(I.JA)
     PB=P(I.JB)
     PZ=(PA-PB)/D2Z
```

```
      TI=T(TL,J)
      TR=T(IR,J)
      TP=(TR-TL)/D2R
      PL=P(IL,J)
      PR=P(IR,J)
      PP=(PR-PL)/D2R
      TPP=(TL+TR-2.*T(I,J))/DRR2
      PPP=(PL+PR-2.*P(I,J))/DRR2
      TAL=T(IL,JA)
      TAR=T(IR,JA)
      TBL=T(IL,JB)
      TBR=T(IR,JB)
      TPZ=(TAR+TBL-TAL-TBR)/DEN
      PAL=P(IL,JA)
      PAR=P(IR,JA)
      PBL=P(IL,JB)
      PBR=P(IR,JB)
      PPZ=(PAR+PBL-PAL-PBR)/DEN
      TZ2=TZ*TZ
      PZ2=PZ*PZ
      TP2=TP*TP
      PP2=PP*PP
      TSR1=SP*CP*(PP*RR*(CST-4.*ST2*DTB)+DST*PPP)
      TSR2=RR2*(SK*CP2+SP2*(TK-ST2*2.*DTB))+CP2*TP2*DSB
     1+PP2*(TK*SP2+CP2*(SK-2.*DTB*ST2))-TZ2*DSB+PZ2*(1.+2.-ST2*DTB)
     2+TSP*(RR*(CP*TZ-SP*TZ*PP+2.*CP*TPZ-SP*TP*PZ)+.0015*H2)
      TSR3=2.*SP*CP*TP*PP*(DST-ST2*DSB)-RR*TP*(TK*SP2+CP2*(1.+CT2*CSB))
      TSR4=RR*SP*PZ*(-DST+DTB-4.*DTB*CT2)-CP*PP*PZ*(DST-DTB+4.*DTB*CT2)
     1-SP*PPZ*DST
      TSR5=DSB*(CT2-ST2)*CP*TP*TZ
      TSR=ST*CT*(TSR1+TSR2)+TSR3+ST2*TSR4+TSR5
      T2PP=(TK*SP2+CP2*(1.+CT2*CSB))/DRR2
      T2ZZ=(1.+ST2*DSB)/DZ2
      T2=(TL+TR)*T2PP+(TA+TB)*T2ZZ
      T(I,J)=.5*(T2-TSR)/(T2PP+T2ZZ)
  965 PSR1=TP2*(CTR-DST)-(RR2+PP2)*(DST+ST2*DTB)
      PSR2=RR*TP*(CST+4.*ST2*DTB)+TPP*CST
      PSR3=2.*TP*PP*(SK*SP2+CP2*(TK-2.*ST2*DTB))+TZ*PZ*(2.+4.*ST2*DTB)
     1+SP*TP*TZ*(CST-CTR)
      PSR4=-RR*PP*(SK*SP2+CP2*(1.+CT2*DTB))-RR*SP*TZ*(1.-4.*CT2)*DTB
     1-SP*TPZ*CST
      PSR5=CTR*(2.*CP*PPZ-SP*PP*PZ+RR*CP*PZ)
      PSR6=(4.*CT2-1.)*CP*(TZ*PP+TP*PZ)*DTB
      PSR=SP*CP*(PSR1+PSR2*CT/ST)-PSR3*CT/ST+PSR4+ST*CT*PSR5+PSR6
      P2PP=(SK*SP2+CP2*(1.+CT2*DTB))/DRR2
      P2ZZ=(1.+ST2*DTB)/DZ2
      P2=(PL+PR)*P2PP+(PA+PB)*P2ZZ
      P(I,J)=.5*(P2-PSR)/(P2PP+P2ZZ)
  100 CONTINUE
C P7=0 AT TOP SURFACE FOR TUS=90
      DO 902 I=2,IM1
  902 P(I,JM)=P(I,JM1)
C EVALUATE PHI AT BOTTOM SURFACE
      DO 903 I=2,IM1
      CT=COS(T(I,1))
      ST=SIN(T(I,1))
      CT2=CT*CT
      ST2=ST*ST
      CP=COS(P(I,1))
      SP=SIN(P(I,1))
```

```
        IF(NDR(I))909,910,911
909 IL=I-1
        IR=I+2
        DRI=DR(I-1)
        GO TO 912
910 IL=I-1
        IR=I+1
        DRI=DR(I)
        GO TO 912
911 IL=I-2
        IR=I+1
        DRI=DR(I)
912 PZ=DTB*ST*CT*(SP/RAD(I)+.5*CP*(P(IR,1)-P(IL,1))/DRI)/(1.+DTB*ST2)
903 P(I,1)=P(1,2)-PZ*DZA(1)
C CONTINUITY OF PHI AT RAD=0
        DO 900 J=1,JM
900 P(1,J)=3.*(P(2,J)-P(3,J))+P(4,J)
950 IM2=IM-2
        IM3=IM-3
C BOUNDARY CONDITIONS ON THE AND PHI AT R=IM
841 DO 840 J=2,JM1
        ST=SIN(T(IM,J))
        CT=COS(T(IM,J))
        ST2=ST*ST
        CT2=CT*CT
        SCT=ST*CT
        SP=SIN(P(IM,J))
        CP=COS(P(IM,J))
        SP2=SP*SP
        CP2=CP*CP
        SCP=SP*CP
        IF(NDZ(J))620,621,622
620 JA=J+2
        JB=J-1
        DZ=DZA(J-1)
        GO TO 623
621 JA=J+1
        JB=J-1
        DZ=DZA(J)
        GO TO 623
622 JA=J+1
        JB=J-2
        DZ=DZA(J)
623 DDZ=2.*DZ
        TZ=(T(IM,JA)-T(IM,JB))/DDZ
        FZ=(P(IM,JA)-P(IM,JB))/DDZ
        PP=(P(IM,J)-P(IM1,J))/DR(IM1)
        TP=(T(IM,J)-T(IM1,J))/DR(IM1)
        TSR=SCT*((TK+CP2*DST)/RAD(IM)-SCP*PP*DST-CP*TZ*DSB)-ST2*SP*PZ*TK
        TTSR=CP2*(1.+CT2*DSB)+TK*SP2
        T(IM,J)=T(IM1,J)-TSR*DR(IM1)/TTSR
843 PSR=SCP*((CT2*DTB-DSB)/RAD(IM)-DST*CT*TP/ST)+SP*TZ*SK
    1-SCT*CP*PZ*DTB
        PPSR=SK*SP2+CP2*(1.+DTB*CT2)
        P(IM,J)=P(IM1,J)-PSR*DR(IM1)/PPSR
840 CONTINUE
        P(IM,1)=3.*(P(IM1,1)-P(IM2,1))+P(IM3,1)
        P(IM,JM)=3.*(P(IM1,JM)-P(IM2,JM))+P(IM3,JM)
920 IF((NPASS/NPW)*NPW-NPASS)150,130,150
130 NFP=1
```

```
  140 TIMR=TIMFXP(C)
       CT55=(T(5.5)-T55)/FLOAT(NPW)
       DP55=(P(5.5)-P55)/FLOAT(NPW)
       T55=T(5.5)
       P55=P(5.5)
       WRITE(6.7)NPASS.TIMR.FKS.DT55.DP55
     7 FORMAT(1H1.5X.'NPASS='.I6.5X.'TIME LEFT IS'.F10.2.5X.'FKS='.F12.4.
      15X.'DT55 ='.E12.5.5X.'CP55='.E12.5)
       WRITE(6.6)(RAD(I).I=1.IM.2)
       DO 63 J=1.JM
       K=JM-J+1
       WRITE(6.2)Z(K).(T(I.K).I=1.IM.2)
       WRITE(6.3)(P(I.K).I=1.IM.2)
    63 CONTINUF
       IF(TIMR-TTF)300.300.150
C FOR PUNCHED OUTPUT IJP=1.NO OUTPUT IJP=-1
   300 IJP=1
       IF(IJP)94.94.95
    95 DO 400 I=1.IM
       WRITE(7.6)(T(I.J).J=1.JM)
       WRITE(7.8)(P(I.J).J=1.JM)
     8 FORMAT(10F7.3)
   400 CONTINUF
    94 ENFR=0.
       T(1.1)=T(2.2)
       T(1.JM)=T(2.JM1)
       DO 500 I=1.IM1
       FTT(I)=0.
       RR=2./(RAD(I)+RAD(I+1))
       D2R=2.*(RAD(I+1)-RAD(I))
       RR2=RR**2
       DO 500 J=1.JM1
       D2Z=2.*DZA(J)
       THE=(T(I.J)+T(I+1.J)+T(I.J+1)+T(I+1.J+1))/4.
       PHI=(P(I.J)+P(I+1.J)+P(I.J+1)+P(I+1.J+1))/4.
       CT=COS(THE)
       ST=SIN(THE)
       CT2=CT*CT
       ST2=ST*ST
       CP=COS(PHI)
       SP=SIN(PHI)
       CP2=CP*CP
       SP2=SP*SP
       TZ=(T(I.J+1)+T(I+1.J+1)-T(I.J)-T(I+1.J))/D2Z
       PZ=(P(I.J+1)+P(I+1.J+1)-P(I.J)-P(I+1.J))/D2Z
       TP=(T(I+1.J)+T(I+1.J+1)-T(I.J)-T(I.J+1))/D2R
       PP=(P(I+1.J)+P(I+1.J+1)-P(I.J)-P(I.J+1))/D2R
       FP(1)=RR2*ST2*(SK*CP2+SP2*(1.+CT2*DTB))
       FP(2)=TP*TP*(TK*SP2+CP2*(1.+DSB*CT2))
       FP(3)=ST2*PP*PP*(SK*SP2+CP2*(1.+CT2*DTB))
       FP(4)=TZ*TZ*(1.+DSB*ST2)
       FP(5)=ST2*PZ*PZ*(1.+DTB*ST2)
       FP(6)=2.*RR*ST*CT*TP*(TK+CP2*DST)
       FP(7)=2.*RR*ST2*SP*CP*PP*(-DSB+CT2*DTB)
       FP(8)=-2.*RR*ST2*CP*TZ*SK
       FP(9)=-2.*RR*ST2*ST*CT*SP*PZ*DTB
       FP(10)=-2.*DST*ST*CT*SP*CP*TP*PP
       FP(11)=-2.*ST*CT*CP*TP*TZ*DSB
       FP(12)=2.*ST2*SP*TZ*PP*SK
       FP(13)=-2.*ST2*SP*TP*PZ*TK
```

```
      FP(14)=-2.*ST2*ST*CT*CP*PP*PZ*DTB
      FP(15)=.0015*ST2*H2
      F(I,J)=0.
      DO 521 N=1,15
  521 F(I,J)=F(I,J)+FP(N)
      FTI(I)=FTI(I)+F(I,J)*DZA(J)
  500 CONTINUE
      WRITE(6,9)
    9 FORMAT(1H1,'ENERGY PER UNIT VOLUME  AT R AND Z')
      WRITE(6,21)(RAD(I),I=1,IM1,2)
   21 FORMAT(7X,20F6.2)
      DO 540 J=1,JM1
      K=JM-J
      WRITE(6,10)Z(K),(F(I,K),I=1,IM1,2)
   10 FORMAT(1X,21F6.3)
  540 CONTINUE
      WRITE(6,11)(FTI(I),I=1,IM1,2)
   11 FORMAT(//5X,'ENERGY PER UNIT RDR',/7X,20F6.2)
      DO 530 I=1,IM1
      FTI(I)=FTI(I)*(RAD(I+1)**2-RAD(I)**2)
  530 ENER =ENER+FTI(I)
      WRITE(6,13)(FTI(I),I=1,IM1,2)
   13 FORMAT(//5X,'ENERGY AT RAD.FV*R*DR*DZ',/7X,20F6.2)
      WRITE(6,12) ENER
   12 FORMAT(//5X,'TOTAL ENERGY IS=',F12.6)
 1000 STOP
      END
//GO.SYSIN DD *
   0.00   0.25   0.50   0.75   1.00   1.25   1.50   2.0    2.5    3.0
   4.0    5.0    6.0    7.0    8.0   10.0   12.0   14.0   16.0   20.0
  24.0   28.0   32.0   40.0   48.0   56.0   64.0   68.0   72.0   74.0
  76.0   77.0   78.0   78.5   79.0   79.25  79.50  79.75  80.0
   0.00   0.25   0.50   0.75   1.00   1.50   2.00   2.50   3.00   4.00
   5.00   6.00   7.00   8.00   9.00  10.00  11.00  12.00  13.00  14.00
  15.00  16.00  16.50  17.00  17.50  18.00  18.25  18.50  18.75  19.00
/*
```

APPENDIX IV

SOME COMPUTER OUTPUTS

The computer output of the equilibrium solution for a cylinder 19 units high and 80 units in radius for the twisted configuration is shown in Table 1. In the top two lines of this table the 39 radial values used are indicated, from 0 to 80 units. The next two lines of numbers, NDR = -1, 0, or 1, indicate that the grid spacing to the right of the grid point is 2^{NDR} times the spacing to the left. The 30 values of z used are shown next followed by the numbers NDZ = -1, 0, or 1 which indicate that the grid spacing above the point of interest is 2^{NDZ} times the grid spacing below.

In the matrix output, the z-values are indicated vertically while the radial values are shown horizontally. At the intersection of lines of constant z and constant ρ are two numbers, the upper one is the equilibrium value for θ while the lower one is the equilibrium value for ϕ in radian measure. θ and ϕ are shown for all values of z used but only for every second value of the radius used. Table 2 shows the equilibrium solution for the normal configuration in which ϕ is zero everywhere.

Tables 3 and 4 show the energy for the twisted and normal configurations, respectively. At the intersection of lines of constant z and constant ρ is the energy density at

TABLE I

RADII TO BE USED ARE

0.0	0.25	0.50	0.75	1.00	1.25	1.50	2.00	2.50	3.00	4.00	5.00	6.00	7.00	8.00	10.00	12.00	14.00	16.00	20.00
24.00	28.00	32.00	40.00	48.00	56.00	64.00	68.00	72.00	74.00	76.00	77.00	78.00	78.50	79.00	79.25	79.50	79.75	80.00	
0	0	0	1	0	0	0	-1	0	-1	0	-1	0	0	0	-1	0	-1	0	
0	0	0	0	0	0	1	0												

Z VALUES TO BE USED ARE

0.0	0.25	0.50	0.75	1.00	1.50	2.00	2.50	3.00	4.00	5.00	6.00	7.00	8.00	9.00
10.00	11.00	12.00	13.00	14.00	15.00	16.00	16.50	17.00	17.50	18.00	18.25	18.50	18.75	19.00
0	0	0	0	1	0	0	0	1	0	0	0	0	0	0
0	0	0	0	0	0	-1	0	0	0	-1	0	0	0	

z	0.0	0.50	1.00	1.50	2.50	4.00	6.00	8.00	12.00	16.00	24.00	32.00	48.00	64.00	72.00	76.00	78.00	79.00	79.50	80.00
19.000	1.571	1.571	1.571	1.571	1.571	1.571	1.571	1.571	1.571	1.571	1.571	1.571	1.571	1.571	1.571	1.571	1.571	1.571	1.571	1.571
	2.067	1.451	1.237	1.094	0.978	0.885	0.809	0.753	0.667	0.597	0.482	0.387	0.242	0.140	0.099	0.080	0.071	0.066	0.064	0.062
18.750	0.0	1.061	1.309	1.398	1.468	1.507	1.527	1.537	1.545	1.549	1.552	1.552	1.553	1.553	1.552	1.551	1.550	1.550	1.549	1.549
	2.067	1.451	1.237	1.094	0.978	0.885	0.809	0.753	0.667	0.597	0.482	0.387	0.242	0.140	0.099	0.080	0.071	0.066	0.064	0.062
18.500	0.0	0.750	1.086	1.237	1.368	1.443	1.484	1.503	1.520	1.527	1.532	1.534	1.535	1.534	1.533	1.531	1.529	1.528	1.528	1.527
	1.896	1.496	1.253	1.123	0.999	0.890	0.811	0.754	0.668	0.598	0.482	0.387	0.242	0.140	0.099	0.080	0.071	0.066	0.064	0.062
18.250	0.0	0.568	0.911	1.096	1.273	1.381	1.443	1.469	1.495	1.505	1.513	1.515	1.516	1.516	1.514	1.511	1.509	1.507	1.506	1.505
	1.734	1.510	1.298	1.161	1.011	0.900	0.819	0.756	0.669	0.598	0.482	0.387	0.242	0.139	0.099	0.080	0.071	0.066	0.064	0.062
18.000	0.0	0.459	0.777	0.975	1.185	1.322	1.398	1.435	1.469	1.483	1.494	1.497	1.498	1.497	1.494	1.491	1.488	1.486	1.485	1.484
	1.661	1.512	1.333	1.198	1.035	0.912	0.821	0.764	0.670	0.599	0.482	0.387	0.242	0.139	0.099	0.080	0.071	0.066	0.064	0.062
17.500	0.0	0.321	0.589	0.787	1.029	1.207	1.315	1.369	1.419	1.440	1.455	1.460	1.462	1.461	1.456	1.451	1.446	1.443	1.442	1.440
	1.551	1.486	1.369	1.253	1.085	0.942	0.837	0.769	0.674	0.601	0.483	0.387	0.242	0.139	0.099	0.080	0.071	0.066	0.064	0.061
17.000	0.0	0.248	0.471	0.652	0.901	1.103	1.236	1.304	1.369	1.397	1.417	1.423	1.425	1.424	1.418	1.411	1.405	1.401	1.399	1.397
	1.494	1.459	1.379	1.287	1.128	0.975	0.857	0.782	0.680	0.604	0.484	0.387	0.242	0.139	0.098	0.080	0.073	0.066	0.064	0.061
16.500	0.0	0.202	0.390	0.553	0.795	1.011	1.162	1.242	1.320	1.354	1.378	1.386	1.389	1.387	1.380	1.371	1.364	1.359	1.357	1.354
	1.458	1.435	1.376	1.305	1.162	1.006	0.878	0.796	0.687	0.608	0.486	0.385	0.242	0.139	0.098	0.079	0.070	0.066	0.063	0.061
16.000	0.0	0.171	0.333	0.478	0.708	0.929	1.092	1.183	1.272	1.311	1.340	1.349	1.353	1.351	1.342	1.332	1.323	1.318	1.315	1.311
	1.434	1.418	1.374	1.315	1.187	1.034	0.901	0.812	0.695	0.613	0.487	0.389	0.242	0.139	0.098	0.079	0.070	0.065	0.063	0.061
15.000	0.0	0.130	0.255	0.373	0.574	0.790	0.967	1.072	1.180	1.228	1.264	1.275	1.281	1.278	1.267	1.253	1.242	1.235	1.232	1.227
	1.392	1.383	1.356	1.316	1.218	1.079	0.940	0.843	0.714	0.624	0.491	0.390	0.241	0.138	0.097	0.078	0.069	0.065	0.062	0.060
14.000	0.0	0.104	0.206	0.303	0.478	0.682	0.859	0.971	1.092	1.147	1.190	1.203	1.209	1.205	1.192	1.176	1.163	1.155	1.150	1.145
	1.360	1.354	1.335	1.307	1.233	1.111	0.975	0.873	0.733	0.636	0.496	0.392	0.241	0.138	0.097	0.078	0.068	0.064	0.061	0.059
13.000	0.0	0.087	0.172	0.254	0.406	0.592	0.767	0.881	1.029	1.069	1.116	1.130	1.138	1.133	1.119	1.100	1.086	1.076	1.071	1.066
	1.334	1.330	1.316	1.295	1.237	1.133	1.004	0.900	0.753	0.649	0.501	0.394	0.241	0.137	0.096	0.077	0.067	0.063	0.060	0.058
12.000	0.0	0.074	0.147	0.218	0.351	0.520	0.686	0.800	0.935	0.994	1.043	1.059	1.067	1.062	1.046	1.026	1.010	1.006	0.994	0.988
	1.312	1.309	1.299	1.283	1.236	1.146	1.027	0.924	0.772	0.662	0.507	0.395	0.240	0.136	0.095	0.076	0.066	0.062	0.059	0.057
11.000	0.0	0.064	0.128	0.190	0.307	0.462	0.617	0.727	0.857	0.921	0.972	0.988	0.997	0.992	0.975	0.953	0.937	0.926	0.920	0.914
	1.293	1.291	1.283	1.270	1.232	1.155	1.045	0.946	0.789	0.675	0.512	0.397	0.239	0.135	0.093	0.074	0.065	0.061	0.058	0.056
10.000	0.0	0.056	0.112	0.167	0.272	0.411	0.556	0.661	0.788	0.851	0.902	0.919	0.927	0.922	0.904	0.882	0.865	0.855	0.849	0.842
	1.277	1.275	1.268	1.258	1.226	1.160	1.061	0.964	0.806	0.686	0.517	0.398	0.239	0.133	0.092	0.073	0.064	0.059	0.057	0.055
9.000	0.0	0.050	0.100	0.149	0.243	0.369	0.504	0.602	0.722	0.784	0.834	0.850	0.858	0.853	0.835	0.813	0.796	0.785	0.779	0.773
	1.263	1.261	1.255	1.247	1.220	1.163	1.072	0.980	0.821	0.698	0.521	0.400	0.238	0.132	0.091	0.072	0.063	0.058	0.056	0.054
8.000	0.0	0.045	0.091	0.135	0.220	0.334	0.457	0.549	0.661	0.719	0.766	0.782	0.790	0.785	0.768	0.746	0.729	0.719	0.713	0.706
	1.250	1.249	1.244	1.237	1.214	1.165	1.081	0.994	0.835	0.708	0.523	0.401	0.237	0.131	0.090	0.071	0.062	0.057	0.055	0.053
7.000	0.0	0.042	0.083	0.123	0.201	0.305	0.417	0.500	0.603	0.656	0.703	0.714	0.722	0.717	0.701	0.681	0.664	0.654	0.648	0.642
	1.241	1.240	1.236	1.230	1.210	1.166	1.090	1.006	0.848	0.718	0.529	0.402	0.236	0.130	0.089	0.070	0.061	0.057	0.054	0.052
6.000	0.0	0.039	0.077	0.115	0.186	0.281	0.381	0.456	0.547	0.595	0.635	0.648	0.655	0.651	0.636	0.617	0.601	0.592	0.586	0.581
	1.235	1.234	1.231	1.225	1.206	1.169	1.098	1.018	0.860	0.727	0.533	0.403	0.236	0.129	0.088	0.069	0.060	0.056	0.053	0.051
5.000	0.0	0.037	0.074	0.110	0.176	0.262	0.351	0.415	0.495	0.536	0.571	0.582	0.588	0.585	0.571	0.554	0.541	0.532	0.527	0.521
	1.234	1.233	1.230	1.225	1.210	1.174	1.107	1.029	0.871	0.735	0.536	0.403	0.235	0.128	0.087	0.068	0.059	0.055	0.053	0.051
4.000	0.0	0.038	0.075	0.109	0.172	0.249	0.325	0.379	0.445	0.479	0.507	0.517	0.522	0.519	0.508	0.494	0.482	0.474	0.469	0.464
	1.241	1.240	1.237	1.232	1.218	1.183	1.118	1.040	0.881	0.742	0.538	0.404	0.234	0.127	0.086	0.067	0.059	0.054	0.052	0.050
3.000	0.0	0.041	0.080	0.116	0.175	0.241	0.303	0.345	0.397	0.423	0.445	0.453	0.457	0.454	0.445	0.434	0.424	0.418	0.414	0.409
	1.259	1.258	1.255	1.250	1.233	1.196	1.130	1.052	0.890	0.748	0.540	0.404	0.233	0.126	0.085	0.067	0.058	0.054	0.052	0.049
2.500	0.0	0.045	0.087	0.123	0.180	0.240	0.293	0.330	0.373	0.395	0.414	0.421	0.424	0.422	0.415	0.405	0.396	0.390	0.387	0.382
	1.275	1.274	1.270	1.264	1.249	1.205	1.137	1.058	0.895	0.751	0.541	0.404	0.233	0.126	0.085	0.066	0.058	0.053	0.051	0.049
2.000	0.0	0.052	0.097	0.134	0.188	0.240	0.285	0.315	0.350	0.368	0.383	0.389	0.391	0.390	0.384	0.376	0.369	0.363	0.360	0.356
	1.296	1.294	1.290	1.282	1.260	1.216	1.144	1.064	0.899	0.753	0.542	0.404	0.232	0.125	0.084	0.066	0.057	0.053	0.051	0.049
1.500	0.0	0.064	0.114	0.151	0.199	0.243	0.278	0.301	0.328	0.341	0.353	0.357	0.359	0.358	0.353	0.347	0.342	0.337	0.334	0.331
	1.324	1.322	1.315	1.309	1.278	1.228	1.152	1.070	0.902	0.755	0.543	0.404	0.232	0.125	0.084	0.065	0.057	0.053	0.051	0.049
1.000	0.0	0.087	0.142	0.176	0.215	0.247	0.272	0.287	0.306	0.315	0.322	0.325	0.327	0.326	0.323	0.319	0.315	0.312	0.309	0.306
	1.363	1.360	1.350	1.334	1.290	1.241	1.161	1.076	0.906	0.757	0.543	0.404	0.232	0.124	0.083	0.065	0.057	0.053	0.051	0.049
0.750	0.0	0.107	0.162	0.192	0.225	0.253	0.269	0.281	0.295	0.301	0.307	0.309	0.310	0.310	0.307	0.304	0.301	0.299	0.297	0.294
	1.389	1.386	1.371	1.352	1.310	1.249	1.165	1.079	0.908	0.758	0.543	0.404	0.232	0.124	0.083	0.065	0.056	0.052	0.051	0.049
0.500	0.0	0.138	0.188	0.212	0.236	0.253	0.266	0.274	0.284	0.288	0.292	0.294	0.294	0.294	0.292	0.290	0.288	0.287	0.285	0.282
	1.429	1.419	1.396	1.370	1.322	1.256	1.170	1.082	0.909	0.759	0.543	0.404	0.231	0.124	0.083	0.065	0.056	0.052	0.050	0.049
0.250	0.0	0.186	0.221	0.235	0.248	0.257	0.264	0.268	0.273	0.275	0.277	0.278	0.278	0.278	0.277	0.276	0.275	0.274	0.273	0.271
	1.517	1.467	1.425	1.390	1.334	1.263	1.174	1.085	0.911	0.760	0.544	0.404	0.231	0.124	0.083	0.065	0.056	0.052	0.050	0.049
0.0	0.262	0.262	0.262	0.262	0.262	0.262	0.262	0.262	0.262	0.262	0.262	0.262	0.262	0.262	0.262	0.262	0.262	0.262	0.262	0.262
	1.757	1.531	1.497	1.411	1.346	1.270	1.179	1.088	0.912	0.760	0.544	0.404	0.231	0.124	0.083	0.065	0.056	0.052	0.050	0.049

TABLE II

RADII TO BE USED ARE
0.0   0.25   0.50   0.75   1.00   1.25   1.50   2.00   2.50   3.00   4.00   5.00   6.00   7.00   8.00   10.00 12.00 14.00 16.00 20.00
24.00 28.00 32.00 40.00 48.00 56.00 64.00 68.00 72.00 74.00 76.00 77.00 78.00 78.50 79.00 79.25 79.50 79.75 80.00
    0   0   1   0   0   0   0   1   0   0   1   0   0   0   1   0   0   0   1   0
    0   0   1   0   0   0   -1   0   -1   0   -1   0   -1   0   -1   0   0   0   0

Z VALUES TO BE USED ARE
0.0   0.25   0.50   0.75   1.00   1.50   2.00   2.50   3.00   4.00   5.00   6.00   7.00   8.00   9.00
10.00 11.00 12.00 13.00 14.00 15.00 16.00 16.50 17.00 17.50 18.00 18.25 18.50 18.75 19.00
    0   0   0   0   1   0   0   0   1   0   0   0   0   0
    0   0   0   0   0   0   -1   0   0   0   -1   0   0   0

	0.0	0.50	1.00	1.50	2.50	4.00	6.00	8.00	12.00	16.00	24.00	32.00	48.00	64.00	72.00	76.00	78.00	79.00	79.50	80.00
19.000																				
	1.571	1.571	1.571	1.571	1.571	1.571	1.571	1.571	1.571	1.571	1.571	1.571	1.571	1.571	1.571	1.571	1.571	1.571	1.571	1.571
18.750																				
	1.115	1.324	1.403	1.469	1.505	1.525	1.535	1.544	1.548	1.551	1.552	1.553	1.552	1.552	1.551	1.550	1.550	1.549	1.549
18.500																				
	0.827	1.116	1.249	1.370	1.441	1.480	1.500	1.518	1.525	1.532	1.533	1.534	1.534	1.533	1.531	1.529	1.528	1.528	1.527
18.250																				
	0.642	0.951	1.114	1.276	1.378	1.436	1.464	1.491	1.503	1.512	1.515	1.516	1.516	1.513	1.511	1.508	1.507	1.506	1.505
18.000																				
	0.519	0.821	0.995	1.189	1.316	1.392	1.429	1.465	1.480	1.492	1.496	1.498	1.497	1.494	1.491	1.488	1.486	1.485	1.484
17.500																				
	0.366	0.633	0.816	1.036	1.202	1.307	1.360	1.412	1.435	1.453	1.459	1.462	1.460	1.456	1.451	1.446	1.443	1.442	1.440
17.000																				
	0.280	0.509	0.682	0.910	1.098	1.226	1.294	1.361	1.391	1.414	1.422	1.425	1.424	1.418	1.411	1.405	1.401	1.399	1.397
16.500																				
	0.225	0.422	0.583	0.816	1.006	1.150	1.230	1.310	1.347	1.376	1.385	1.389	1.387	1.380	1.371	1.364	1.359	1.357	1.354
16.000																				
	0.188	0.355	0.502	0.719	0.924	1.079	1.168	1.261	1.303	1.337	1.348	1.353	1.351	1.342	1.332	1.323	1.318	1.315	1.311
15.000																				
	0.140	0.271	0.397	0.584	0.786	0.952	1.055	1.165	1.218	1.260	1.274	1.281	1.278	1.267	1.253	1.242	1.236	1.232	1.227
14.000																				
	0.110	0.216	0.314	0.484	0.675	0.844	0.952	1.075	1.136	1.185	1.201	1.209	1.205	1.192	1.176	1.163	1.155	1.150	1.146
13.000																				
	0.090	0.177	0.261	0.409	0.585	0.750	0.861	0.991	1.056	1.111	1.129	1.138	1.134	1.119	1.100	1.086	1.077	1.071	1.066
12.000																				
	0.075	0.149	0.227	0.351	0.512	0.669	0.779	0.912	0.981	1.039	1.057	1.067	1.062	1.046	1.026	1.010	1.000	0.995	0.989
11.000																				
	0.064	0.125	0.189	0.304	0.451	0.599	0.706	0.838	0.908	0.967	0.987	0.997	0.992	0.975	0.954	0.937	0.926	0.921	0.914
10.000																				
	0.056	0.111	0.165	0.267	0.399	0.538	0.640	0.769	0.838	0.898	0.917	0.927	0.922	0.905	0.883	0.866	0.855	0.849	0.842
9.000																				
	0.049	0.098	0.145	0.236	0.356	0.485	0.581	0.704	0.771	0.829	0.849	0.858	0.853	0.836	0.814	0.796	0.786	0.780	0.773
8.000																				
	0.044	0.087	0.129	0.211	0.320	0.438	0.528	0.644	0.707	0.762	0.781	0.790	0.785	0.768	0.746	0.729	0.719	0.713	0.707
7.000																				
	0.039	0.078	0.117	0.190	0.289	0.398	0.480	0.587	0.645	0.696	0.714	0.722	0.718	0.701	0.681	0.665	0.654	0.649	0.643
6.000																				
	0.036	0.072	0.107	0.174	0.264	0.362	0.437	0.533	0.586	0.632	0.647	0.655	0.651	0.636	0.617	0.602	0.592	0.587	0.581
5.000																				
	0.034	0.068	0.101	0.163	0.245	0.333	0.398	0.482	0.528	0.568	0.582	0.589	0.585	0.571	0.554	0.541	0.532	0.527	0.521
4.000																				
	0.034	0.066	0.098	0.157	0.231	0.308	0.364	0.434	0.472	0.506	0.517	0.522	0.519	0.508	0.494	0.482	0.474	0.469	0.464
3.000																				
	0.036	0.070	0.102	0.159	0.225	0.288	0.333	0.389	0.418	0.444	0.452	0.457	0.454	0.445	0.434	0.424	0.418	0.414	0.409
2.500																				
	0.035	0.075	0.108	0.163	0.225	0.281	0.319	0.366	0.391	0.413	0.420	0.424	0.422	0.414	0.405	0.396	0.390	0.387	0.382
2.000																				
	0.044	0.083	0.118	0.172	0.227	0.274	0.306	0.345	0.365	0.383	0.388	0.391	0.390	0.384	0.376	0.369	0.363	0.360	0.356
1.500																				
	0.053	0.098	0.134	0.184	0.231	0.269	0.294	0.324	0.339	0.352	0.357	0.359	0.358	0.353	0.347	0.341	0.337	0.334	0.331
1.000																				
	0.073	0.125	0.163	0.203	0.238	0.265	0.283	0.303	0.313	0.322	0.325	0.326	0.326	0.323	0.318	0.315	0.311	0.309	0.306
0.750																				
	0.091	0.146	0.178	0.215	0.243	0.264	0.277	0.292	0.300	0.307	0.309	0.310	0.310	0.307	0.304	0.301	0.299	0.297	0.294
0.500																				
	0.120	0.174	0.201	0.229	0.249	0.263	0.272	0.282	0.287	0.292	0.293	0.294	0.294	0.292	0.290	0.288	0.286	0.285	0.282
0.250																				
	0.172	0.212	0.229	0.244	0.255	0.262	0.267	0.272	0.275	0.277	0.278	0.278	0.278	0.277	0.276	0.275	0.274	0.273	0.271
0.0																				
0.262	0.262	0.262	0.262	0.262	0.262	0.262	0.262	0.262	0.262	0.262	0.262	0.262	0.262	0.262	0.262	0.262	0.262	0.262	0.262

TABLE III

ENERGY PER UNIT VOLUME AT R AND Z

R \ Z	0.0	0.50	1.00	1.50	2.50	4.00	6.00	8.00	12.00	16.00	24.00	32.00	48.00	64.00	72.00	76.00	78.00	79.00	79.50
18.750	52.204	2.797	0.642	0.225	0.175	0.023	0.009	0.004	0.002	0.001	0.001	0.002	0.002	0.003	0.003	0.004	0.004	0.004	0.005
18.500	11.374	2.644	0.721	0.247	0.180	0.023	0.009	0.004	0.002	0.001	0.001	0.002	0.002	0.003	0.003	0.004	0.004	0.005	0.004
18.250	4.452	2.111	0.765	0.275	0.187	0.025	0.010	0.004	0.002	0.001	0.001	0.002	0.002	0.003	0.003	0.004	0.004	0.004	0.005
18.000	2.377	1.556	0.731	0.296	0.196	0.027	0.010	0.004	0.002	0.001	0.001	0.001	0.002	0.003	0.003	0.004	0.004	0.004	0.004
17.500	1.296	1.012	0.612	0.297	0.197	0.030	0.011	0.004	0.002	0.001	0.001	0.002	0.002	0.003	0.003	0.004	0.004	0.004	0.004
17.000	0.675	0.599	0.443	0.269	0.185	0.035	0.013	0.005	0.002	0.001	0.001	0.002	0.002	0.003	0.003	0.004	0.004	0.004	0.004
16.500	0.419	0.390	0.324	0.226	0.174	0.038	0.014	0.006	0.002	0.001	0.001	0.002	0.002	0.003	0.003	0.004	0.004	0.004	0.004
16.000	0.286	0.240	0.245	0.185	0.147	0.041	0.016	0.006	0.002	0.001	0.001	0.002	0.002	0.003	0.003	0.004	0.004	0.004	0.004
15.000	0.185	0.180	0.165	0.137	0.112	0.039	0.017	0.007	0.003	0.001	0.001	0.002	0.002	0.003	0.003	0.004	0.004	0.004	0.004
14.000	0.112	0.111	0.105	0.094	0.092	0.034	0.018	0.008	0.003	0.002	0.001	0.002	0.002	0.003	0.003	0.004	0.004	0.004	0.004
13.000	0.074	0.075	0.072	0.067	0.072	0.029	0.018	0.009	0.003	0.002	0.002	0.002	0.003	0.003	0.003	0.004	0.004	0.004	0.004
12.000	0.053	0.054	0.052	0.049	0.055	0.024	0.017	0.009	0.004	0.002	0.002	0.002	0.003	0.003	0.003	0.004	0.004	0.004	0.004
11.000	0.040	0.040	0.039	0.037	0.042	0.020	0.016	0.009	0.004	0.002	0.002	0.002	0.003	0.003	0.003	0.003	0.004	0.004	0.004
10.000	0.030	0.031	0.030	0.029	0.033	0.017	0.014	0.008	0.004	0.003	0.002	0.003	0.003	0.003	0.003	0.003	0.004	0.003	0.003
9.000	0.024	0.024	0.024	0.023	0.026	0.014	0.012	0.007	0.004	0.003	0.002	0.003	0.003	0.003	0.003	0.003	0.003	0.003	0.003
8.000	0.019	0.019	0.019	0.018	0.021	0.012	0.010	0.006	0.004	0.003	0.003	0.003	0.003	0.003	0.003	0.003	0.003	0.003	0.003
7.000	0.016	0.016	0.016	0.015	0.017	0.010	0.009	0.005	0.004	0.003	0.003	0.003	0.003	0.003	0.003	0.003	0.003	0.003	0.003
6.000	0.014	0.013	0.013	0.013	0.014	0.008	0.007	0.004	0.004	0.003	0.003	0.003	0.003	0.003	0.003	0.003	0.003	0.003	0.003
5.000	0.012	0.012	0.012	0.011	0.012	0.006	0.006	0.004	0.003	0.003	0.003	0.003	0.004	0.003	0.003	0.003	0.003	0.003	0.003
4.000	0.012	0.012	0.011	0.010	0.010	0.005	0.005	0.003	0.003	0.003	0.003	0.003	0.004	0.004	0.003	0.003	0.003	0.003	0.003
3.000	0.014	0.013	0.012	0.010	0.009	0.004	0.004	0.003	0.003	0.003	0.003	0.004	0.004	0.004	0.003	0.003	0.003	0.003	0.003
2.500	0.016	0.015	0.013	0.010	0.008	0.004	0.003	0.002	0.002	0.003	0.003	0.004	0.004	0.004	0.003	0.003	0.003	0.003	0.003
2.000	0.020	0.019	0.015	0.012	0.007	0.004	0.003	0.002	0.002	0.003	0.003	0.004	0.004	0.004	0.003	0.003	0.003	0.003	0.003
1.500	0.029	0.025	0.019	0.014	0.007	0.003	0.002	0.002	0.002	0.003	0.003	0.004	0.004	0.004	0.003	0.003	0.003	0.002	0.002
1.000	0.054	0.038	0.024	0.016	0.007	0.003	0.002	0.002	0.002	0.003	0.004	0.004	0.004	0.004	0.003	0.003	0.003	0.003	0.002
0.750	0.098	0.055	0.030	0.018	0.007	0.003	0.001	0.002	0.002	0.003	0.004	0.004	0.004	0.004	0.003	0.003	0.003	0.003	0.002
0.500	0.181	0.076	0.037	0.020	0.008	0.003	0.001	0.001	0.002	0.003	0.004	0.004	0.004	0.004	0.003	0.003	0.002	0.002	0.002
0.250	0.423	0.108	0.043	0.022	0.008	0.003	0.001	0.001	0.002	0.003	0.004	0.004	0.004	0.004	0.003	0.003	0.003	0.002	0.002
0.0	1.566	0.159	0.053	0.022	0.008	0.002	0.001	0.001	0.002	0.003	0.003	0.004	0.004	0.004	0.003	0.003	0.003	0.002	0.002

ENERGY PER UNIT RDR

20.17	4.16	2.17	1.31	0.74	0.36	0.20	0.11	0.06	0.04	0.04	0.05	0.06	0.06	0.06	0.06	0.06	0.06	0.06

ENERGY AT RAD, FV*R*DR*DZ

1.26	1.30	1.22	2.29	2.03	3.27	2.54	3.87	3.02	6.34	9.25	29.06	48.05	32.57	18.36	9.72	5.01	2.55	2.58

TOTAL ENERGY IS= 394.354492

TABLE IV

ENERGY PER UNIT VOLUME AT R AND Z

R	0.0	0.50	1.00	1.50	2.50	4.00	6.00	8.00	12.00	16.00	24.00	32.00	48.00	64.00	72.00	76.00	78.00	79.00	79.50
18.750	45.590	0.325	0.038	0.007	0.001	0.000	0.000	0.000	0.001	0.001	0.001	0.002	0.002	0.003	0.003	0.004	0.004	0.004	0.005
18.500	22.645	1.620	0.261	0.055	0.010	0.002	0.001	0.000	0.001	0.001	0.001	0.002	0.003	0.003	0.003	0.004	0.004	0.004	0.004
18.250	10.306	2.050	0.482	0.122	0.024	0.004	0.001	0.001	0.001	0.001	0.001	0.002	0.002	0.003	0.003	0.004	0.004	0.004	0.004
18.000	5.590	1.912	0.602	0.185	0.041	0.007	0.001	0.001	0.001	0.001	0.001	0.002	0.002	0.003	0.003	0.004	0.004	0.004	0.004
17.500	2.954	1.487	0.630	0.240	0.066	0.013	0.002	0.001	0.001	0.001	0.001	0.002	0.002	0.003	0.003	0.004	0.004	0.004	0.004
17.000	1.449	0.996	0.556	0.264	0.090	0.021	0.006	0.002	0.001	0.001	0.001	0.002	0.002	0.003	0.003	0.004	0.004	0.004	0.004
16.500	0.857	0.681	0.447	0.251	0.102	0.028	0.009	0.003	0.001	0.001	0.001	0.002	0.002	0.003	0.003	0.004	0.004	0.004	0.004
16.000	0.564	0.483	0.356	0.225	0.105	0.033	0.011	0.004	0.002	0.001	0.001	0.002	0.002	0.003	0.003	0.004	0.004	0.004	0.004
15.000	0.348	0.316	0.259	0.181	0.099	0.037	0.014	0.005	0.002	0.001	0.002	0.002	0.003	0.003	0.003	0.004	0.004	0.004	0.004
14.000	0.200	0.190	0.167	0.132	0.085	0.038	0.017	0.007	0.003	0.002	0.002	0.002	0.003	0.003	0.003	0.004	0.004	0.004	0.004
13.000	0.128	0.124	0.114	0.096	0.069	0.036	0.017	0.008	0.003	0.002	0.002	0.003	0.003	0.003	0.003	0.004	0.004	0.004	0.004
12.000	0.088	0.086	0.081	0.071	0.055	0.032	0.017	0.009	0.004	0.002	0.002	0.003	0.003	0.003	0.003	0.004	0.004	0.004	0.004
11.000	0.063	0.062	0.059	0.054	0.044	0.028	0.016	0.009	0.004	0.002	0.002	0.003	0.003	0.003	0.003	0.004	0.003	0.003	0.003
10.000	0.046	0.046	0.044	0.041	0.035	0.024	0.015	0.008	0.004	0.003	0.003	0.003	0.003	0.003	0.003	0.003	0.003	0.003	0.003
9.000	0.036	0.036	0.034	0.032	0.028	0.020	0.013	0.008	0.004	0.003	0.003	0.003	0.003	0.003	0.003	0.003	0.003	0.003	0.003
8.000	0.028	0.027	0.026	0.026	0.022	0.017	0.011	0.007	0.004	0.003	0.003	0.003	0.003	0.003	0.003	0.003	0.003	0.003	0.003
7.000	0.023	0.022	0.022	0.020	0.018	0.014	0.010	0.006	0.004	0.003	0.003	0.004	0.003	0.003	0.003	0.003	0.003	0.003	0.003
6.000	0.018	0.018	0.018	0.017	0.015	0.012	0.008	0.005	0.003	0.003	0.003	0.004	0.004	0.003	0.003	0.003	0.003	0.003	0.003
5.000	0.016	0.016	0.015	0.014	0.013	0.010	0.007	0.005	0.003	0.003	0.003	0.004	0.004	0.004	0.003	0.003	0.003	0.003	0.003
4.000	0.015	0.014	0.014	0.013	0.011	0.008	0.006	0.004	0.003	0.003	0.003	0.004	0.004	0.004	0.003	0.003	0.003	0.003	0.003
3.000	0.016	0.015	0.014	0.013	0.010	0.007	0.004	0.003	0.003	0.003	0.003	0.004	0.004	0.004	0.003	0.003	0.003	0.003	0.003
2.500	0.018	0.017	0.015	0.013	0.010	0.006	0.004	0.002	0.002	0.003	0.003	0.004	0.004	0.004	0.003	0.003	0.003	0.003	0.003
2.000	0.022	0.020	0.018	0.014	0.015	0.005	0.003	0.002	0.002	0.003	0.004	0.004	0.004	0.004	0.003	0.003	0.003	0.003	0.002
1.500	0.031	0.027	0.022	0.016	0.016	0.004	0.002	0.002	0.002	0.003	0.004	0.004	0.004	0.004	0.003	0.003	0.003	0.002	0.002
1.000	0.056	0.044	0.031	0.020	0.016	0.004	0.002	0.002	0.002	0.003	0.004	0.004	0.004	0.004	0.003	0.003	0.002	0.002	0.002
0.750	0.102	0.068	0.044	0.024	0.012	0.004	0.002	0.001	0.002	0.003	0.004	0.004	0.004	0.004	0.003	0.003	0.002	0.002	0.002
0.500	0.193	0.099	0.052	0.028	0.012	0.004	0.002	0.001	0.002	0.003	0.004	0.004	0.004	0.004	0.003	0.002	0.002	0.002	0.002
0.250	0.494	0.157	0.068	0.031	0.012	0.004	0.001	0.001	0.002	0.003	0.004	0.004	0.004	0.004	0.003	0.003	0.002	0.002	0.002
0.0	2.242	0.263	0.089	0.037	0.013	0.004	0.001	0.001	0.002	0.003	0.003	0.004	0.004	0.004	0.003	0.003	0.003	0.002	0.002

ENERGY PER UNIT RDR

0.0	0.50	1.00	1.50	2.50	4.00	6.00	8.00	12.00	16.00	24.00	32.00	48.00	64.00	72.00	76.00	78.00	79.00	79.50
25.79	4.47	2.31	1.35	0.74	0.34	0.18	0.10	0.05	0.04	0.05	0.05	0.06	0.06	0.06	0.06	0.06	0.06	0.06

ENERGY AT RAD,FV*R*DR*DZ

| 1.61 | 1.41 | 1.30 | 2.37 | 2.03 | 3.16 | 2.31 | 3.45 | 2.77 | 6.25 | 9.53 | 29.86 | 48.78 | 32.79 | 18.43 | 9.75 | 5.03 | 2.56 | 2.59 |

TOTAL ENERGY IS= 397.384033

at the point (ρ, z). Below each column is the total energy in a column of unit area at the radius ρ while in the next row of numbers this has been multiplied by the total area of which this energy density was representative. The final number gives the total volume energy of the configuration.

Table 5 shows the equilibrium solution for the twisted configuration in a 10 kG magnetic field. The two regions of opposite twist are separated by a region with θ close to zero where ϕ rotates very rapidly. This switchover region is at a height of about 7 microns from the bottom (air) interface of the 19 micron thick droplet.

TABLE V

```
RADII TO BE USED ARE
 0.0   0.50  0.75  1.00  1.25  1.50  2.00  2.50  3.00  4.00  5.00  6.00  7.00  8.00 10.00 12.00 14.00 16.00 20.00
24.00 28.00 32.00 40.00 48.00 56.00 64.00 68.00 72.00 74.00 76.00 77.00 78.00 78.50 79.00 79.25 79.50 79.75 80.00
  0    0    0    0    0    1    0   -1    0   -1    0   -1    0   -1    0   -1    0    0    0
  0    0    0    1    0    0    0    1    0   -1    0    0    0    0

 Z VALUES TO BE USED ARE
 0.0   0.25  0.50  0.75  1.00  1.50  2.00  2.50  3.00  4.00  5.00  6.00  7.00  8.00  9.00
10.00 11.00 12.00 13.00 14.00 15.00 16.00 16.50 17.00 17.50 18.00 18.25 18.50 18.75 19.00
  0    0    0    0    1    0    0    0    1    0    0    0    0    0    0
  0    0    0    0    0    0   -1    0    0    0   -1    0    0    0
```

```
       0.0   0.50  1.00  1.50  2.50  4.00  6.00  8.00 12.00 16.00 24.00 32.00 48.00 64.00 72.00 76.00 78.00 79.00 79.50 80.00
19.000
       1.571 1.571 1.571 1.571 1.571 1.571 1.571 1.571 1.571 1.571 1.571 1.571 1.571 1.571 1.571 1.571 1.571 1.571 1.571 1.571
       2.208 1.724 1.528 1.435 1.334 1.238 1.136 1.045 0.900 0.776 0.581 0.436 0.236 0.106 0.057 0.035 0.025 0.020 0.017 0.014
18.750
       0.0   1.017 1.250 1.345 1.410 1.441 1.455 1.459 1.462 1.463 1.463 1.463 1.463 1.463 1.461 1.458 1.455 1.451 1.445
       2.208 1.724 1.528 1.435 1.334 1.238 1.136 1.045 0.900 0.776 0.581 0.436 0.236 0.106 0.057 0.035 0.025 0.020 0.017 0.014
18.500
       0.0   0.685 1.000 1.140 1.256 1.315 1.340 1.349 1.355 1.356 1.357 1.357 1.356 1.356 1.356 1.353 1.348 1.340 1.333 1.322
       2.090 1.777 1.581 1.472 1.353 1.247 1.141 1.052 0.901 0.777 0.581 0.436 0.236 0.106 0.057 0.035 0.025 0.020 0.017 0.014
18.250
       0.0   0.500 0.801 0.963 1.113 1.194 1.230 1.242 1.250 1.252 1.253 1.253 1.253 1.252 1.252 1.248 1.240 1.229 1.220 1.204
       1.974 1.802 1.635 1.519 1.382 1.262 1.150 1.057 0.904 0.778 0.582 0.436 0.236 0.105 0.056 0.035 0.025 0.019 0.017 0.014
18.000
       0.0   0.384 0.652 0.816 0.983 1.080 1.124 1.140 1.150 1.153 1.154 1.154 1.153 1.153 1.152 1.148 1.137 1.124 1.112 1.094
       1.930 1.816 1.676 1.564 1.415 1.282 1.161 1.065 0.907 0.780 0.532 0.436 0.235 0.105 0.056 0.035 0.024 0.019 0.017 0.014
17.500
       0.0   0.246 0.447 0.594 0.766 0.878 0.933 0.953 0.966 0.969 0.970 0.970 0.970 0.970 0.968 0.962 0.949 0.933 0.919 0.900
       1.858 1.811 1.720 1.627 1.476 1.324 1.186 1.081 0.915 0.784 0.583 0.436 0.235 0.104 0.055 0.034 0.024 0.019 0.016 0.014
17.000
       0.0   0.170 0.320 0.440 0.597 0.710 0.769 0.791 0.805 0.809 0.810 0.810 0.810 0.810 0.808 0.801 0.787 0.770 0.756 0.738
       1.821 1.795 1.735 1.662 1.521 1.361 1.211 1.058 0.924 0.789 0.585 0.436 0.234 0.104 0.055 0.033 0.023 0.018 0.016 0.013
16.500
       0.0   0.124 0.237 0.332 0.467 0.573 0.631 0.654 0.668 0.672 0.674 0.674 0.673 0.673 0.671 0.664 0.649 0.633 0.621 0.607
       1.794 1.777 1.735 1.677 1.552 1.392 1.234 1.114 0.932 0.793 0.586 0.436 0.233 0.103 0.054 0.033 0.023 0.018 0.016 0.014
16.000
       0.0   0.053 0.179 0.255 0.367 0.462 0.516 0.538 0.553 0.557 0.558 0.558 0.558 0.558 0.556 0.549 0.535 0.520 0.511 0.499
       1.774 1.761 1.724 1.680 1.570 1.415 1.253 1.127 0.939 0.797 0.587 0.436 0.233 0.102 0.053 0.032 0.022 0.018 0.016 0.014
15.000
       0.0   0.054 0.106 0.153 0.225 0.300 0.345 0.364 0.377 0.380 0.382 0.382 0.381 0.381 0.379 0.373 0.362 0.352 0.345 0.339
       1.724 1.716 1.695 1.663 1.575 1.441 1.279 1.148 0.951 0.804 0.589 0.437 0.233 0.102 0.053 0.032 0.022 0.018 0.016 0.015
14.000
       0.0   0.043 0.065 0.095 0.145 0.195 0.230 0.245 0.256 0.259 0.260 0.260 0.260 0.259 0.258 0.252 0.244 0.239 0.234 0.230
       1.674 1.662 1.654 1.631 1.566 1.448 1.294 1.163 0.960 0.813 0.592 0.438 0.233 0.102 0.053 0.032 0.022 0.019 0.017 0.016
13.000
       0.0   0.021 0.041 0.060 0.092 0.128 0.153 0.165 0.174 0.176 0.177 0.177 0.176 0.176 0.174 0.170 0.165 0.161 0.158 0.156
       1.627 1.623 1.612 1.594 1.543 1.447 1.301 1.173 0.969 0.817 0.597 0.442 0.235 0.103 0.053 0.032 0.023 0.020 0.019 0.018
12.000
       0.0   0.013 0.026 0.038 0.060 0.084 0.102 0.111 0.118 0.120 0.120 0.120 0.119 0.118 0.117 0.114 0.110 0.108 0.106 0.105
       1.583 1.581 1.572 1.558 1.517 1.432 1.304 1.182 0.981 0.828 0.607 0.450 0.240 0.106 0.056 0.034 0.026 0.022 0.021 0.021
11.000
       0.0   0.009 0.017 0.025 0.039 0.056 0.069 0.076 0.081 0.082 0.081 0.081 0.079 0.079 0.078 0.075 0.073 0.071 0.070 0.070
       1.547 1.545 1.539 1.527 1.494 1.423 1.310 1.196 1.001 0.849 0.628 0.469 0.253 0.114 0.062 0.040 0.031 0.028 0.027 0.026
10.000
       0.0   0.006 0.012 0.017 0.027 0.039 0.048 0.053 0.056 0.055 0.055 0.054 0.052 0.051 0.050 0.048 0.046 0.045 0.045 0.045
       1.524 1.522 1.517 1.509 1.482 1.424 1.327 1.225 1.042 0.896 0.676 0.514 0.286 0.136 0.079 0.053 0.042 0.039 0.038 0.038
 9.000
       0.0   0.004 0.008 0.012 0.020 0.028 0.035 0.039 0.040 0.040 0.038 0.036 0.032 0.031 0.030 0.028 0.027 0.026 0.026 0.026
       1.524 1.523 1.519 1.513 1.494 1.449 1.372 1.287 1.127 0.993 0.786 0.624 0.371 0.195 0.125 0.090 0.076 0.071 0.070 0.070
 8.000
       0.0   0.004 0.007 0.010 0.016 0.023 0.028 0.031 0.032 0.031 0.027 0.024 0.019 0.016 0.014 0.013 0.012 0.012 0.011 0.011
       1.560 1.559 1.557 1.553 1.541 1.513 1.461 1.400 1.282 1.182 1.026 0.893 0.638 0.412 0.311 0.252 0.222 0.212 0.211 0.213
 7.000
       0.0   0.003 0.007 0.010 0.016 0.022 0.027 0.029 0.029 0.028 0.024 0.020 0.013 0.010 0.008 0.008 0.007 0.007 0.007 0.007
       1.622 1.622 1.622 1.621 1.618 1.608 1.587 1.560 1.506 1.468 1.434 1.434 1.463 1.490 1.558 1.692 1.778 1.807 1.814 1.816
 6.000
       0.0   0.004 0.008 0.012 0.019 0.025 0.030 0.032 0.032 0.031 0.027 0.024 0.019 0.016 0.015 0.015 0.015 0.015 0.015 0.015
       1.674 1.679 1.681 1.683 1.690 1.701 1.710 1.715 1.726 1.749 1.838 1.971 2.275 2.525 2.643 2.721 2.760 2.775 2.779 2.780
 5.000
       0.0   0.006 0.012 0.017 0.026 0.034 0.039 0.041 0.041 0.041 0.038 0.036 0.033 0.031 0.031 0.031 0.030 0.030 0.030 0.030
       1.706 1.708 1.712 1.718 1.734 1.762 1.795 1.823 1.875 1.932 2.073 2.236 2.536 2.734 2.816 2.868 2.896 2.908 2.912 2.915
 4.000
       0.0   0.010 0.019 0.027 0.038 0.049 0.054 0.057 0.058 0.057 0.056 0.054 0.052 0.051 0.051 0.051 0.050 0.050 0.049 0.049
       1.709 1.712 1.719 1.729 1.754 1.795 1.842 1.882 1.954 2.025 2.180 2.343 2.621 2.792 2.862 2.907 2.933 2.945 2.950 2.954
 3.000
       0.0   0.017 0.032 0.044 0.064 0.073 0.079 0.082 0.083 0.083 0.082 0.081 0.080 0.079 0.079 0.079 0.078 0.077 0.077 0.076
       1.699 1.703 1.714 1.729 1.764 1.812 1.866 1.913 1.993 2.069 2.227 2.387 2.653 2.813 2.878 2.921 2.947 2.960 2.965 2.970
 2.500
       0.0   0.023 0.042 0.057 0.077 0.090 0.096 0.099 0.100 0.100 0.100 0.099 0.098 0.098 0.097 0.097 0.096 0.095 0.095 0.094
       1.692 1.698 1.712 1.730 1.769 1.821 1.877 1.923 2.004 2.081 2.240 2.399 2.660 2.818 2.882 2.924 2.950 2.963 2.970 2.975
 2.000
       0.0   0.042 0.058 0.076 0.097 0.111 0.117 0.120 0.121 0.121 0.121 0.120 0.120 0.119 0.119 0.118 0.118 0.117 0.116 0.115
       1.683 1.692 1.711 1.733 1.776 1.829 1.884 1.931 2.012 2.090 2.248 2.406 2.666 2.821 2.884 2.926 2.952 2.966 2.973 2.979
 1.500
       0.0   0.047 0.081 0.102 0.124 0.137 0.143 0.145 0.147 0.147 0.147 0.146 0.146 0.146 0.146 0.145 0.145 0.143 0.142 0.140
       1.673 1.684 1.714 1.741 1.785 1.838 1.892 1.938 2.019 2.096 2.254 2.411 2.669 2.824 2.885 2.927 2.953 2.967 2.975 2.983
 1.000
       0.0   0.074 0.116 0.139 0.159 0.170 0.175 0.177 0.178 0.178 0.178 0.178 0.178 0.177 0.177 0.177 0.177 0.175 0.174 0.172
       1.662 1.693 1.727 1.756 1.799 1.848 1.900 1.945 2.024 2.101 2.258 2.415 2.671 2.825 2.886 2.928 2.953 2.968 2.977 2.985
 0.750
       0.0   0.096 0.141 0.162 0.181 0.190 0.194 0.195 0.196 0.196 0.196 0.196 0.196 0.196 0.196 0.195 0.195 0.194 0.193 0.190
       1.660 1.702 1.739 1.767 1.808 1.854 1.904 1.948 2.027 2.103 2.260 2.416 2.672 2.825 2.886 2.928 2.953 2.968 2.977 2.986
 0.500
       0.0   0.129 0.172 0.190 0.205 0.211 0.214 0.215 0.216 0.216 0.216 0.216 0.216 0.216 0.216 0.216 0.215 0.215 0.213 0.211
       1.666 1.722 1.757 1.782 1.818 1.861 1.909 1.951 2.029 2.105 2.261 2.417 2.672 2.826 2.886 2.928 2.953 2.968 2.977 2.987
 0.250
       0.0   0.181 0.212 0.223 0.232 0.235 0.237 0.237 0.238 0.238 0.238 0.238 0.238 0.238 0.238 0.238 0.237 0.236 0.233
       1.724 1.760 1.782 1.800 1.829 1.868 1.914 1.955 2.032 2.106 2.262 2.418 2.673 2.826 2.886 2.927 2.953 2.968 2.977 2.988
 0.0
       0.262 0.262 0.262 0.262 0.262 0.262 0.262 0.262 0.262 0.262 0.262 0.262 0.262 0.262 0.262 0.262 0.262 0.262 0.262 0.262
       1.554 1.824 1.814 1.821 1.842 1.875 1.918 1.958 2.034 2.108 2.263 2.418 2.673 2.826 2.886 2.927 2.953 2.968 2.976 2.987
```

APPENDIX V

THE OPTICS COMPUTER CALCULATION

The system of equations given by Eqs. V.9, V.14, and V.16 can be solved by computer using a finite central-difference expansion as was done in solving the bulk equations in App. III.

The crystal gets divided into N regions of equal thickness

$$\Delta = L/N \tag{AV.1}$$

This produces (N-1) interior points, at each of which there are the unknowns E_x^j and E_y^j where j refers to the jth grid point. Eqs. V.9 can then be written as

$$0 = \frac{E_x^{j+1} - 2 E_x^j + E_x^{j-1}}{\Delta^2}$$

$$+ \frac{\omega^2}{c^2}\left[\begin{array}{l} E_x^j\left(\epsilon^j(11) - \dfrac{\epsilon^j(13)\epsilon^j(31)}{\epsilon^j(33)}\right) \\ + E_y^j\left(\epsilon^j(12) - \dfrac{\epsilon^j(13)\epsilon^j(32)}{\epsilon^j(33)}\right) \end{array}\right] \tag{AV.2}$$

and

$$0 = \frac{E_y^{j+1} - 2 E_y^j + E_y^{j-1}}{\Delta^2}$$

$$+ \frac{\omega^2}{c^2}\left[\begin{array}{l} E_x^j\left(\epsilon^j(21) - \dfrac{\epsilon^j(23)\epsilon^j(31)}{\epsilon^j(33)}\right) \\ + E_y^j\left(\epsilon^j(22) - \dfrac{\epsilon^j(23)\epsilon^j(32)}{\epsilon^j(33)}\right) \end{array}\right] \tag{AV.3}$$

At the bottom surface, from Eq. V.14 one has

$$E_x^1 - \frac{c}{i\omega\, n_{ext}}\left(\frac{E_x^2 - E_x^1}{\Delta}\right) = 2\, E_{xi} \qquad (AV.4)$$

and

$$E_y^1 - \frac{c}{i\omega\, n_{ext}}\left(\frac{E_y^2 - E_y^1}{\Delta}\right) = 2\, E_{yi} \qquad (AV.5)$$

while at the top surface, from Eq. V.16 one has

$$E_x^{N+1} + \frac{c}{i\omega\, n_{ext}}\left(\frac{E_x^{N+1} - E_x^N}{\Delta}\right) = 0 \qquad (AV.6)$$

and

$$E_y^{N+1} + \frac{c}{i\omega\, n_{ext}}\left(\frac{E_y^{N+1} - E_y^N}{\Delta}\right) = 0 . \qquad (AV.7)$$

There are $2(N-1)$ bulk equations (Eq. AV.2 and AV.3) plus two equations at both the top and bottom surfaces which makes a total of $2(N+1)$ equations in the $2(N+1)$ unknowns. This system of equations can be solved by the method of guassian elimination to determine the nature of the light that has been transmitted through the anisotropic liquid crystalline medium. Only E_x^{N+1} and E_y^{N+1}, the electric field amplitudes at the upper surface, are evaluated absolutely since the interior values are not really of interest. This avoids the necessity of having to store a large array of intermediate numbers.

The computer program OPT5 which solves the equations follows.

```
//A122CPT5 JOB (*****,*****),*PRESS*,TIME=3
//*JOBPARM FORMS=6E19
// EXEC FORTGCLG
//FORT.SYSIN DD *
      IMPLICIT COMPLEX*8(A-H)
      DIMENSION D(3,5),DR(3),E(3,3),RS(180),RC(180),EX(2),EY(2),VA(180),
     17(30),T(30),P(30)
      R=1.
      THK=.025
      WALTH=1.
      WALTH=10.
      V=.12
      V=.06
      PI=3.1415927/180.
      READ(5,5)7
    5 FORMAT(10F6.2)
      WRITE(6,7)7
C  NR=NO. OF RADII USED
      NR=10
      DO 700 I=1,NR
C
      READ(5,8)RAD
    8 FORMAT(F6.2)
      WRITE(6,9)RAD
    9 FORMAT(//5X,*RAD=*,F6.2)
      READ(5,6)T
      READ(5,6)P
    6 FORMAT(10F7.2)
      WRITE(6,7)T
      WRITE(6,7)P
    7 FORMAT(1X,10F7.3)
      DO 50 J=1,180
      RC(J)=COS(PI*FLOAT(J))
   50 RS(J)=SGRT(1.-RC(J)**2)
      RATIO=(2.*3.1415927*THK/WALTH)**2
      A1=CMPLX(0.,1./(RATIO**.5*R))
      DO 502 K=1,2
      GO TO(20,30),K
   20 EXINC=CMPLX(1.,0.)
      EYINC=CMPLX(0.,0.)
      GO TO 35
   30 EXINC=CMPLX(0.,0.)
      EYINC=CMPLX(1.,0.)
   35 CONTINUE
      D(1,1)=CMPLX(1.,0.)-A1
      D(1,2)=CMPLX(0.,0.)
      D(1,3)=A1
      D(1,4)=D(1,2)
      D(1,5)=D(1,2)
      D(2,1)=D(1,2)
      D(2,2)=D(1,1)
      D(2,3)=D(1,2)
      D(2,4)=A1
      D(2,5)=D(1,2)
      NXY=1
      DR(1)=2.*EXINC
      DR(2)=2.*EYINC
      DO 400 N=1,29
      XZ=Z(N+1)-Z(N)
      M=2*(IFIX((XZ+.001)/THK)+N/29)
```

```
      XT=T(N+1)-T(N)
      XF=P(N+1)-F(N)
      XP=FLOAT(M)
      DC 400 MM=1.M
      IF(N-79)110.111.111
111   IF(MM-M-1)130.130.110
110   GC TO(70.82).NXY
70    THE=T(N)+FLOAT(MM-1)*XT/XM
      PHI=P(N)+FLOAT(MM-1)*XP/XM
      THEC=CCS(THE)
      THES=SORT(1.-THEC**2)
      FHIC=CNS(PHI)
      PHIS=SORT(1.-PHIC**2)
      TC2=THEC**2
      TS2=THES**2
      PC2=PHIC**2
      FS2=PHIS**2
      F(1.1)=CMPLX(1.-V*(1.-2.*TS2*PS2).0.)
      F(1.2)=CMPLX(-2.*V*TS2*PHIS*PHIC.0.)
      F(1.3)=CMPLX(2.*V*THES*THEC*PHIS.0.)
      F(2.1)=CCNJG(E(1.2))
      F(2.2)=CMPLX(1.-V*(1.-2.*TS2*PC2).0.)
      F(2.3)=CMPLX(-2.*V*THES*THEC*PHIC.0.)
      F(3.1)=CCNJG(E(1.3))
      F(3.2)=CCNJG(E(2.3))
      F(3.3)= CMPLX(1.+V*(TC2-TS2).0.)
      D(3.1)=1.
      C(3.2)=0.
      D(3.3)=RATIO*(E(1.1)-E(1.3)*E(3.1)/E(3.3))-2.
      D(3.4)=RATIO*(E(1.2)-E(1.3)*E(3.2)/E(3.3))
      C(3.5)=1.
      NXY=2
      GO TO 80
82    C(3.1)=1.
      C(3.2)=RATIO*(E(2.1)-E(2.3)*E(3.1)/E(3.3))
      F(3.3)=RATIO*(E(2.2)-E(2.3)*E(3.2)/E(3.3))-2.
      C(3.4)=0.
      D(3.5)=1.
      NXY=1
      GC TO 80
130   D(3.1)=A1
      C(3.2)=CMPLX(0..0.)
      D(3.3)=CMPLX(1..0.)-A1
      D(3.4)=D(3.2)
      C(3.5)=C(3.2)
80    DR(3)=CMPLX(C..0.)
      P=1./C(1.1)
      FC 85 KA=1.5
85    D(1.KA)=D(1.KA)*B
      CR(1)=DR(1)*E
      DC 86 KB=2.3
      B=CMPLX(-1..C.)*D(KB.1)
      CC 87 KA=1.5
87    C(KB.KA)=D(KB.KA)+B*D(1.KA)
86    CR(KB)=CR(KB)+B*DR(1)
      C(1.1)=C(2.2)
      D(1.2)=D(2.3)
      C(1.3)=D(2.4)
      C(1.4)=C(2.5)
      D(1.5)=CMPLX(0..0.)
```

```
      C(2,1)=C(3,2)
      C(2,2)=D(3,3)
      C(2,3)=C(3,4)
      C(2,4)=C(3,5)
      D(2,5)=CMPLX(0.,0.)
      CR(1)=CR(2)
      DR(2)=DR(3)
  400 CONTINUE
      P=1./C(1,1)
      D(1,1)=CMPLX(1.,0.)
      C(1,2)=D(1,2)*R
      CR(1)=CR(1)*P
      B=D(2,1)*CMPLX(-1.,0.)
      C(2,2)=D(2,2)+C(1,2)*B
      DR(2)=DR(2)+DR(1)*B
      FYOUT=DR(2)/D(2,2)
      FXOUT=DR(1)-C(1,2)*EYOUT
      OUT=CABS(EXOUT)**2+CABS(EYOUT)**2
      WRITE(6,1)WALTH,EXOUT,EYOUT,OUT
    1 FORMAT( /5X,'WALTH=',F12.6,5X,'EXOUT=',2F12.8,5X,'EYOUT=',2F12.8/
     15X,'OUT INT=',F12.8)
      FX(K)=FXOUT
      FY(K)=FYOUT
  500 CONTINUE
      DO 600 J=1,180
      BV=RS(J)*RC(J)*(FY(2)-EX(1))-EX(2)*RS(J)**2+EY(1)*RC(J)**2
  600 VA(J)=CABS(BV)**2
      DO 675 J1=1,2
      NN=(J1-1)*90
      VMIN=VA(1+NN)
      MINAN=1+NN
      NL=1+NN
      NU=90+NN
      DO 650 J=NL,NU
      IF(VA(J)-VMIN)660,660,650
  660 VMIN=VA(J)
      MINAN=J
  650 CONTINUE
      NL=3+NN
      NU=90+NN
      WRITE(6,3)(VA(J),J=NL,NU,3)
    3 FORMAT(10F10.6)
      WRITE(6,4)VMIN,MINAN
    4 FORMAT(10X,'VMIN=',F12.6,5X,'MINAN=',I6)
  675 CONTINUE
  700 CONTINUE
      STOP
      END
//GO.SYSIN DD *
  0.00  0.25  0.50  0.75  1.00  1.50  2.00  2.50  3.00  4.00
  5.00  6.00  7.00  8.00  9.00 10.00 11.00 12.00 13.00 14.00
 15.00 16.00 16.50 17.00 17.50 18.00 18.25 18.50 18.75 19.00
/*
```

SIMPLIFIED CALCULATION OF SOME DROPLET ENERGIES

Using the one constant approximation, Eq. III.21, the approximate nature of the minimum energy configuration of the liquid crystal droplet can be obtained. This will again point out the important feature of splay cancellation.

The calculation will be done about the point singularity at the water surface, with the water surface at $z=0$, the point singularity at $\rho=0$, and the air surface moved to plus infinity, i.e., the air surface will be neglected. (Note the coordinate system of Fig. IV-2b has been shifted and inverted for the convenience of the following mathematics.)

With $\phi=0$ and $H=0$, Eq. III.21 becomes

$$\Theta_{\rho\rho} + \frac{1}{\rho}\Theta_\rho + \Theta_{zz} = \sin\Theta \cos\Theta/\rho^2 \qquad \text{(AVI.1)}$$

which has among its solutions

$$\tan\Theta = \pm \rho/z . \qquad \text{(AVI.2)}$$

Eq. AVI.2 has the correct boundary condition since at $z=0$, $\Theta = \frac{\pi}{2}$, in agreement with the hard pinning condition at the water surface. The + solution correspoinds to a radial configuration of the molecules in the ρ-z plane about the point singularity while the − sign corresponds to a hyperbolic configuration of the molecules (as in Fig. IV.2b).

The energy/volume in the one constant approximation with $\sin\phi$ and H zero can be obtained from Eq. III.20,

$$F = \sin^2\theta\left[\frac{1}{\rho^2} - \frac{2}{\rho}\cos\phi \, \theta_z\right] + \theta_\rho^2 + \theta_z^2 + \frac{2}{\rho}\sin\theta\cos\theta \, \theta_\rho \tag{AVI.3}$$

which using Eq. AVI.2 gives

$$F_R = \frac{4}{\rho^2 + z^2} \tag{AVI.4}$$

for the radial configuration and

$$F_H = \frac{4z^2}{(\rho^2 + z^2)^2} \tag{AVI.5}$$

for the hyperbolic configuration.

Performing the z-integration from z=0 to z=∞ gives

$$E_R(\rho) = \frac{2\pi S}{\rho} \tag{AVI.6}$$

as the energy/area for the radial configuration and

$$E_H(\rho) = \frac{\pi S}{\rho} \tag{AVI.7}$$

as the energy/area for the hyperbolic configuration. Thus

$$E_R(\rho)/E_H(\rho) = 2 , \tag{AVI.8}$$

the radial configuration has twice the energy density of the hyperbolic configuration. This is a result of the splay cancellation which takes place in the hyperbolic configuration but not in the radial configuration.

The total energy about the singularity to a radius R is $2\pi RS$ for the radial configuration and πRS for the hyperbolic configuration. The radial configuration is twice as expensive as the hyperbolic configuration.

In the real droplet the molecular configurations about the

singularity at the water surface given by Eq. AVI.2 are approximately correct as long as the air surface doesn't have much influence. This is satisfied for small enough radii (less than about 3 micron) where the polar angle Θ becomes very small away from the surfaces, Eq. AVI.7 then predicts that the energy/ area should vary inversely with the radius which is verified by the computer calculation shown in Table IV. Instead of a constant of proportionality of πS as derived in Eq. AVI.7 one finds 2.5S from the computer calculation. A smaller value is not unreasonable since the finite droplet occupies less volume than the semi-infinite medium for which Eq. AVI.7 was derived.

As explained in Ch. III and App. II where there are singularities in the volume energy the surface can distort and/or there can be a relaxation in the hard pinning angle. If the surface distorts it will form a depression, or anti-nipple, since this allows a decrease in the polar angle at the surface with a resultant reduction in the volume energy. An elevation or nipple would increase the polar angle as can be seen from Fig. IV.2b, which would worsen the volume singularity.

The reduction of the energy/area (the integral of the volume energy density from the air to the water surface) is proportional to the decrease in the polar angle at the water surface. This was verified by changing the pinning angle at the water surface, finding the new equilibrium solution, and calculating the energy. From the computer calculations the energy/area at the radius $\mathcal{G}$ for small radii can be written as

$$E(g) = S\left(\frac{2.5 - 2\Delta\Theta_{us}}{g}\right) \qquad \text{(AVI.9)}$$

where $\Delta\Theta_{us}$ is the amount of the decrease of the polar angle at the upper surface from $\pi/2$.

When the surface is distorted the surface area and therefore the surface energy increases quadratically with the slope of the surface for small distortions. For hard pinning the slope of the surface is equal to the decrease of the polar angle at the surface. Thus the total energy/area with distorted surface is

$$E_g = S\left(\frac{2.5 - 2\Delta\Theta_{us}}{g}\right) + \frac{1}{2}\sigma\,\Delta\Theta_{us}^2 \qquad \text{(AVI.10)}$$

where σ is the interfacial surface tension. This is minimized if

$$\Delta\Theta_{us} = \frac{2S}{\sigma g} \qquad \text{(AVI.11)}$$

With $S \sim 10^{-6}$ dynes, $\sigma \sim 10^2$ dynes/cm (Kmetz (Km-72)), and at a radius of 1 micron the amount of the distortion is 2×10^{-4} radians which is sufficiently small to be neglected.

The hard pinning energy increases quadratically with the change of the pinning angle from its equilibrium value. Assuming no surface distortions the change in the pinning angle is equal to the change in the polar angle at the surface. Thus the total energy/area is

$$E(g) = S\left(\frac{2.5 - 2\Delta\Theta_{us}}{g}\right) + \frac{1}{2}k_p\,\Delta\Theta_{us}^2 \qquad \text{(AVI.12)}$$

where K_p is the strength of the pinning energy. This is minimized if

$$\Delta \Theta_{us} = \frac{2S}{k_s \rho} \qquad \text{(AVI.13)}$$

With $S \sim 10^{-6}$ dynes, $K_p \sim 10$ dynes/cm (if it were any smaller the optical data in Ch. V could not have been theoretically fit), and at a radius of 1 micron, the amount of distortion is 2×10^{-3} radians which again is sufficiently small to be neglected.

This justifies the flat cylinder model used in Ch. III which neglected the volume singularities occuring at the axis of symmetry which would be relieved in a real material by surface distortions or relaxing of the hard pinning.

REFERENCES

Ai-31 Airy, G. B., "On The Nature Of The Light In The Two Rays Produced By The Double Refraction Of Quartz", Transactions of the Cambridge Phil. Soc., Vol. IV, Part I, 79-123, 199-208, 21 February 1831.

Bo-71 Bouchiat, M. A., and Langevin-Cruchon, D., "Molecular Order At The Free Surface Of A Nematic Liquid Crystal From Light Reflectivity Measurements", Physics Letters, Vol. 34A, 331-2, 5 April 1971.

Ch-72 Chou, S. C., Cheung, L., and Meyer, R. B., "Effects Of A Magnetic Field On The Optical Transmission In Cholesteric Liquid Crystals", Solid State Communications, Vol. 11, 997-81, 1972.

Cl-73 Cladis, P. E., "Study of the Bend Elastic Constant Near a Smectic-A-Nematic Phase Transition", Physical Review Letters, Vol. 31, #19, 1200-3, 1973.

Du-69 Dubois-Violette, E., and Parodi, O., "Emulsions Nematiques. Effets De Champ Magnetiques Et Effets Piezoelectriques", Journal De Physique Colloque C4, Supplement #11-12, Tome 30, 57-64, 1969.

Fr-58 Frank, F. C., "I. Liquid Crystals , On The Theory Of Liquid Crystals", Discussions Of The Faraday Society, Vol. 25, 19-28, 1958.

Ga-64 Garabedian, P. R., "Partial Differential Equations", John Wiley And Sons, New York, 1964, Ch. 15.

Ha-72a Haller, I., "Elastic Constants Of The Nematic Liquid Crystalline Phase Of p-Methoxybenzylidene-p-n-Butyaniline (MBBA)", The Journal Of Chemical Physics, Vol. 57, #4, 1400-5, 15 August 1972.

Ha-72b Haller, I., Huggins, H. A., and Freiser, M. J., "On The Measurement Of Indices Of Refraction Of Nematic Liquids", Molecular Crystals and Liquid Crystals, Vol. 16, 53-59, 1972.

Jo-69 Johnson, J. F., Porter, R. S., and Barrall II, E. M., "Thermodynamics Of Mesophase Transitions From Calorimetric Measurements", Molecular Crystals and Liquid Crystals, Vol. 8, 1-7, 1969.

Kl-72   Kleman, M., "Defauts Dans les Cristaux Liquides",
         Societe Francais De Mineralogie et de Cristallographie,
         Paris, Bulletin, Vol. 95, #2, 215-30,1972.

Km-72   Kmetz, A. R., amd Creagh, L., "Mechanism of Surface
         Alignment in Nematic Liquid Crystals", 4th International
         Liquid Crystal Conference, Kent State, 1972, (to be
         published).

Le-72   Le Roy, P., Debauvais, F., and Candau, S., "Effets
         de Champ Magnetic Sur La Structure de Goutelettes de
         Cristaux Liquides Nematiqes en Emulsion dans un
         Liquid Isotrope", C. R. Acad. Sc., Paris, Serie B,
         T. 274, 419-22, 1972.

Me-72   Meyer, R. B., "Point Disclinations at a Nematic-
         Isotropic Liquid Interface", Molecular Crystals and
         Liquid Crystals, Vol. 16, 355-69, 1972.

Pr-69   Princen, H. M., "The Equilibrium Shape Of Interfaces,
         Drops, And Bubbles. Rigid And Deformable Particles
         At Interfaces", Surface And Colloid Science, Editor
         Egon Matijevic, Vol. 2, 1-84, Wiley-Interscience,1969.

Pr-71   Prost, J., and Gasparoux, H., "Modification, Sous
         L'action D'un Champ Magnetique, De L'orientation Des
         Molecules Au Sein D'une Goutte De Substance Nematique

         (p, p'-methoxybenzene-aminobutylbenzene)", C. R. Acad.
         Sc. Paris. T. 273, Serie B,335-8, 30 Aout 1971.

Pr-73   Press, M. J. and Arrott, A. S., "Expansion Coefficient
         Of Methoxybenzylidene Butylaniline Through The Liquid
         Crystal Phase Transition", Physical Review A, Vol. 8,
         #3, 1459-65, September 1973.

Ra-71   Rault, J., "Sur Une Methode Nouvelle D'etude De
         L'orientation Moleculaire A La Surface D'un Cholester-
         ique", C. R. Acad. Sc. Paris. T. 273, Serie B, 1275-6,
         2 Juin 1971.

Sa-73   Saupe, A., "Disclinations and Properties of the
         Directorfield in Nematic and Cholesteric Liquid
         Crystals", Molecular Crystals and Liquid Crystals,
         Vol. 21, 211-38, 1973.

BIBLIOGRAPHY

Cladis, P. E., amd Kleman, M., "Non-Singular Disclinations Of Strength S=+1 in Nematics", Le Journal De Physique, Tome 33, 591-8, Mai 1972.

De Gennes, P. G., "Liquid Crystal Physics", To be published.

De Gennes, P. G., "Structures En Domaines Dans Un Nematique Sous Champ Magnetique", Solid State Communications, Vol. 8, 213-6, 1970.

Meyer, R. B., "On The Existence Of Even Indexed Disclinations In Nematic Liquid Crystals", Phil. Mag., Vol. 27, #2, 405-24, 1973.

Nehring, J., and Saupe, A., "On The Elastic Theory Of Uniaxial Liquid Crystals", The Journal Of Chemical Physics, Vol. 54, #1, 337-43, 1971.

Pieranski, P., Brochard, F., and Guyon, E., "Static And Dynamic Behavior Of A Nematic Liquid Crystal In A Magnetic Field. Part I: Static Results", Le Journal De Physique, T.33, 681-9, 1972.

Williams, C., and Cladis, P. E., "On The Measurement Of The Elastic Constants Of Twist And Bend For The Nematic Liquid Crystal p-n-Methoxy Benzilidene-p.Butylaniline (MBBA)", Solid State Communications, Vol. 10, 357-9, 1972.

Williams, C., Pieranski, P., and Cladis, P. E., "Nonsingular S=+1 Screw Disclination Lines In Nematics", Physical Review Letters, Vol. 29, #2, 90-2, 1972.